Chapter 3
The Reservoir Liquids

Abstract Over 1000 chemical analyses of reservoir liquids coming from different geothermal systems were reconstructed combining the chemical analyses of the liquid and vapor phases discharged from drilled wells and collected at known separation temperature and pressure. All these reservoir liquids, apart from a few exceptions, have probably attained or closely approached the condition of chemical equilibrium with the hydrothermal (secondary) minerals occurring in the geothermal reservoirs of provenance at temperatures of 100-350°C. Therefore, they can be used to test geothermometers and f_{CO_2}-indicators, both the traditional ones and those derived in this work. The chemical characteristics of these reservoir liquids are illustrated through a comprehensive water-classification approach, including not only the triangular diagram of major anions but also the triangular diagram of main cations and suitable salinity plots, all prepared from concentrations in equivalent units. The fractions of free Na^+, K^+, Mg^{2+}, and Ca^{2+} ions and undissociated $SiO_{2(aq)}$ and the activity coefficients of these entities are examined to highlight the effects of relevant association-dissociation reactions as well as of solute-solvent and solute-solute interactions.

The data from the real world used to test the traditional geothermometers and f_{CO_2}-indicators as well as the theoretical, activity-based geoindicators that we intend to propose in this work are 1013 chemical analyses of reservoir liquids, which can be reasonably assumed to be representative of mineral-solution thermochemical equilibrium at aquifer temperatures in the range 100–350 °C. The criteria adopted to select these reservoir liquids are provenance from drilled wells and availability of sufficiently complete chemical and physical data for the calculation of reservoir (aquifer) composition. Upon complete purging of drilling fluids, initial discharge fluids are of particular interest, being representative of the natural, pre-exploitation

Electronic supplementary material The online version of this chapter (https://doi.org/10.1007/978-3-030-54318-1_3) contains supplementary material, which is available to authorized users.

R. Cioni and L. Marini, *A Thermodynamic Approach to Water Geothermometry*, Springer Geochemistry, https://doi.org/10.1007/978-3-030-54318-1_3

state, whereas fluids sampled at later stages may be affected by production-induced processes, such as mixing with re-injected fluids (brines and steam condensates) and inflow of external waters into the geothermal reservoir due to its depressurization.

3.1 Calculation of the Chemical Composition of Reservoir Liquids

In most cases, the chemical composition of reservoir liquids, including pH, was computed by merging the chemical analyses of liquid and vapor phases, separated at known temperature and pressure, and considering both total-discharge enthalpy and aquifer temperature in calculations. These calculations were generally carried out by means of the computer code WATCH, version 2.4 (Arnórsson et al. 1982; Bjarnason 2010). Further details are given in Sect. 2.3 and in the following sections. Only the composition of a few reservoir liquids (some of Salton Sea and those of Asal, Aluto-Langano, and Latera) was taken as reported by the authors due to the unavailability of data for the separated liquid and vapor phases. The boiling spring model was adopted for the Icelandic systems of medium temperature (details in Sect. 3.1.3).

3.1.1 Calculation of Reservoir Liquid Chemistry for Liquid Enthalpy Wells

For the liquid enthalpy wells, whose total discharge enthalpy is close to that of the saturated liquid water at the aquifer temperature, it is reasonable to assume that the system of interest, including the well and the nearby aquifer zones, behaves as an ***isolated system*** and that adiabatic boiling occurs from the reservoir temperature to the vapor-liquid separation temperature. If so, the steam fraction, y, in the two-phase fluid (in mass units)[1] at the separation temperature is computed using the simple relation:

$$y = \frac{H_O - H_L}{H_V - H_L} \tag{3.1}$$

which is obtained by rearranging the enthalpy conservation equation:

$$H_O = H_L \cdot (1 - y) + H_V \cdot y. \tag{3.2}$$

[1]The steam fraction is defined by the ratio $y = Q_V/(Q_V + Q_L)$, where Q_V and Q_L are the mass flow-rates of the vapor and liquid phases, respectively, at vapor-liquid separation conditions.

Please note that the equations have been renumbered to maintain sequential order. I noted that the correct numbers (3.8) and (3.9) were assigned to the first two equations in section 3.8.1. Thank you!

In Eqs. (3.1) and (3.2), H indicates the specific enthalpy of the specified phase and subscripts O, L, and V stand for the reservoir liquid, the separated liquid, and the separated vapor, respectively. Since water is by far the major constituent of geothermal fluids, the specific enthalpies of pure water (tabulated by Lemmon et al. 2017) are generally used in Eqs. (3.1) and (3.2).

The composition of the single liquid phase in the reservoir is then computed through the simple mass balance:

$$C_{i,O} = C_{i,L} \cdot (1 - y) + C_{i,V} \cdot y \tag{3.3}$$

where $C_{i,O}$, $C_{i,L}$, and $C_{i,V}$ represent the concentrations of the i-th chemical component in the reservoir liquid, the separated liquid, and the separated vapor, respectively, in consistent measurement units.

However, the pH of the reservoir liquid can neither be calculated by this simple mass balance [Eq. (3.3)] nor measured in situ, but requires the use of a relatively complex calculation procedure, which takes into account the dissociation constants of weak acids and bases and a suitable balance, either on total ionizable hydrogen ion, or titration alkalinity, or the electrical charge (e.g., Truesdell and Singers 1974; Arnórsson et al. 1982; Reed and Spycher 1984; Henley et al. 1984).

Therefore, a suitable speciation code is needed and the best option is WATCH because it calculates automatically the composition of reservoir fluids, having been specifically developed for this purpose. In contrast, a relatively intricate approach must be followed if other software packages, such as EQ3/6 (Wolery 1992; Wolery and Daveler 1992) and PHREEQC Interactive (Parkhurst and Appelo 2013; Charlton and Parkhurst 2002) are used.

For instance, Marini et al. (2003) used the software package EQ3/6 for reconstructing the chemistry of Miravalles deep waters, assuming that a single saturated liquid phase is present in the reservoir, which is a reasonable hypothesis for this geothermal system. The calculation approach is schematically summarized in Fig. 3.1 and is briefly illustrated here below.

1. First, two distinct EQ3 runs were performed to compute the chemical speciation of the liquid and vapor phases separated at known P, T conditions and cooled at 25 °C. This is the temperature at which the pH and alkalinity of the separated liquid were measured. Since the pH of the condensed vapor phase was not measured, it was assumed to be fixed by the electric charge balance in EQ3 calculations. In general, it is not a good idea to compute the pH by balancing on H^+. In this case, however, this choice is reasonable because H^+ is expected to be a major component and the concentrations of other major components, i.e., CO_2, H_2S and NH_3, are known.

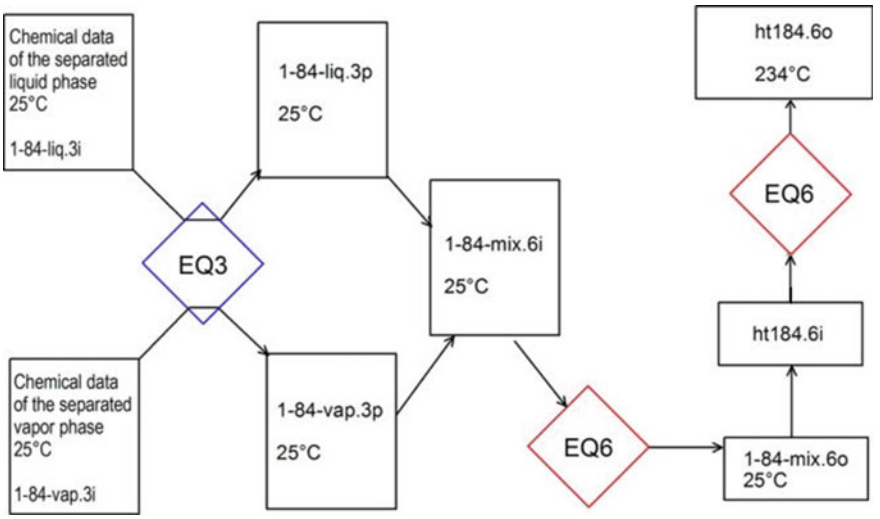

Fig. 3.1 Approach adopted by Marini et al. (2003) to compute the chemical composition of the single liquid phase presumably present in the Miravalles geothermal reservoir using the software package EQ3/6. The fourth step, in which the reservoir liquid is equilibrated with a suitable Al-silicate, is not shown

2. Second, EQ6 was run for mixing the separated, cooled liquid and vapor phases, keeping the temperature at 25 °C, and considering the steam fraction, y, computed for adiabatic boiling from the reservoir temperature to the separation temperature.
3. Third, EQ6 was run for heating the mixture obtained in the previous step from 25 °C to the reservoir temperature.
4. Fourth, EQ3 was run to equilibrate the aqueous solution with a suitable Al-silicate, either muscovite or kaolinite, because analytical Al data are not available.

The same calculations can be carried out by PHREEQC Interactive using the following keyword data blocks (Fig. 3.2):

- SOLUTION_1 to define the temperature and chemical composition of the separated liquid cooled at room temperature and to perform related speciation-saturation calculations (simulation 1);
- SOLUTION_2 to define the temperature and chemical composition of the separated vapor condensed and cooled at room temperature and to perform related speciation-saturation calculations (simulation 2);
- MIX_1 to mix together the separated liquid and condensed vapor at room temperature (simulation 3);
- REACTION_TEMPERATURE_1 to heat the liquid + condensed vapor mixture from room temperature to reservoir temperature (simulation 4);
- EQUILIBRIUM_PHASES_1 to equilibrate the reservoir liquid with the selected Al-silicate (low-albite in this example), which is dissolved or precipitated to attain saturation (simulation 5).

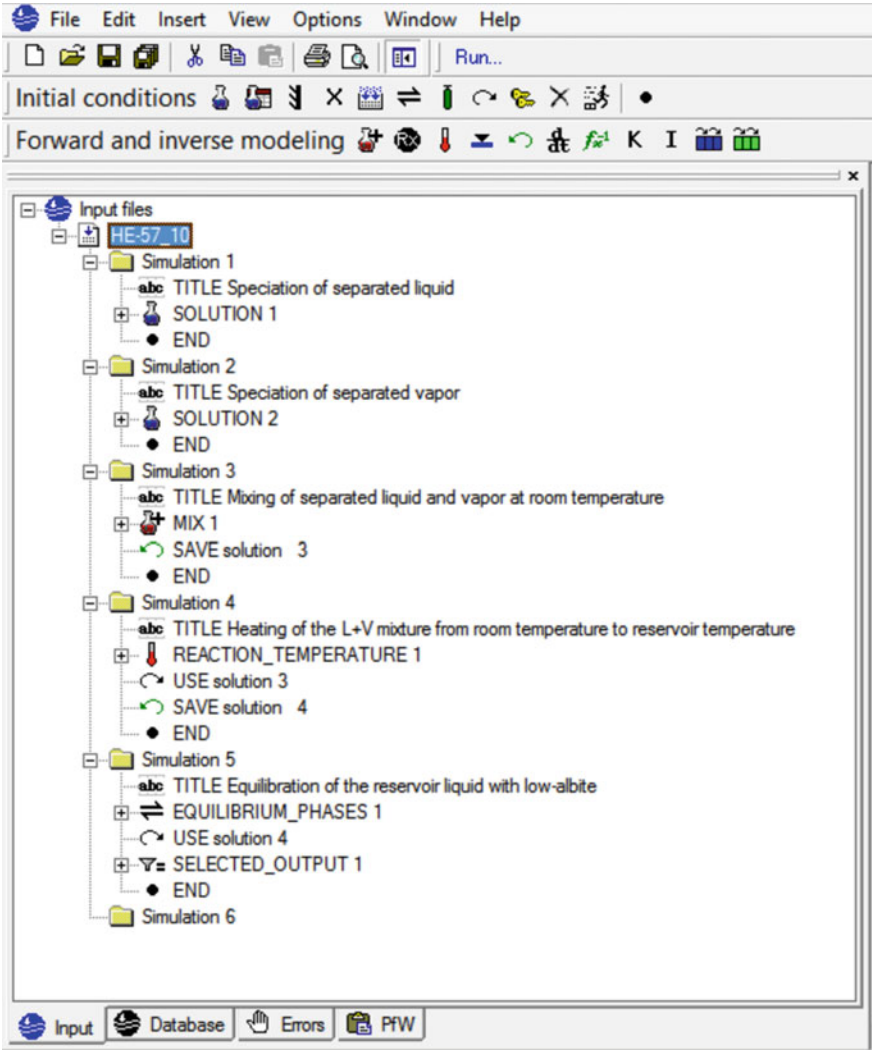

Fig. 3.2 Keyword data blocks used to compute the chemical composition of the liquid phase under reservoir condition for liquid enthalpy wells by means of PHREEQC Interactive

3.1.2 Calculation of Reservoir Liquid Chemistry for Excess Enthalpy Wells

The assumptions of isolated system behavior and adiabatic boiling are questionable for the wells with excess enthalpy or excess steam (e.g., Arnórsson and Stefansson 2005b; Arnórsson et al. 2007, 2010). In fact, because of extensive boiling in the producing aquifers of a wet-steam well, its discharge enthalpy is larger than that of

the fluid present in the undisturbed aquifer, that is beyond the depressurization zone around the well as recognized by several authors (e.g., Truesdell 1979; Glover et al. 1981; Henley et al. 1984; Truesdell et al. 1995). Consequently, the system including the aquifer and the well is not isolated.

For the excess enthalpy wells, Arnórsson and coworkers proposed different models to explain the cause of the excess enthalpy by invoking the effects of depressurization boiling, liquid phase segregation in the depressurization zones around the wells, conductive heat transfer from the aquifer rock to the flowing fluid as well as loss of steam from the fluid flowing into the wells.

In addition, Arnórsson and coworkers derived the equations needed to calculate the aquifer steam fractions and fluid chemistry for excess enthalpy wells. In detail:

1. Liquid phase segregation means that liquid water is partially or almost completely retained in the aquifer because of its adhesion onto the surfaces of mineral grains by capillary forces, whereas the vapor phase is totally transferred from the aquifer into the well. Liquid phase segregation changes both the enthalpy and the chemical composition of the well discharge compared to those of the undisturbed aquifer fluid. Therefore, the system comprising the aquifer and the well acts as an ***open system***.
2. Loss of steam from the fluid flowing into the well may occur in a sub-horizontal aquifer downstream of the upflow zone. Due to this vapor loss the well discharge suffers a depletion of volatile components and a decrease in enthalpy compared to the undisturbed aquifer. Also in this case, the system including the aquifer and the well acts as an ***open system***.
3. Conductive heat transfer from the aquifer rock to the fluid flowing into the well occurs because depressurization boiling cools the fluid. This heat transfer changes the enthalpy of the fluid but not its chemical composition. Therefore, the system comprising the aquifer and the well acts as a ***closed system***.

For all the models (as in the isolated system case), it is necessary to specify the aquifer temperature and, in general, it is also necessary to assume a suitable value for the temperature (or pressure) in the intermediate zone or depressurization zone, where the considered process (either phase segregation or loss of liquid water or loss of vapor or conductive rock-to-fluid heat transfer) occurs.

Using WATCH, these models were applied to different geothermal systems, such as Hellisheidi, Nesjavellir, and Krafla in Iceland, Olkaria in Kenya, Mahanagdong and Pataan in the Philippines (Arnórsson et al. 1990, 2010; Angcoy 2010; Karingithi et al. 2010; Remoroza 2010; Scott 2011; Scott et al. 2014). The open-system model with liquid retained in the formation provided realistic results in these applications, with concentrations of volatile components and pH values significantly different from those obtained using the isolated-system model. In contrast, concentrations of non-volatile components for the open-system (phase segregation) model resulted to be similar to those for the isolated-system model.

To gain further insight into this matter, the results of the open-system (phase segregation) model for Olkaria well discharges (from Karingithi et al. 2010) are compared, here below, with the results of both the isolated-system (gas partitioning)

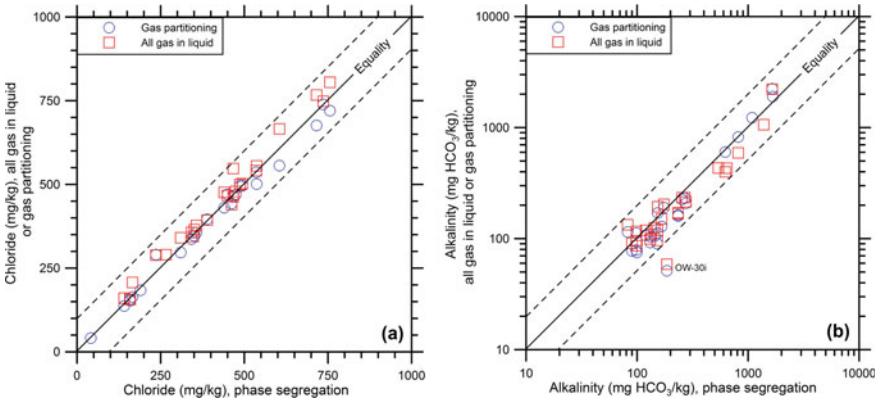

Fig. 3.3 **a** Chloride concentration and **b** total alkalinity of the Olkaria reservoir liquids given by the open-system model with liquid retained in the formation (phase segregation) are compared with those given by the isolated-system model (gas partitioning) and the all-gas-in-liquid model. The dashed lines show deviations from the equality condition

model and those obtained through a still different approach, which is based on the assumption that all gas species are contributed by the liquid phase initially stored in the geothermal aquifer and that the vapor phase is gas-free pure water. This is a realistic hypothesis if vapor is produced through boiling (evaporation) of a gas-poor liquid, as is the case of injection-derived steam (e.g., Panichi 2004). WATCH calculations were performed by merging the chemical analyses of the separated liquid and vapor phases, specifying the reservoir temperature, but omitting total-discharge enthalpy. Since enthalpy is not given to WATCH, the code computes it, assuming that the enthalpy corresponds to that of pure liquid water saturated with steam at the chosen reservoir temperature.

As expected, the three models provide similar results for the non-volatile components, such as chloride (Fig. 3.3a), and relatively similar outcomes for total alkalinity (Fig. 3.3b). In fact, for chloride, the absolute average deviation from the open-system (phase segregation) model is 6.1 ± 5.9% for the isolated-system (gas partitioning) model and 3.4 ± 4.2% for the all-gas-in-liquid model. For total alkalinity, the absolute average deviation from the open-system (phase segregation) model is 26 ± 21% for the isolated-system (gas partitioning) model and 26 ± 22% for the all-gas-in-liquid model.

Part of the discrepancies between the three models are due to the different reservoir temperatures, with an absolute average deviation from the open-system (phase segregation) model of 8.8 ± 7.6 °C for the isolated-system (gas partitioning) model and of 8.1 ± 7.6 °C for the all-gas-in-liquid model.

For the volatile components, such as total CO_2 (Fig. 3.4a) and total H_2S (Fig. 3.4b), the results of the isolated-system model (gas partitioning) are significantly lower than those of the open-system (phase segregation) model and of the all-gas-in-liquid model, whereas the latter two models give relatively similar outcomes.

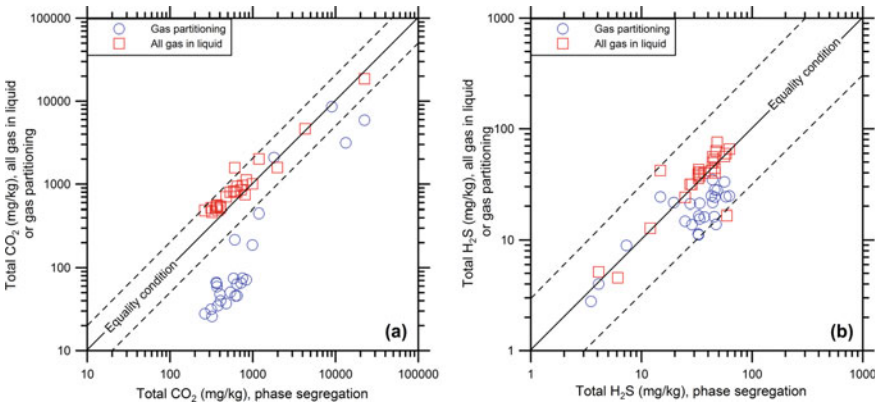

Fig. 3.4 **a** Total CO_2 and **b** total H_2S concentrations of the Olkaria reservoir liquids given by the open-system model with liquid retained in the formation (phase segregation) are compared with those given by the isolated-system model (gas partitioning) and the all-gas-in-liquid model. The dashed lines show deviations from the equality condition

In detail, the absolute average deviation of the isolated-system (gas partitioning) model from the open-system (phase segregation) model is 140 ± 45% for total CO_2 and 58 ± 29% for total H_2S, whereas the absolute average deviation of the all-gas-in-liquid model from the open-system (phase segregation) model is 32 ± 18% for total CO_2 and 21 ± 27% for total H_2S. These figures are similar to those for alkalinity (see above).

The pH of reservoir liquids is computed by WATCH starting from the low-temperature pH value and based on the assumption of constant alkalinity, apart from the increase brought about by steam separation (Arnórsson et al. 1982). In WATCH calculations, alkalinity is the sum of the concentrations (in equivalent units) of OH^-, $H_3SiO_4^-$, $H_2SiO_4^{2-}$, HCO_3^-, CO_3^{2-}, HS^- and S^{2-}, and related complexes with Na^+, Ca^{2+}, and Mg^{2+} ions, that is $CaHCO_3^+$, $MgHCO_3^+$, $CaCO_3°$, $MgCO_3°$, and $NaH_3SiO_4°$, minus H^+ molality.

Consequently, the discrepancies between the pH values computed by the three models are chiefly due to the distinct values of total alkalinity which, in turn, are essentially controlled by the differences in total CO_2 and total H_2S, whereas the differences in non-volatiles components and temperature are less important.

As shown by Fig. 3.5, the pH values given by the isolated-system model (gas partitioning) are significant higher than those of the open-system (phase segregation) model, whereas the pH values given by the all-gas-in-liquid model are similar to or somewhat lower than those of the open-system (phase segregation) model. In detail, the absolute average deviation of the isolated-system (gas partitioning) model from the open-system (phase segregation) model is 0.67 ± 0.26 pH units, whereas the absolute average deviation of the all-gas-in-liquid model from the open-system (phase segregation) model is 0.22 ± 0.15 pH units.

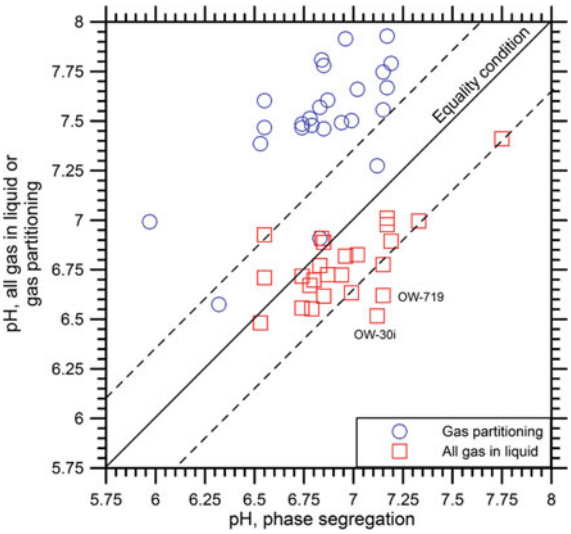

Fig. 3.5 pH values of the Olkaria reservoir liquids given by the open-system model with liquid retained in the formation (phase segregation) are compared with those given by the isolated-system model (gas partitioning) and the all-gas-in-liquid model. The dashed lines show deviations from the equality condition

Summing up, results of the all-gas-in-liquid model are not significantly different from those of the open-system model with liquid retained in the formation (phase segregation). However, the second model requires to specify the temperature (or pressure) in the intermediate zone or depressurization zone, where phase segregation occurs, whereas this information is not required by the first model. Therefore, the first model was preferred and the second model was abandoned. The next step is to choose the best model between the isolated-system model (gas partitioning) and the all-gas-in-liquid model. To this purpose, the mineral-solution equilibrium pH (definition in Sect. 3.9) was taken as reference. The isolated-system (gas partitioning) model was chosen if the difference between the pH computed using this model and the mineral-solution equilibrium pH is less than one pH unit, whereas the all-gas-in-liquid model was adopted when this pH difference resulted to be higher than one pH unit.

In this work, modeling of reservoir liquid chemistry for excess enthalpy wells was carried out using WATCH. The same calculations can be performed by other computer programs, such as SOLVEQ-XPT and CHIM-XPT (Reed 1998; Reed et al. 2014) or PHREEQC Interactive. Using PHREEQC Interactive, the initial four simulations are exactly the same as for the liquid enthalpy wells (see Fig. 3.2 and related discussion in Sect. 3.1.1). Again, the following keyword data blocks are used (Fig. 3.6):

- SOLUTION_1 to define the temperature and chemical composition of the separated liquid cooled at room temperature and to perform related speciation-saturation calculations (simulation 1);
- SOLUTION_2 to define the temperature and chemical composition of the separated vapor condensed and cooled at room temperature and to perform related speciation-saturation calculations (simulation 2);

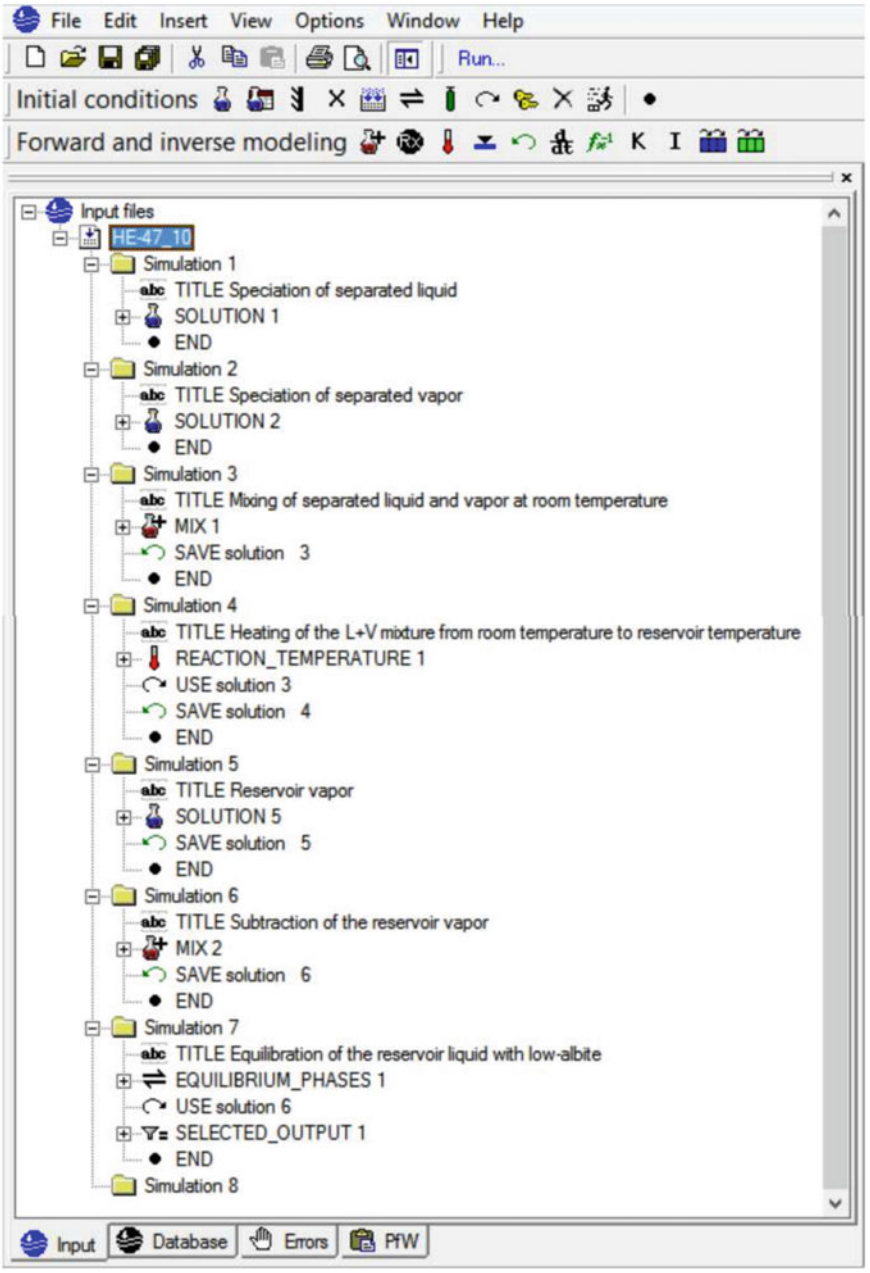

Fig. 3.6 Keyword data blocks used to compute the chemical composition of the liquid phase under reservoir condition for excess enthalpy wells by means of PHREEQC Interactive

- MIX_1 to mix together the separated liquid and condensed vapor at room temperature, considering the steam fraction at collection (simulation 3);
- REACTION_TEMPERATURE_1 to heat the liquid + condensed vapor mixture from room temperature to reservoir temperature (simulation 4).

Initially, only the 4 simulations mentioned so far are performed and the concentrations of aqueous CO_2, H_2S, and NH_3 in total discharge (obtained through simulation 4) are used to compute the concentrations of gaseous CO_2, H_2S, and NH_3 in the equilibrium vapor phase by means of the relation:

$$C_{i,V} = \frac{C_{i,O}}{y + \frac{1-y}{B_i}}. \tag{3.4}$$

Equation (3.4) is obtained by inserting the vapor-liquid gas distribution coefficient of the i-th gas species, $B_i = C_{i,V}/C_{i,L}$, into Eq. (3.3) and rearranging it. The vapor-liquid gas distribution coefficients of CO_2, H_2S, and NH_3 depend on temperature according to the following equations (T in °C; Giggenbach 1980):

$$\log B_{CO_2} = 4.7593 - 0.01092 \cdot T \tag{3.5}$$

$$\log B_{H_2S} = 4.0547 - 0.00981 \cdot T \tag{3.6}$$

$$\log B_{NH_3} = 1.4113 - 0.00292 \cdot T \tag{3.7}$$

which are valid from 100 to 340 °C. The concentrations of gaseous CO_2, H_2S, and NH_3 in the equilibrium vapor phase thus computed are then used as input data in simulation 5 to model the condensed reservoir vapor, whose pH is computed imposing the charge balance. The keyword data block SOLUTION_5 is used.

Then, in simulation 6, the keyword data block MIX_2 is utilized to subtract the condensed reservoir vapor from the total reservoir fluid, considering the aquifer steam fraction, which is obtained by plugging the enthalpies of total discharge and of vapor and liquid H_2O at reservoir temperature into Eq. (3.1).

Finally, in simulation 7, the reservoir liquid is equilibrated with low-albite, as in the last simulation for the liquid enthalpy wells, utilizing the keyword data block EQUILIBRIUM_PHASES_1.

3.1.3 Further Details on the Reconstruction of Reservoir Liquid Chemistry

The choice of the reservoir temperature depends largely on the available information. Temperatures measured in the producing sector of the well were used when available.

Enthalpy-temperatures were used for liquid enthalpy wells when measured temperatures were not available and silica temperatures appeared to be unreliable. Nevertheless, in most cases, the reservoir temperatures were considered equal to silica saturation temperatures, which were computed using the quartz/chalcedony function, i.e., Eq. (4.57), above 180 °C or the chalcedony geothermometer of Fournier (1977), i.e., Eq. (5.18), at lower temperatures. When the computed pH of the reservoir liquid resulted to be relatively high and the computed concentration of silicic acid resulted to be significantly lower than that of total dissolved silica, an iterative procedure was used, running again WATCH at the reservoir temperature given by the silica geothermometric function for the silicic acid concentration computed in the previous run. The procedure was stopped for reservoir temperatures differing by less than 0.1 °C in two consecutive runs. Usually four or five iterations are needed to attain this condition.

The reservoir temperatures of Miravalles fluids were computed averaging (1) in-hole temperature measurements performed in the same period of sampling, (2) temperatures corresponding to total discharge enthalpy, assuming the presence of a single saturated liquid in the reservoir, and (3) results of the quartz/chalcedony function, i.e., Eq. (4.57), because of the small deviations between these different temperature types.

When the liquid sample was collected at the weir box, under atmospheric pressure, and the vapor phase was obtained at higher pressure, simple preliminary calculations were carried out to compute the composition of the vapor phase at atmospheric pressure (Arnórsson et al. 2005). The alternative approach, that is the calculation of the liquid phase composition at the temperature and pressure of vapor sampling, was not adopted because it requires use of geochemical modeling for pH calculation.

Only boiled liquids were generally collected for the Icelandic systems of medium temperature (100–175 °C) whereas steam samples are not available. Therefore, the boiling spring model was adopted, selecting a suitable degassing factor to approach calcite saturation for the deep liquids, because *it is reasonable to assume that deep geothermal waters are calcite saturated* (Arnórsson et al. 1983b). Aquifer temperatures were reconstructed on the basis of in-hole temperature measurements. The chalcedony geothermometer was not used due to the usual presence of considerable amounts of silicate ion at the relatively high pH of these reservoir liquids.The citation "Arnórsson et al. (1982)" has been changed to "Arnórsson (1983a, b)" to match the author name/date in the reference list. Please check here and in subsequent occurrences, and correct if necessary. Here the correct citation is Arnórsson (1983b). I tried to correct the text but I could not. Here and in subsequent occurrences I added a comment.

Although WATCH performs speciation-saturation calculations, the chemical compositions computed by WATCH, including pH and the redox potential fixed by the HS^-/SO_4^{2-} couple, were given as input data to PHREEQC Interactive 3.1.1 to improve data processing. PHREEQC Interactive was run using a modified version the LLNL database containing the thermodynamic data of solid phases, including variably ordered adularia, from Helgeson et al. (1978). In PHREEQC Interactive

runs, aluminum was assumed to be fixed by saturation with low-albite. The reasons for this choice are discussed in Sect. 4.2.3.

In most cases, the extended Debye-Hückel equation, also known as B-dot equation (see Sect. 2.3.3), was adopted to calculate activity coefficients of individual ions. However, the high-salinity geothermal liquids of Salton Sea and Asal were processed directly by EQ3, without running WATCH beforehand, and using a thermodynamic database which is consistent with the Pitzer's theory (see Sect. 2.3.4) and comprises the data of solid phases, including variably ordered adularia, from Helgeson et al. (1978).

3.1.4 *Presentation of the Main Results of Speciation-Saturation Calculations and Approach Adopted for the Chemical Classification of Reservoir Liquids*

Only the aqueous solutions with percent error on total charge lower than 10% and reservoir pH (from speciation calculations) corresponding with the mineral-solution equilibrium pH within ±1.3 pH unit were considered in data interpretation. The analytical data of reservoir liquids, main results of speciation-saturation calculations and outcomes of traditional geothermometers and f_{CO_2}-indicators as well as of the theoretical activity-based geoindicators derived in this book are reported as electronic supplementary material (file Reservoir_Liquids.XLS). The ordering parameter of hydrothermal adularia in hypothetical equilibrium with these reservoir liquids is also given. The results of speciation-saturation calculations listed in this file comprise: pH, Eh, pe, carbonate alkalinity,[2] Alk_C, the activities and molalities of H^+, Na^+, K^+, Ca^{2+}, Mg^{2+}, Al^{3+} and HCO_3^- ions, $SiO_{2(aq)}$, and $CO_{2(aq)}$, the logarithm of CO_2 fugacity, and the concentration of total dissolved Al constrained by equilibrium with low-albite.

In the following sections of this chapter, the chemical composition of reservoir liquids is investigated by means of the triangular plots of major anions (i.e., Cl, SO_4, and carbonate alkalinity) and major cations (i.e., Na, K, and Ca). Magnesium was excluded because it is generally present in very low concentrations in geothermal liquids and the relative concentration of Mg is negligible with respect to those of Na, K, and Ca. Since these triangular plots do not convey any information on total ionic salinity (Σ_{eq}), this parameter is inspected by using the binary diagrams of Cl versus $SO_4 + Alk_C$. In fact, the Σ_{eq} of the considered reservoir liquids can be appreciated in these diagrams, by comparing the position of each reservoir liquid with the lines of slope −1 which are iso-Σ_{eq} lines (see Tonani et al. 1998 for further details). All these graphs were prepared using concentrations in equivalent units, in contrast with the

[2]Carbonate alkalinity is the sum of the concentrations, in equivalent units, of HCO_3^- and CO_3^{2-} ion, including related aqueous complexes, e.g., $CaHCO_3^+$, $MgHCO_3^+$, $CaCO_3°$, and $MgCO_3°$.

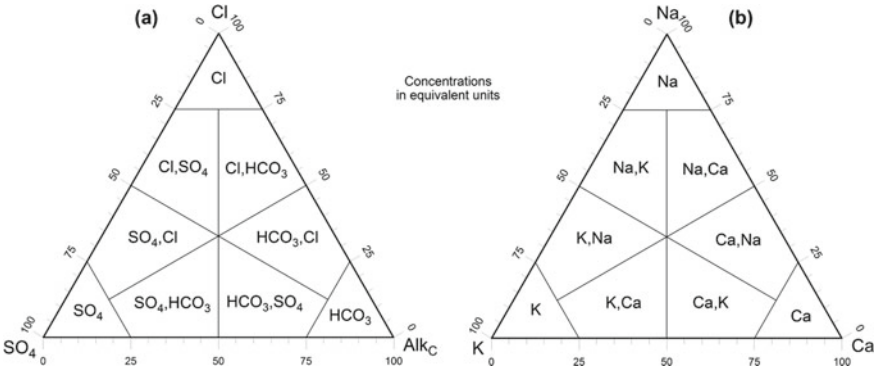

Fig. 3.7 Triangular plots of **a** major anions and **b** major cations showing the different sectors used for the chemical classification of reservoir liquids

consolidated procedure which is based on the use of concentrations in weight units. The reason for our choice is that equivalent units are proportional to the amount of electrical charges carried by each ion and, therefore, are more suitable than weight units for the chemical classification of natural waters as recognized long ago (e.g., Zaporozec 1972 and references therein). Average seawater composition (Nordstrom et al. 1979) is also represented in the relevant plots for comparison.

The terminology adopted for the chemical classification of reservoir liquids is consistent with the two triangular diagrams of Fig. 3.7. For instance a reservoir liquid positioned in the [Cl,SO_4] sector in Fig. 3.7a and in the [Na] sector in Fig. 3.7b belongs to the Na–Cl,SO_4 chemical type or chemical facies, whereas a reservoir liquid situated in the [HCO_3,SO_4] sector in Fig. 3.7a and in the [Ca] sector in Fig. 3.7b is attributed to the Ca–HCO_3,SO_4 chemical type or chemical facies, and so on.

3.2 The Reservoir Liquids from the Geothermal Systems in Iceland

Iceland is located along the Mid-Atlantic Ridge between 63°20′ N, 18°44′ W and 66°11′ N, 18°50′ W and is the largest emerged sector of a mid-oceanic ridge system all over the world. Iceland belongs to a large volcanic province which extends from Greenland to Scotland and is associated to a hotspot or a deep mantle plume (Wilson 2007).

The high-temperature (>175 °C) geothermal systems of Iceland considered here are Hellisheidi (data from Scott 2011), Hveragerdi (data from Arnórsson 1978b, Arnórsson et al. 1978, 1983b, Ping 1991; Zhanxue 1998), Krafla (data from Arnórsson et al. 1983b; Ping 1991; Gudmunsson and Arnórsson 2002; Giroud 2008; Hermanska et al. 2019), Námafjall (data from Arnórsson 1978b; Arnórsson et al. 1978, 1983b; Gudmunsson and Arnórsson 2002; Giroud 2008; Malimo 2012),

Fig. 3.8 Google Earth map showing the location of the high-temperature geothermal fields of Krafla and Námafjall in northeastern Iceland

Nesjavellir (data from Arnórsson 1978b; Arnórsson et al. 1978; Giroud 2008), Reykjanes (data from Arnórsson 1978a, b; Arnórsson et al. 1978, 1983b; Giroud 2008; Hardardóttir 2011; Berehannu 2014), and Svartsengi (data from Arnórsson 1978a, b; Arnórsson et al. 1978, 1983b; Giroud 2008). The number of accepted chemical analyses is 153.

Krafla and Námafjall are located at short distance from each other, in the northern part of Iceland (Fig. 3.8). The Krafla–Námafjall area was affected by volcanic eruptions in 1975–1984.

Hellisheidi, Nesjavellir, Hveragerdi, Svartsengi, and Reykjanes are situated in the southern part of the country (Fig. 3.9). Hellisheidi, Nesjavellir, and Hveragerdi are next to each other, in the Hengill volcano area, on the inland termination of the Reykjanes peninsula. Reykjanes and Svartsengi are positioned in the extreme southwest of Iceland, on the tip of the Reykjanes peninsula, towards the ocean, and are recharged by sea-water, at least partly.

A thorough description of the Icelandic high-temperature geothermal fields is given in the review paper of Ármansson (2016) and references therein.

For what concerns the medium-temperature ($100 < T < 175$ °C) geothermal systems of Iceland taken into account in this work, most data come from Bakki, with 18 entries (data from Arnórsson et al. 1983b; Arnórsson 1995b, Ping 1991, and Zhanshi 2001), whereas the other 11 data (from Arnórsson 1978b; Arnórsson et al. 1983b; Arnórsson 1995b) refer to different sites, for a total of 29 chemical analyses.

Fig. 3.9 Google Earth map showing the location of the high-temperature geothermal fields of Hellisheidi, Nesjavellir, Hveragerdi, Svartsengi, and Reykjanes in southwestern Iceland

3.2.1 Chemistry of the Reservoir Liquids from the High-Temperature Geothermal Systems in Iceland

In the triangular diagram of main cations (Fig. 3.10), all the high-temperature reservoir liquids of Iceland are positioned in the [Na] sector, indicating that sodium is by far the prevailing cation in all these aqueous solutions. The reservoir liquids of Krafla, Námafjall, Hellisheidi, Nesjavellir, and Hveragerdi are situated close to the Na vertex, whereas those of Reykjanes and Svartsengi have somewhat lower Na/Ca molar ratio, due to acquisition of Ca during high-temperature basalt-seawater interaction. In the triangular diagram of major anions for the high-temperature geothermal systems of Iceland there is a large scatter of sample points (Fig. 3.11). Based on both triangular plots the considered reservoir liquids can be attributed to eight different chemical types. In detail:

1. The Na–Cl chemical type comprises 62 of the 152 reservoir liquids of interest, that is 41% of the cases. The Na–Cl reservoir liquids come from Hellisheidi, Námafjall, Nesjavellir, Reykjanes and Svartsengi. In particular, the reservoir liquids of Reykjanes and Svartsengi are positioned exactly on the chloride vertex in Fig. 3.11.
2. The Na–Cl,HCO_3 chemical facies includes 32 reservoir liquids (21% of the total) proceeding from Hellisheidi, Hveragerdi, Krafla, Námafjall, and Nesjavellir.

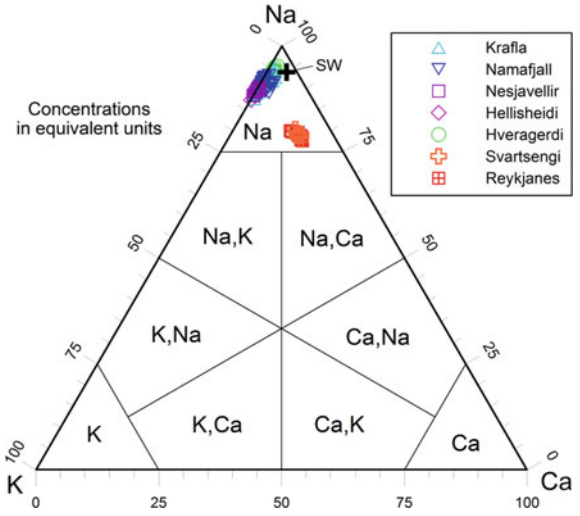

Fig. 3.10 Triangular plot of major cations for the reservoir liquids from the high-temperature Icelandic geothermal systems. Average seawater is also shown for comparison

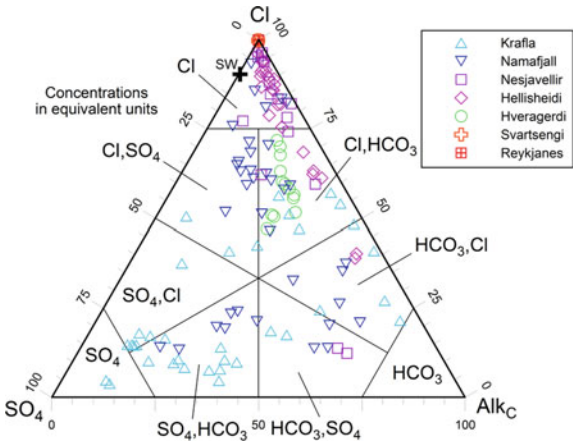

Fig. 3.11 Triangular plot of major anions for the reservoir liquids from the high-temperature Icelandic geothermal systems. Average seawater is also shown for comparison

3. The Na–HCO_3,Cl chemical facies is represented by 12 reservoir liquids (8% of the total), coming from Hellisheidi, Krafla, and Námafjall.
4. The Na–HCO_3,SO_4 chemical type groups 7 reservoir liquids (5% of the cases), proceeding from Krafla, Námafjall, and Nesjavellir.
5. The Na–SO_4,HCO_3 chemical facies includes 18 reservoir liquids (12% of the total) coming from Krafla and Námafjall.
6. The Na–SO_4 chemical facies is represented by 2 reservoir liquids (1% of the total), both from Krafla.
7. The Na–SO_4,Cl chemical type comprises 7 reservoir liquids (5% of the cases) proceeding from Krafla.

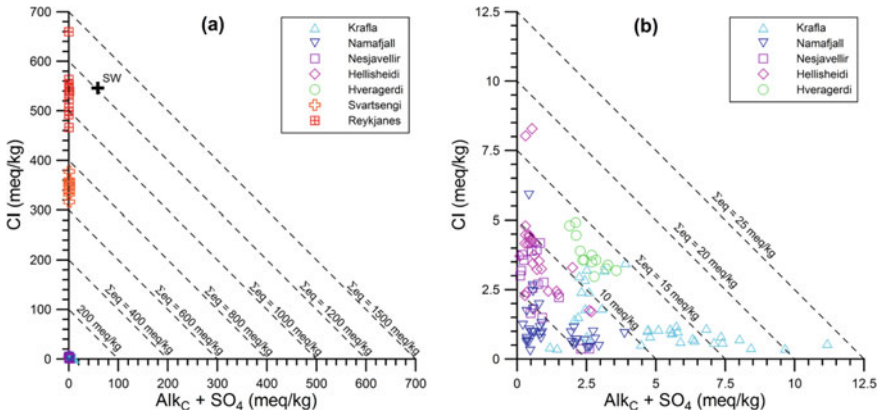

Fig. 3.12 Correlation diagrams of Cl versus SO_4 + Alk_C for the reservoir liquids from the high-temperature geothermal systems in Iceland. Plot (**b**) shows a zoomed view of the zone close to the origin of the axes in plot (**a**). Average seawater is also displayed for comparison in plot (**a**)

8. The Na–Cl,SO_4 chemical type groups 12 reservoir liquids (8% of the cases) coming from Krafla and Námafjall.

As shown by the binary diagrams of Cl versus SO_4 + Alk_C (Fig. 3.12), the reservoir liquids of Krafla, Námafjall, Hellisheidi, Nesjavellir, and Hveragerdi have low Σ_{eq}, ranging from 5.0 to 23.5 meq/kg[3]. These low values are not surprising because these geothermal circuits are recharged by meteoric waters and the extent of water-rock interaction is limited (Arnórsson 1995a). In contrast, the reservoir liquids of Reykjanes and Svartsengi have high Σ_{eq}, in the range 946–1312 meq/kg, and 643–732 meq/kg, respectively, due to the variable involvement of seawater and meteoric waters in the recharge of these geothermal circuits (Arnórsson 1978a, 1995a).

In fact, the seawater-dominated Reykjanes geothermal system is positioned along the Mid-Atlantic Ridge and is considered to be the subaerial equivalent to mid-ocean-ridge hydrothermal systems (Hardardóttir et al. 2009).

Chloride is of marine origin at Reykjanes and Svartsengi, whereas it is mainly derived from rock leaching at Hellisheidi, Nesjavellir, Hveragerdi, Námafjall and Krafla, where dissolved chloride is low because local basaltic rocks have low Cl contents (Arnórsson 1995a). Nevertheless, supply of magmatic HCl occurred at Krafla when fresh magma was intruded into the roots of Krafla volcano (Ármannsson et al. 1982).

Sulfur species are chiefly contributed by magma degassing at Námafjall and Krafla. However, the high SO_4 concentrations of the reservoir liquids of lower temperature and enthalpy from Krafla are probably due to dissolution of anhydrite, whose solubility increases with decreasing temperature (Gudmundsson and

[3]Incidentally, these low Σ_{eq} values are similar to those of bottled oligomineral waters. However, these reservoir liquids have very high concentrations of SiO_2, representing 32–84% of the TDS. Therefore, TDS values are significantly higher than those of oligomineral waters.

Arnórsson 2002). Carbon dioxide is probably supplied by magma degassing to all the high-temperature Icelandic geothermal systems (Arnórsson 1995a).

3.2.2 *Chemistry of the Reservoir Liquids from the Medium-Temperature Geothermal Systems in Iceland*

In the triangular plot of main cations (Fig. 3.13), all the medium-temperature reservoir liquids of Iceland, except those of Seltjarnarnes, are found in the [Na] sector, indicating that sodium is by far the prevailing cation in most cases. Of the two Seltjarnarnes reservoir liquids, one is positioned in the [Ca,Na] sector, whereas the other is situated in the [Na,Ca] sector of Fig. 3.13.

In the triangular diagram of main anions (Fig. 3.14), the reservoir liquids from the medium-temperature geothermal systems in Iceland are located in the sectors of [Cl], [Cl,SO_4], [Cl,HCO_3] and [HCO_3,SO_4]. The reservoir liquids of Bakki and Seltjarnarnes are positioned close to the seawater point in this plot. Six different chemical types are recognized based on both triangular diagrams. In detail:

1. The Na–Cl chemical type comprises 18 of the 29 reservoir liquids of interest (62% of the cases), all from Bakki.
2. The Na,Ca–Cl chemical facies includes one of the two reservoir liquids of Seltjarnarnes (3% of the cases).
3. The Ca,Na–Cl chemical type is represented by the other reservoir liquid of Seltjarnarnes (3% of the cases).

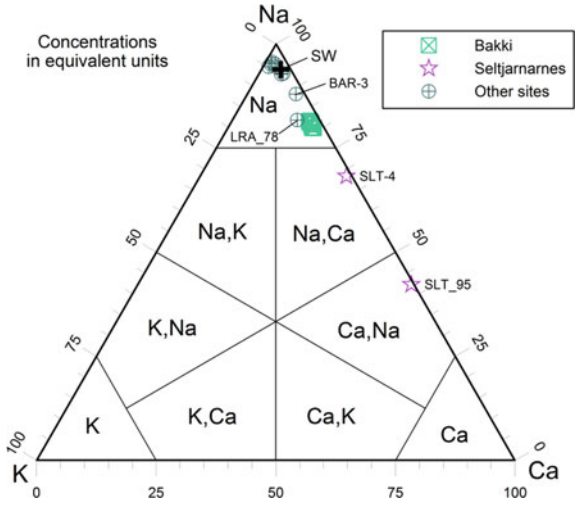

Fig. 3.13 Triangular plot of major cations for the reservoir liquids from the medium-temperature geothermal systems in Iceland. Average seawater is also shown for comparison

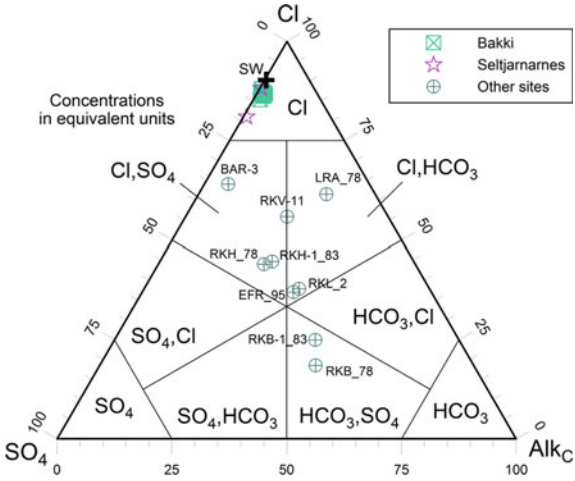

Fig. 3.14 Triangular plot of major anions for the reservoir liquids from the medium-temperature geothermal systems in Iceland. Average seawater is also shown for comparison

4. The Na–Cl,HCO_3 chemical facies groups 4 reservoir liquids (14% of the total) proceeding from Efri-Reykir, Leirà, Reykholar, and Reykjavik.
5. The Na–Cl,SO_4 chemical type comprises 3 reservoir liquids (10% of the cases) coming from Baer and Reykholt.
6. The Na–HCO_3,SO_4 chemical facies includes 2 reservoir liquids (7% of the cases), both proceeding from Reykjabol.

As shown by the correlation diagram of Cl versus SO_4 + Alk_C (Fig. 3.15), the

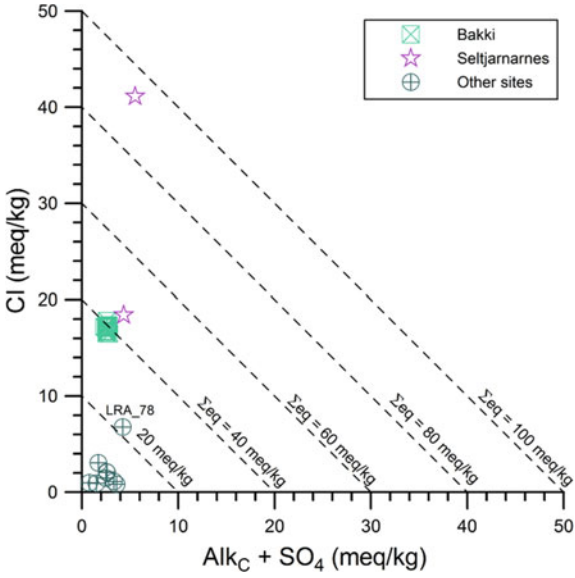

Fig. 3.15 Correlation diagram of Cl versus SO_4 + Alk_C for the reservoir liquids from the medium-temperature geothermal systems in Iceland

reservoir liquids of most geothermal sites have low Σ_{eq} values, ranging from 4 to 10 meq/kg, whereas somewhat higher Σ_{eq} values are displayed by the reservoir liquids of Leirà (code LRA_78), with Σ_{eq} of 22 meq/kg, Bakki, with Σ_{eq} of 39–41 meq/kg, and Seltjarnarnes, with Σ_{eq} values of 45 and 96 meq/kg.

The peculiar chemistry of Bakki is probably due to an appreciable seawater contribution in the recharge of this geothermal circuit or to leaching of halite contained in local marine sediments alternating with volcanic rocks (Zhanshi 2001). Similar explanations apply to Seltjarnarnes, whose high Ca concentrations are likely acquired through interaction with basalts.

3.3 The Reservoir Liquids from the Geothermal Systems in Northern and Central America

The geothermal systems in Northern and Central America taken into account in this work are: Dixie Valley (data from Reed 1989; Goff et al. 2002), Long Valley (data from White and Peterson 1991), Coso (data from Moore et al. 1989), Valles (data from Truesdell and Janik 1986; White 1986), Salton Sea (data from Helgeson 1968b; Michels 1986; Thompson and Fournier 1988; Williams and McKibben 1989) and Heber (data from Adams et al. 1989) in the USA, Cerro Prieto (data from Reed 1976; Mañon et al. 1977; Truesdell et al. 1981) and Los Azufres (data from González-Partida et al. 2000, 2005; Arellano et al. 2005) in México, Berlín in El Salvador (data from Renderos 2002), and Miravalles in Costa Rica (data from Giggenbach and Corrales Soto 1992; Yock Fung 1998; Gherardi et al. 2002; Marini et al. 2003). The accepted chemical analyses are 35 from Dixie Valley, 10 from Long Valley, 5 from Coso, 7 from Valles, 23 from Salton Sea, 16 from Heber, 19 from Cerro Prieto, 26 from Los Azufres, 55 from Berlín, and 105 from Miravalles, for a total of 301 entries.

3.3.1 Dixie Valley

The Dixie Valley in central Nevada is the site of a fault-controlled geothermal system of the Basin and Range tectonic province (Fig. 3.16). In the Dixie Valley geothermal system, hot fluids are produced from the permeable sectors of a normal fault, known as Stillwater, and associated fractured rocks at depths of 2800–3050 m (Goff et al. 2002 and references therein). The local stratigraphic sequence includes marine quartzite, siltstone, and shale, silicic and basaltic volcanic and volcaniclastic rocks as well as granodiorite of Cretaceous age (Waibel 1987). Local rocks were affected by several thermal and metasomatic events characterized by temperatures ranging from 50 to 250 °C, which compare with the interval of present-day temperatures.

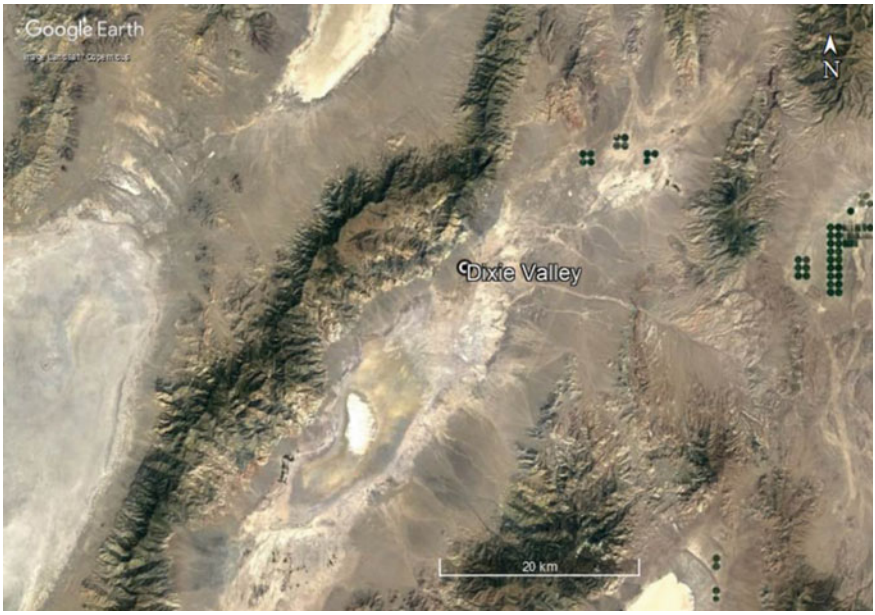

Fig. 3.16 Google Earth map showing the location of the Dixie Valley geothermal field

3.3.2 Long Valley

The Long Valley geothermal system in east-central California is hosted within the homonymous caldera, a 17 by 32 km elliptical depression on the eastern front of the Sierra Nevada (Fig. 3.17). The Long Valley caldera formed 730 ka ago during the Bishop Tuff eruption that emitted ~600 km^3 of rhyolite magma (Bailey et al. 1976). Rhyolites and rhyodacites were erupted during the subsequent intracaldera volcanic activity. The currently active geothermal system is hosted in Paleozoic and Mesozoic metasedimentary rocks situated at depths of at least 3 km. The geothermal system is recharged by meteoric waters infiltrating in the western rim of the Long Valley caldera along the Sierra Nevada front. Thermal fluids upflow in the western part of the caldera, flow eastwards in a confined, shallow aquifer and mix progressively with dilute meteoric groundwaters before discharging through the hot springs located in the southeastern parts of the caldera (Tempel et al. 2011 and references therein).

3.3.3 Coso

The Coso geothermal field in east-central California is situated between the Basin and Range and Sierra Nevada tectonic provinces (Fig. 3.18), at a releasing bend stepover in a dextral strike-slip fault system (Monastero et al. 2005).

Fig. 3.17 Google Earth map showing the location of the Long Valley geothermal field

Fig. 3.18 Google Earth map showing the location of the Coso geothermal field

Permeability is probably controlled by active normal faults accommodating the regional dextral transtension. Although the reservoir does not appear to be confined to a specific lithotype, it is prevailingly hosted in granitic rocks and subordinately in mafic and metamorphic rocks associated with the Sierra Nevada composite batholith.

Basement rocks are covered by the Late Tertiary and Quaternary volcanic rocks of the Coso volcanic field, including rhyolite domes and flows younger than 300 ka (Wohletz and Heiken 1992). A silicic magma body, possibly partially molten, underlies the Coso volcanic field at a depth of at least 8 km, acting as heat source of the geothermal system (Bacon et al. 1980).

Measured temperatures in wells used as producers vary from 340 °C, at depths of 2500 m in the south, to 230 °C, in the shallow part of the system in the north, reflecting the presence of an upflowing plume of thermal water, which is also indicated by chemical and fluid inclusion data (Moore et al. 1989).

3.3.4 Valles

The Valles caldera is a Quaternary volcanic collapse structure with a diameter of 22 km (Fig. 3.19). It was formed by the eruption of the Upper Member of the Bandelier Tuff, which occurred 1.25 Ma ago and is the latest catastrophic volcanic eruption in

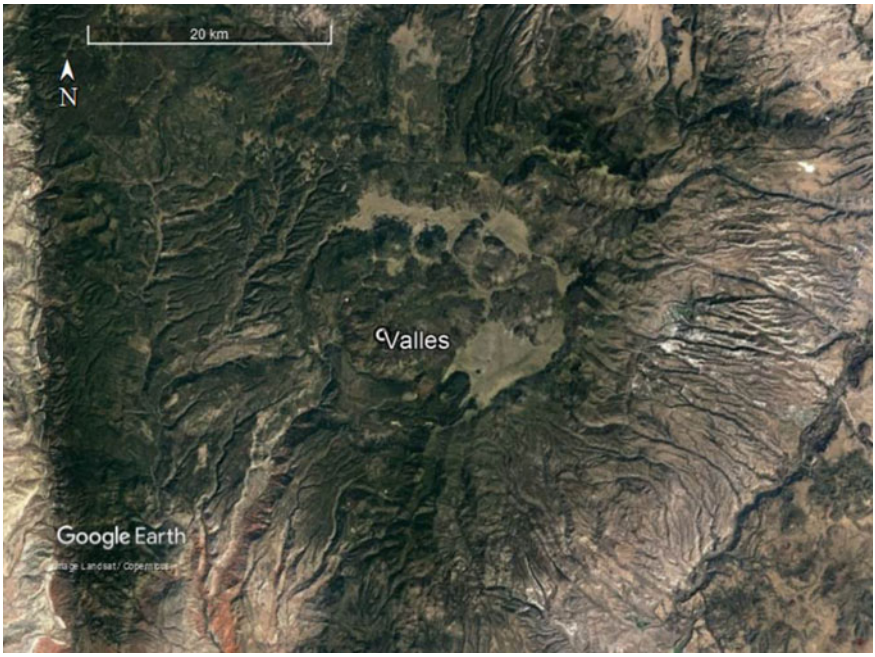

Fig. 3.19 Google Earth map showing the location of the Valles geothermal field

the Jemez Mountains volcanic field of north-central New Mexico (Smith and Bailey 1966).

The Valles caldera is located at the intersection of the Jemez Lineament and the western edge of the Rio Grande Rift, a major extensional structure that stretches over 1000 km. A geothermal system at temperatures of 225–330 °C is hosted within the Valles caldera, in caldera-fill ignimbrites and pre-caldera rocks, at depths of 600–2500 m (Nielson and Hulen 1984).

The Valles geothermal system comprises two drilled reservoirs: the Redondo Creek (formerly called Baca) reservoir and the Sulphur Springs reservoir. Deep reservoir fluids have neutral sodium-chloride chemical composition, TDS lower than 8000 mg/kg, and gas content of 0.4–1.5 wt%. About 10 km outside the Valles caldera, along the pre-caldera Jemez fault zone, there are two sets of neutral-chloride hot springs representing the outflows of the Valles geothermal system (Goff et al. 1988).

3.3.5 Salton Sea, Heber, and Cerro Prieto

Several active geothermal systems, including Salton Sea, Heber, and Cerro Prieto, are located into the extensional basins linking different sectors of strike-slip faulting within the Salton Trough, which comprises the Imperial Valley in southern California, U.S.A, and the Mexicali Valley in the northern part of Baja California, México (Fig. 3.20).

Since 4 Ma ago, the Imperial Valley has been isolated from the Gulf of California by the Colorado River sedimentation, with the consequent deposition of evaporite rocks, whose dissolution explains the high or relatively high salinity of local geothermal fluids (Williams and McKibben 1989 and references therein). The stratigraphic sequence of the region comprises Pliocene and Pleistocene fluvial, deltaic, lacustrine and evaporite sediments. These sediments were locally intruded by both mafic and felsic igneous rocks and experienced widespread metamorphism generating greenschist and even amphibolite facies hornfelses.

Hypersaline geothermal brines (20–27 wt% TDS) occupy the deep hot (260–340 °C) central sectors of the Salton Sea geothermal system, whereas lower salinity fluids (<10 wt% TDS) generally occur in the cooler (<260 °C) shallow or boundary portions of the field (Williams and McKibben 1989). The two fluid types are separated by a few hundred meter thick interface, roughly coinciding with the 260 °C isotherm.

The Heber geothermal system comprises three major units, characterized by distinct permeability, namely: (1) the low permeability capping clays from 150 to 550 m, (2) the high matrix permeability sandstone "outflow reservoir" from 550 to 1700 m, and (3) the indurated sediments, at depths of 1700 to ~3200 m, whose high permeability is controlled by both strike-slip and normal faults (James et al. 1987). A maximum bottom-hole temperature of 199 °C was measured in well GTW-6, which is probably the closest to the upflow zone in the south. The geothermal fluids traveling northeastward have higher B and Li concentrations, lower Ca and SO_4 concentrations, as well as somewhat different deuterium and oxygen-18 compared to the geothermal

Fig. 3.20 Google Earth map showing the location of the Salton Sea, Heber, and Cerro Prieto geothermal fields

fluids moving northwestward. These differences suggest that the northwestern fluids mix with small amounts of low-temperature waters and re-equilibrate with anhydrite at weakly lower temperatures than the northeastern fluids (Adams et al. 1989). Apart from these limited differences, Heber geothermal brines have close to 15,000 mg/kg TDS and low gas contents.

The wells drilled at Cerro Prieto to depths of 1250–3550 m have encountered the same temperature interval of Salton Sea and similar rocks (Reed 1976; Izquierdo et al. 2006). Moreover, the distribution of hydrothermal minerals as a function of temperature compares with that recognized at Salton Sea. In contrast, the reservoir liquids of Cerro Prieto have salinities of 17,000–36,000 mg/kg, which are significantly lower than those of the hypersaline geothermal brines of Salton Sea. The lower salinity of Cerro Prieto reservoir liquids is chiefly controlled by mixing of Colorado River water with seawater evaporated to about six times its initial salinity (Truesdell et al. 1981). During deep circulation, this mixture acquired heat as well as Li, K, Ca, B, SiO_2 and rare alkalis released from rocks, whereas Mg, SO_4, and a minor amount of Na were transferred from the aqueous solution to the rocks. After these processes, the brine was finally diluted to its present interval of temperature and salinity.

3.3.6 *Los Azufres*

The geothermal field of Los Azufres in the Michoacán state, México comprises two distinct production areas, separated by an intermediate zone without surface manifestations (Fig. 3.21). Multiple caldera collapses occurred during pre-Quaternary times in the area of the geothermal field (Ferrari et al. 1991). Based on the evidence provided by deep wells of total depth up to 3600 m, the local stratigraphic sequence includes:

1. Late Miocene to Early Pliocene volcanic rocks, primarily andesitic and basaltic lava flows and breccias, locally interstratified with pyroclastic deposits, and
2. younger rhyodacites, rhyolites, and dacites, which were emplaced between 1 and 0.15 Ma ago (Arellano et al. 2005 and references therein).

In the natural-state, the reservoir hosted a single-phase liquid below 1280 m asl, overlain by a two-phase liquid-dominated region, ranging from 1280 to 1830 m asl, and a two-phase steam-dominated region extending upward to approximately 2400 m asl (Iglesias et al. 1985). The chloride concentrations of the reservoir liquids varied from about 1750–2050 mg/kg.

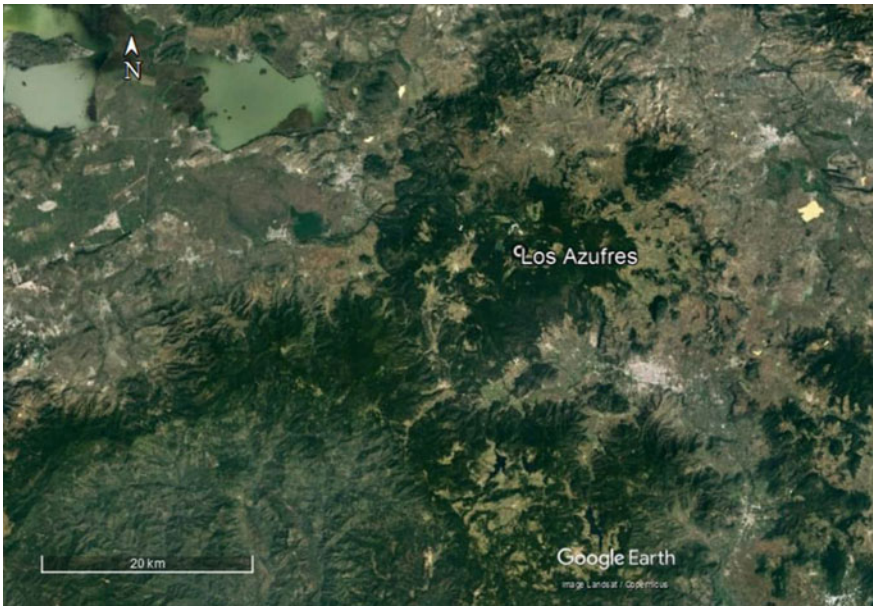

Fig. 3.21 Google Earth map showing the location of the geothermal field of Los Azufres

3.3.7 *Berlin*

The Berlin geothermal field is positioned on the northern slopes of the Berlin-Tecapa volcanic complex (Fig. 3.22). Reservoir rocks consist of altered lava flows and pyroclastics. An elliptical caldera with major axis close to 6–7 km and a 3–4 km wide NNW-SSE trending graben are the main geological features of the area, controlling the circulation, uprising, and migration of geothermal fluids.

The wells used as producers are clustered within an area of about 2 km^2. Reservoir temperatures generally vary from 270 to 305 °C. Deep wells meet neutral chloride waters, with pH of 5.30–6.70, Cl concentration from 3100 to 5600 mg/kg and low SO_4 concentration, 2.5–19 mg/kg, under reservoir conditions.

As observed by D'Amore and Mejia (1999), the isotopic composition of produced fluids is intermediate between that of local meteoric waters recharging the geothermal reservoir and that of injected fluids, because reinjection was carried out since the beginning of production. Consequently, available data are not representative of the natural pre-exploitation condition.

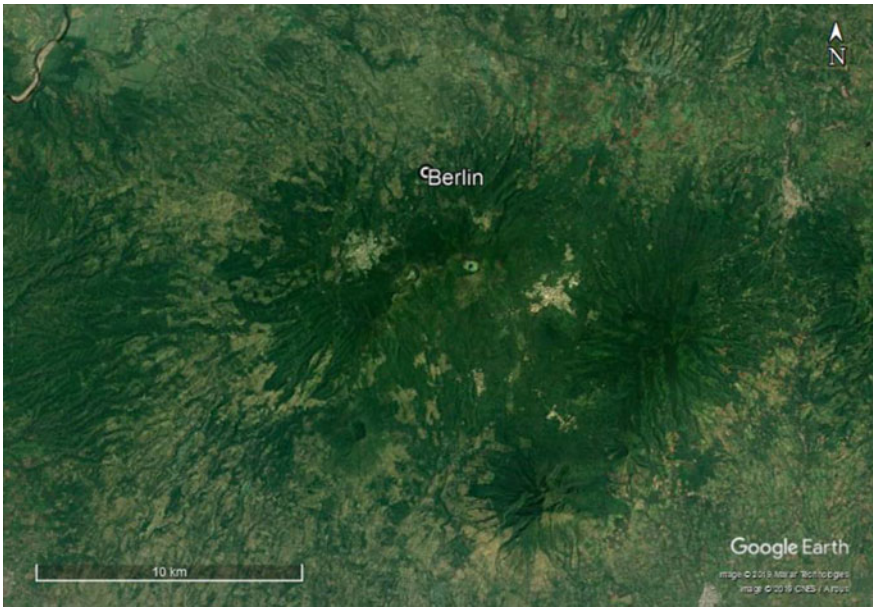

Fig. 3.22 Google Earth map showing the location of the Berlin geothermal field

3.3.8 *Miravalles*

The Miravalles geothermal field extends over an area greater than 21 km^2 on the southwestern flanks of the Miravalles volcano (Fig. 3.23), which belongs to the Guanacaste Cordillera in north-western Costa Rica. The geothermal reservoir is confined within the Guayabo caldera and main production zones are chiefly correlated with andesitic and dacitic lavas.

Reservoir temperatures usually vary from 230 to 240 °C, but the highest measured value is 255 °C. Most deep wells encountered neutral chloride waters, with pH of 5.27–6.31, Cl concentration from 2500 to 3300 mg/kg and low SO_4, 20–70 mg/kg, under reservoir conditions.

However, a few wells located in a small area of the field met acidic liquids, with pH of 2.80–4.05, Cl concentration of 2800–3400 mg/kg, and SO_4 concentration of 360–540 mg/kg, under reservoir conditions. These acid Cl–SO_4 liquids are not considered here because they are close to equilibrium with the hydrothermal minerals of the acid alteration suite (sensu Reyes 1990), including chalcedony, anhydrite, kaolinite (as a proxy of dickite), illite, and alunite (Marini et al. 2003).

Reservoir liquids are produced through mixing of deeply circulating meteoric waters and andesitic (arc-type) magmatic waters, accounting for 80–90% and 10–20%, respectively (Giggenbach and Corrales Soto 1992; Gherardi et al. 2002).

Fig. 3.23 Google Earth map showing the location of the Miravalles geothermal field

3.3.9 *Chemistry of the Reservoir Liquids from the Geothermal Systems in Northern and Central America*

Most reservoir liquids from the geothermal systems in Northern and Central America are located in the [Na] sector of the triangular diagram of main cations (Fig. 3.24). However, 20 of the 23 reservoir liquids from Salton Sea and 1 of the 16 reservoir liquids from Heber are situated in the [Na,Ca] sector. Hence, the prevailing cation in all these aqueous solutions is sodium, although most Salton Sea reservoir liquids have relative Ca concentrations varying from 30 to 39 eq% and one Heber reservoir liquid exhibits a relative Ca concentration of 22 eq%. These enrichments in calcium are expected owing to the high salinity of these aqueous solutions.

In the triangular diagram of major anions (Fig. 3.25) most reservoir liquids are positioned in the [Cl] sector, close to the Cl vertex. Only the reservoir liquids of Dixie Valley and Long Valley are distributed elsewhere, namely in the sectors of [Cl,SO_4], [Cl,HCO_3], and [HCO_3,Cl]. Five distinct chemical facies are recognized on the basis of both triangular diagrams. In detail:

1. The Na–Cl chemical type is by far the most frequent, comprising 235 of the 301 reservoir liquids of interest, that is 78% of the cases. The Na–Cl reservoir liquids come from Coso, Valles, Salton Sea, Heber, Cerro Prieto, Los Azufres, Berlin, and Miravalles.
2. The Na,Ca–Cl chemical facies comprises 21 reservoir liquids (7% of the cases), all proceeding from Salton Sea apart one from Heber.
3. The Na–Cl,SO_4 chemical type groups 34 reservoir liquids (11% of the cases), all coming from Dixie Valley.
4. The Na–Cl,HCO_3 chemical facies includes 7 reservoir liquids (2% of the total), six of which proceed from Long Valley and one from Dixie Valley.

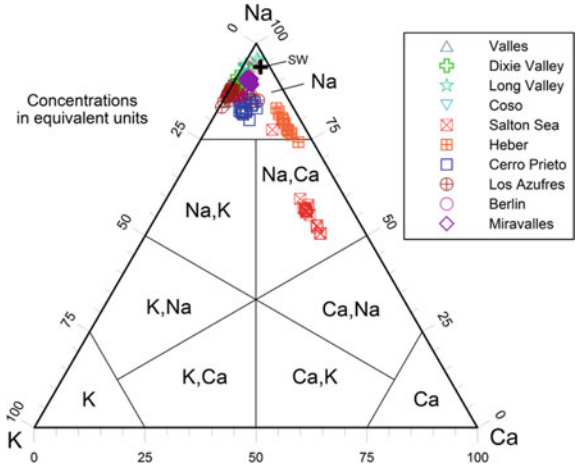

Fig. 3.24 Triangular plot of major cations for the reservoir liquids from the geothermal systems in Northern and Central America. Average seawater is also shown for comparison

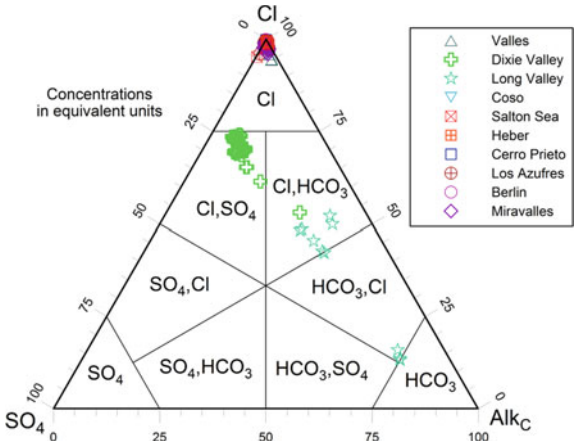

Fig. 3.25 Triangular plot of major anions for the reservoir liquids from the geothermal systems in Northern and Central America

5. The Na–HCO_3,Cl chemical type is represented by 4 reservoir liquids (1% of the total), all coming from Long Valley.

As shown by the binary diagrams of Cl versus $SO_4 + Alk_C$ (Fig. 3.26), the reservoir liquids from the geothermal systems in Northern and Central America distribute over a large range of Σ_{eq}, from the relatively low values of Na–Cl,SO_4, Na–Cl,HCO_3, and Na-HCO_3,Cl waters of Long Valley and Dixie Valley, 31–41 meq/kg (Fig. 3.26c), to the very high values of the Na,Ca–Cl hypersaline geothermal brines from Salton Sea, 6440–9080 meq/kg (Fig. 3.26a). However, most reservoir liquids, all belonging to the Na–Cl chemical type, have intermediate Σ_{eq} values, varying from 100 to 720 meq/kg (Fig. 3.26b). The distinct Σ_{eq} values of the reservoir liquids from the geothermal systems in Northern and Central America are controlled by different sources and processes.

As already recalled above, dissolution of evaporite rocks accounts for the very high Σ_{eq} values of the Na,Ca–Cl hypersaline geothermal brines from Salton Sea (Williams and McKibben 1989) whereas dilution of evaporated seawater explains the origin of the Na–Cl reservoir liquids from Cerro Prieto (Truesdell et al. 1981).

The low Σ_{eq} values of the Long Valley and Dixie Valley reservoir liquids are probably governed by meteoric recharge and rock dissolution sustained by titration of acid gases, chiefly CO_2, whose emission has experienced a considerable increase since 1989 (Farrar et al. 2003 and references therein). The reservoir liquids of Long Valley probably acquire chloride, boron and lithium through rock leaching, but only chloride has conservative behavior, whereas boron and lithium are partly incorporated in alteration minerals (White and Peterson 1991).

The intermediate Σ_{eq} values of the Na–Cl reservoir liquids from the other considered geothermal systems are probably controlled by meteoric recharge, inflow of magmatic fluids and related rock dissolution sustained by titration of acid gases. According to Gherardi et al. (2002), the reservoir liquids of Miravalles are originated through a multi-step process, consistent with the conceptual model of volcanic-hydrothermal systems situated along convergent plate boundaries proposed by

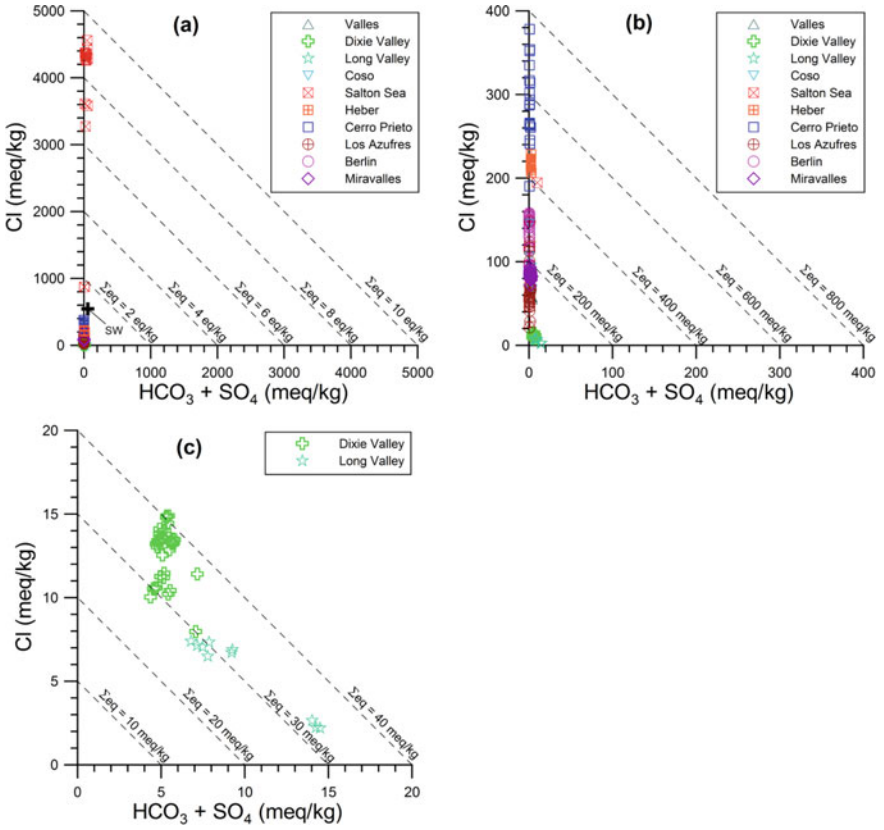

Fig. 3.26 Correlation diagrams of Cl versus $SO_4 + Alk_C$ for the reservoir liquids from the geothermal systems of Northern and Central America. Different Σ_{eq} intervals are considered in the three diagrams **(a)**, **(b)**, and **(c)** in order to accommodate all the liquids of interest

several authors (e.g., Hedenquist 1986; Hedenquist and Lowenstein 1994; Giggenbach 1988, 1997a; Reed 1997). First, magmatic gases (mainly consisting of H_2O, CO_2, SO_2, H_2S and HCl) are absorbed into deep circulating groundwaters of meteoric origin, thus generating acid, relatively oxidized, and highly reactive fluids. Second, these fluids are partly reduced and neutralized through isochemical dissolution of wall rocks in a zone of primary neutralization. Third, further water-rock interaction converts these fluids into neutral Na–Cl waters.

3.4 The Reservoir Liquids from the Geothermal Systems in Japan

The geothermal systems in Japan considered in this work are: Mori-Nigorikawa (data from Yoshida 1991), Sumikawa (data from Ueda et al 1991; Sakai et al. 1993), Uenotai-Wasabizawa (data from Kuriyama 1985; Klein et al. 1991; Naka and Okada 1992; Takeno 2000), Onikobe (data from Truesdell and Nakanishi 2005), Oku-aizu (data from Seki 1990, 1991; Nitta et al. 1991, 1995), Takigami (data from Takenaka and Furuya 1991; Takenaka et al. 1995), Oguni (data from Sasada 1987; Yamada et al. 2000), and Fushime (data from Akaku 1990; Akaku et al. 1991; Okada et al. 2000). The accepted chemical analyses are 21 from Mori-Nigorikawa, 14 from Sumikawa, 4 from Uenotai-Wasabizawa, 7 from Onikobe, 31 from Oku-aizu, 13 from Takigami, 6 from Oguni, and 25 from Fushime, for a total of 121 entries.

3.4.1 Mori-Nigorikawa

The Nigorikawa geothermal field is located in the homonymous caldera and provides fluids to the Mori geothermal power plant (Fig. 3.27). The geochemical characteristics of Nigorikawa fluids summarized here below are from Yoshida (1991).

Fig. 3.27 Google Earth map showing the location of the Nigorikawa geothermal field and the Mori geothermal power plant

Deuterium and oxygen-18 data indicate that the geothermal liquids are mixtures made up of isotopically light meteoric water and isotopically heavy fluids, namely magmatic water and/or altered seawater. Relative He, Ar and N_2 contents suggest that geothermal fluids are mixtures of N_2-rich magmatic gases and air-saturated water. Enthalpy-chloride relations were initially controlled by mixing between deep reservoir liquids and Cl-free steam-heated waters, but reinjection of high-Cl brines has complicated this simple mixing pattern. Calcite scaling was experienced in the early power plant operation and was solved through injection of a scale inhibitor. Stevensite scaling was experienced in well ND-1 and related equipment, probably due to inflow of Mg-rich, low-enthalpy shallow water.

3.4.2 Sumikawa

The characteristics of the Sumikawa geothermal system reported here below are from Ueda et al. (1991) and Ariki et al. (2000). The Sumikawa geothermal field is positioned within a north–south oriented graben. To the south of the field, the graben is crossed by an east–west trending volcanic chain, comprising the Akita-Yake volcano to the west and the Hachimantai volcano to the east. At short distances from Sumikawa there are the geothermal fields of Ohnuma, Kakkonda, and Matsukawa (Fig. 3.28). The last one is the only vapor-dominated geothermal system in Japan.

Subsurface temperature increases progressively southward, that is towards the upflow zone and heat source beneath Akita-Yake, and decreases abruptly northwards, towards the outflow zone. The geothermal reservoir hosts a single liquid phase at depth, overlain by a bi-phase zone whose thickness increases southward.

The deepest Sumikawa wells met temperatures often exceeding 300 °C and neutral Na–Cl liquids. These are diluted by relatively shallow SO_4- and/or HCO_3-rich waters of enthalpy close to 850 kJ/kg heated by conductive heat transfer or steam inflow. Enthalpy-chloride relationships suggest that the Sumikawa Na–Cl parent fluid has an enthalpy of 1300 kJ/kg and chloride concentration of 280 mg/kg. Deuterium and oxygen-18 indicate that reservoir fluids are mainly of meteoric origin and have a small oxygen isotope shift, lower than 2‰ units, which might be attributed to minor contributions of magmatic fluids. This interpretation is supported by relative contents of He, Ar, and N_2 in separated vapors.

Well S-2 is unique having encountered both neutral Na–Cl liquids and acidic SO_4–Cl waters coming from two distinct productive zones at depths of 905 and 1065 m, respectively. Acidic alteration minerals, including alunite and kaolinite, are present close to the deeper feed zone. The acidic fluids are possibly of magmatic origin and are excluded from this compilation.

Fig. 3.28 Google Earth map showing the location of the Sumikawa geothermal field as well as the nearby geothermal fields of Ohnuma, Kakkonda, and Matsukawa

3.4.3 Uenotai-Wasabizawa

The characteristics of the Uenotai geothermal system (Fig. 3.29) presented here below are from Takeno (2000). The Uenotai geothermal system is situated 16 km west of Kurikoma volcano in an area affected by intense faulting. Uenotai was probably a single-phase liquid system in natural state, but exploitation has triggered boiling in a large, central portion of the aquifer, where several wells have excess enthalpy and some wells produce superheated steam. Measured temperatures exceed 300 °C and increase south-eastwards. Enthalpy-chloride relations suggest that reservoir liquids are derived from a deep parent liquid, with chloride concentration close to 700–750 mg/kg and temperature close to 300 °C, through vapor loss, vapor gain, and mixing with shallow vapor condensates.

Although the Wasabizawa geothermal field is situated few kilometers to the south-west of Uenotai, reservoir liquids derive from a distinct parent liquid, with chloride concentration of 1800 mg/kg and enthalpy close to 1300 kJ/kg (Suzuki et al. 2000).

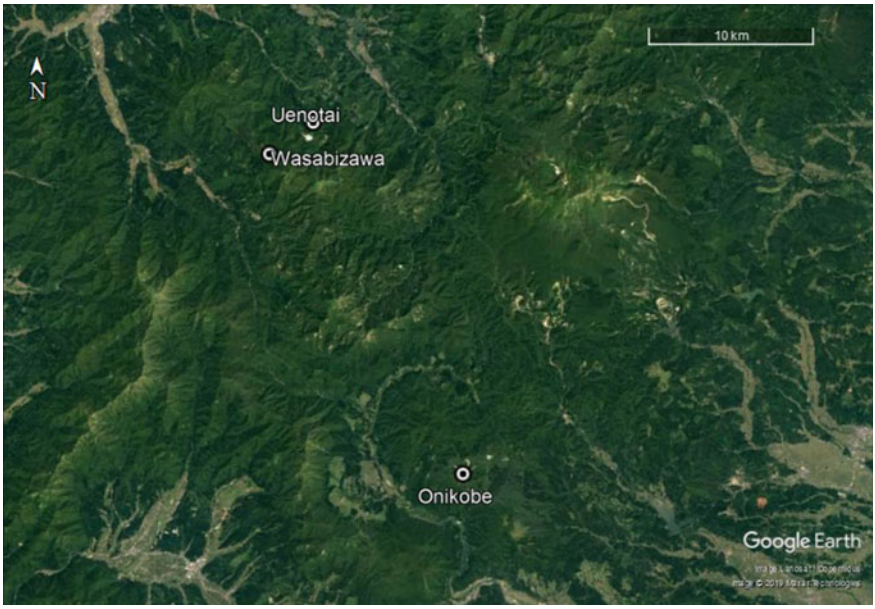

Fig. 3.29 Google Earth map showing the location of the Uenotai-Wasabizawa and Onikobe geothermal fields

3.4.4 Onikobe

The Onikobe geothermal field is located within the homonymous caldera, an elliptical depression with maximum axis close to 10 km, to the south of the Uenotai-Wasabizawa geothermal fields (Fig. 3.29). Seki et al. (1983) report the results obtained by the early mineralogical, petrological, and geochemical investigations performed at Onikobe on core samples collected in several boreholes drilled at depths up to 1352 m as well as temperature logs and chemical analyses of hot springs, waters and vapors discharged from the boreholes, whereas enthalpy data are not given. Unfortunately, these early data do not allow a reliable reconstruction of the chemistry of reservoir fluids.

More recently, Truesdell and Nakanishi (2005) have shown that Onikobe fluids have measured reservoir temperatures varying from 230 to 255 °C, little excess steam (with inlet vapor fraction <0.1), and chloride concentration ranging from 985 to 3920 mg/kg. The largest variations are observed for pH, which ranges from 2.8 to 8.0 for the waters collected at atmospheric pressure. The main acidity source is HCl, but H_2SO_4 could act as subordinate acidity source. Part of the acidity might have been suppressed through dissolution of reservoir rocks and well casings, leading to acquisition of Fe (0.01–371 mg/kg), Mg (0.39–58.3 mg/kg), and Ca (8.4–721 mg/kg). Large variations are observed also for volatile species with pH-dependent volatility, such as H_3BO_3 (from 3.2 to 77.2 mg/kg as B). Re-injected waters enriched in dissolved

solids and depleted in gases are contributing to production fluids. In this work, only the samples not impacted by acidic fluids and related processes were selected, but some Onikobe reservoir liquids might not be representative of the mineral-solution equilibrium condition at aquifer temperatures.

Both deuterium and oxygen-18 values of separated brines discharged from Onikobe wells are inversely correlated with pH, suggesting that the enrichment in heavy isotopes is related to the proportion of unneutralized magmatic water (Pang 2006).

3.4.5 Oku-Aizu

The characteristics of the Oku-aizu geothermal system (Fig. 3.30) reported here below are chiefly from Seki (1991). The Oku-aizu field is located in the "Green Tuff region", which was affected by submarine volcanic activity during the Neogene. The nearest Quaternary volcano, Numazawa, is located 10 km to the west. There, a Plinian eruption occurred about 4600 years BP emitting the Numazawako pumice flow and causing the formation of the 1.5 km × 2 km Numazawako caldera, now largely filled by a lake.

The main feed zones of production wells are at depths of 1000–2600 m, where measured formation temperatures vary from 200 to 350 °C (Nitta et al. 1995). The

Fig. 3.30 Google Earth map showing the location of the Oku-aizu geothermal field

Oku-aizu geothermal aquifer is considered to have experienced little boiling in its natural state before the beginning of production. However, due to the pressure drop induced by exploitation, reservoir boiling occurred close to the geothermal wells. Therefore, most wells show excess enthalpy and their discharge enthalpy increases progressively with time, suggesting extension of the boiling front around the wells into the reservoir. As a consequence of steam separation in the aquifer, the total discharge composition is rarely representative of the reservoir liquid chemistry prior to boiling (Seki 1990).

The steam separated at 6.5 bar contains 2–10 vol.% of non-condensable gases, mostly CO_2 (95–99 vol.%) and H_2S (0.1–4 vol.%). The brine separated at atmospheric pressure has the second highest salinities of the geothermal systems in Japan after Fushime, with chloride concentrations of 5300 to 22,000 mg/kg, sodium concentrations of 2700–10,600 mg/kg, and lower but significant contents of potassium (180–2550 mg/kg), calcium (26–1750 mg/kg), and silica (440–1010 mg/kg). A peculiarity of the Oku-aizu reservoir liquids is the high manganese concentrations, up to 420 mg/kg, and the appreciable contents of Cu, Zn, and Pb. Consequently, sulfide scales were found on the casing wall of well 84N-2t, and in the two-phase line of well 87N-15T (Seki 1991; Nitta et al. 1991).

According to the calculations performed by Seki using the chemical speciation code PECS, reservoir liquids are expected to have pH ranging from 4.1 to 5.5, in substantial agreement with the results obtained in this work using WATCH.

Enthalpy-chloride relations indicate that the deep parent fluid (1) has temperature close to 320 °C and chloride concentration of 11,500 mg/kg and (2) mixes with a shallower water with nil to negligible chloride content and temperature less than 200 °C, heated by conductive heat transfer and/or steam inflow.

Deuterium versus oxygen-18 relationships suggest that the Oku-aizu reservoir liquids are produced by mixing of meteoric waters with either arc-type magmatic water or fossil seawater.

3.4.6 Takigami

This brief synthesis on Takigami is based on Takenaka and Furuya (1991) and Furuya et al. (2000). The Takigami geothermal field is located northeast of the Hatchobaru geothermal field at a distance of about 15 km (Fig. 3.31). The Takigami geothermal reservoir comprises two distinct portions. The south-western portion is deeper, with elevations of −1500 to −600 m asl, lower permeability and higher temperatures, from 230 to 260 °C, whereas the north-eastern portion is shallower, with elevations of −600 to 0 m asl, has high secondary permeability and temperatures of 160–210 °C. The reservoir liquids of the south-western reservoir have relatively high chloride concentrations and comparatively low sulfate concentrations. In contrast, the reservoir liquids of the north-eastern reservoir have relatively low chloride concentrations and comparatively high sulfate concentrations. These findings indicate the upflow of a hot, chloride-rich, sulfate-poor fluid in the southwest, which is gradually cooled

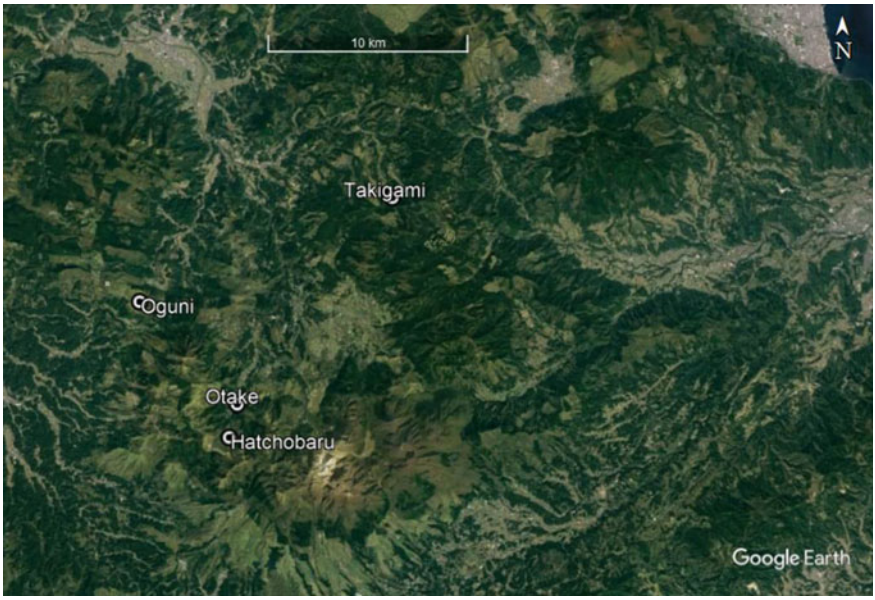

Fig. 3.31 Google Earth map showing the location of the Takigami and Oguni geothermal fields. Also shown are the nearby geothermal fields of Otake and Hatchobaru

as it flows northeast through mixing with shallow chloride-poor, sulfate-rich waters of temperature close to 100 °C. The mixing trend is clearly recognizable in the enthalpy-chloride diagram, which leads to exclude occurrence of boiling, and in the chloride plot of boron, owing to the conservative behaviour of both Cl and B. In contrast, considerable deviations from the mixing trend are observed in the chloride plots of other chemical components, which are evidently controlled by water-rock interaction and possible attainment of equilibrium between the aqueous solution and hydrothermal minerals, including anhydrite and calcite (Chiba 1991). Deuterium and oxygen-18 indicate that the Takigami geothermal fluids derive from meteoric waters.

3.4.7 Oguni

The main features of the Oguni geothermal system (Fig. 3.31) reported here below are from Abe et al. (1995). Oguni is located in the Hohi region, together with the geothermal fields of Takigami (see above), Hatchobaru (supplying steam to the main geothermal power plant in Japan), and Otake. The central part of the Oguni geothermal field is crossed by the northwest to southeast striking Takenoyu fault and related parallel faults forming altogether a nearly vertical high-permeability zone of several hundred meters in width. The wells drilled in this fault zone (e.g., GH-10, GH-11, GH-12, and GH-20) encountered the hottest, undiluted reservoir fluids with

temperatures of 240–250 °C and chloride concentrations of 1050–1150 mg/kg. Wells drilled elsewhere (e.g., wells BS-3 and DY-1) met diluted, cooler reservoir fluids.

The Oguni geothermal reservoir is composed by two different parts, separated by a nearly vertical impermeable zone situated to the south of the Takenoyu fault. Both reservoirs hosts relatively similar neutral Na–Cl fluids with low concentrations of non-condensable gases. Carbonate scaling occurs in some production wells.

3.4.8 Fushime

The brief synthesis given here below on the Fushime geothermal field (Fig. 3.32) is based on Akaku et al. (1991). The geothermal system comprises: (1) a shallow hot zone in the upper 800 m, with temperatures up to 240 °C and (2) a deep hot zone, at depths greater than 1200 m, with temperatures between 300 and 360 °C. These two hot zones are separated by a cooler zone, marked by strong inversions in temperature profiles, at intermediate depths.

Since the temperatures in the deep production zone lie close to the boiling point curve, discharge-induced depressurization triggers boiling in the deep production zone, with development of excess enthalpy conditions in most Fushime wells.

The reservoir fluids have high salinity and maximum C1 concentration similar to the seawater value. Moreover, they are depleted in Mg and SO_4, but are enriched in

Fig. 3.32 Google Earth map showing the location of the Fushime geothermal field

several chemical components (e.g., SiO_2, K, Ca, Fe, Mn, Zn, and Pb) with respect to seawater, indicating that the reservoir fluids are generated through high-temperature seawater-rock interaction.

Chloride-enthalpy relationships suggest the occurrence of steam loss, steam gain, and dilution of reservoir liquids. The latter process probably involves the cold groundwaters overlying the geothermal system. The parent water has temperature of 330 °C and chloride concentration of 17,000 mg/kg.

The variations in K and Ca concentrations of reservoir fluids suggest occurrence of both (1) precipitation of K-bearing hydrothermal minerals, most likely K-feldspar and sericite, which are abundant around the feed zones of the Fushime wells, and (2) dissolution of at least one Ca-bearing mineral, probably anhydrite, which is also present close to the feed zones of the Fushime wells.

3.4.9 Chemistry of the Reservoir Liquids from the Geothermal Systems in Japan

The majority of the reservoir liquids from the geothermal systems in Japan (that is 104 of the 121 entries) are situated in the [Na] sector of the triangular diagram of major cations (Fig. 3.33). However, there are 17 exceptions, comprising 15 reservoir liquids from Oku-aizu, Onikobe, and Fushime which are located in the [Na,Ca] sector and 2 reservoir liquids from Oku-aizu which are positioned in the [Na,K] sector. Therefore, sodium is the prevailing cation in all these aqueous solutions, although calcium and/or potassium are significant in some cases.

In the triangular diagram of main anions (Fig. 3.34) most reservoir liquids are located in the [Cl] sector, and several are very close to the chloride vertex. Only some reservoir liquids of Takigami and Sumikawa are situated in the [Cl,SO_4] sector.

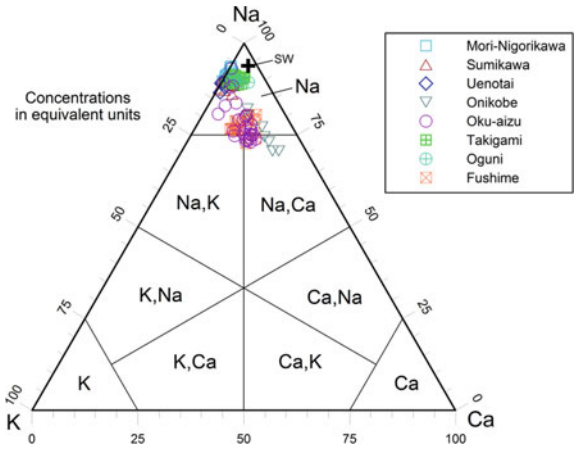

Fig. 3.33 Triangular plot of major cations for the reservoir liquids from the geothermal systems in Japan. Average seawater is also shown for comparison

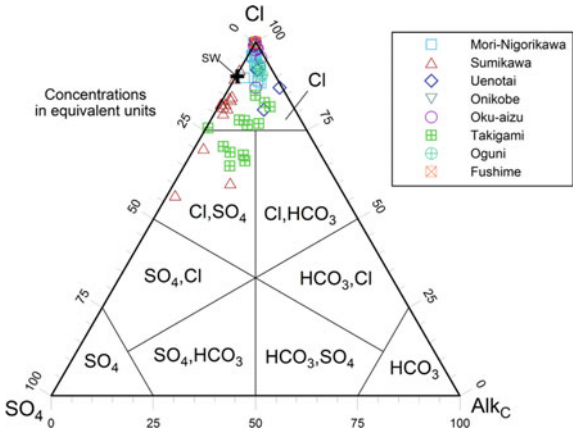

Fig. 3.34 Triangular plot of major anions for the reservoir liquids from the geothermal systems in Japan. Average seawater is also shown for comparison

Based on both triangular diagrams, it is possible to recognize four different chemical facies. In detail:

1. The Na–Cl chemical facies is by far the most common, comprising 96 of the 121 reservoir liquids of interest, that is 79% of the entries. Moreover, the Na–Cl reservoir liquids are found in all the geothermal systems in Japan.
2. The Na,Ca–Cl chemical type includes 15 reservoir liquids (12% of the cases), proceeding from Oku-aizu, Onikobe, and Fushime.
3. The Na,K–Cl chemical type is represented by 2 reservoir liquids only (2% of the total), both from Oku-aizu.
4. The Na–Cl,SO_4 chemical type groups 8 reservoir liquids (7% of the cases), coming from Takigami and Sumikawa.

The reservoir liquids from the geothermal systems in Japan span a large interval of Σ_{eq} (Fig. 3.35). Low to relatively low Σ_{eq} values are encountered at Sumikawa, 12–43 meq/kg, Takigami, 36–41 meq/kg, Oguni, 52–67 meq/kg, and Uenotai, 12–29 meq/kg, apart from the Wasabizawa well N57-T0-3 which has Σ_{eq} of 95 meq/kg. The reservoir liquids of Fushime exhibit the highest Σ_{eq} values, varying from 612 to 1190 meq/kg, whereas intermediate Σ_{eq} values are found in the geothermal systems of Oku-aizu (118–789 meq/kg), Mori-Nigorikawa (243–509 meq/kg), and Onikobe (74–166 meq/kg).

The distinct Σ_{eq} values of the reservoir liquids from the geothermal systems in Japan are governed by different processes and sources. As already noted above, the highest Σ_{eq} values of Fushime are similar to that of seawater (Fig. 3.35a), which recharges the deep reservoir of this geothermal system. In contrast, the low Σ_{eq} values of the reservoir liquids of Sumikawa, Takigami, Oguni, and Uenotai (Fig. 3.35b) are probably controlled by the prevailingly meteoric recharge and by the occurrence of limited rock dissolution processes sustained by titration of acid gases.

The intermediate Σ_{eq} values of the reservoir fluids of Oku-aizu and Mori-Nigorikawa (Fig. 3.35a) are ascribable to a mixed recharge, with significant contributions of meteoric water as well as of Cl-rich magmatic waters and/or fossil/altered

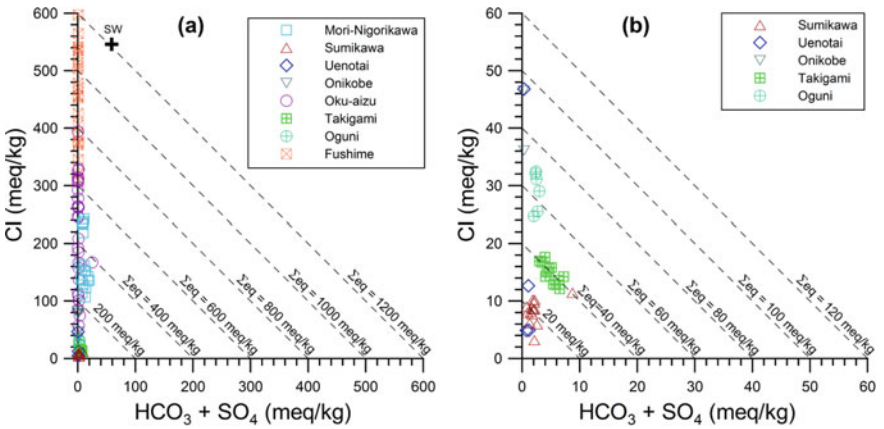

Fig. 3.35 Correlation diagrams of Cl versus $SO_4 + Alk_C$ for the reservoir liquids from the geothermal systems of Japan. Different Σ_{eq} intervals are considered in the two diagrams **(a)** and **(b)** to accommodate all the liquids of interest

seawater, as indicated by deuterium and oxygen-18 data (see above). In both sites, a further supply of solutes is provided by rock dissolution sustained by titration of acid gases. The Onikobe geothermal reservoir is recharged by both meteoric waters and magmatic fluids. The acidity of these meteoric-magmatic fluids is partly titrated through dissolution of reservoir rocks and well casings (see above).

3.5 The Reservoir Liquids from the Geothermal Systems in the Philippines

The geothermal systems in the Philippines taken into account in this work are: Bacon-Manito (data from Ruaya et al. 1995; See 1995), Tongonan-Mahanagdong (data from Baltasar 1980; Balmes 1994; Angcoy 2010), Alto Peak (data from Reyes et al. 1993), and Palinpinon (data from Jordan 1982; Rae 2002). The accepted chemical analyses are 51 from Bacon-Manito, 39 from Tongonan-Mahanagdong, 27 from Alto Peak, and 29 from Palinpinon, for a total of 146 entries.

3.5.1 Bacon-Manito

The Bacon-Manito (Bacman) geothermal field is situated in the southwestern portion of the Luzon Island, along the volcanic chain of the Bicol Arc, between the two active volcanoes Bulusan, which is found 30 km to the SSE, and Mayon, which is located 30 km to the NW (Fig. 3.36).

Fig. 3.36 Google Earth map showing the location of the Bacon-Manito geothermal field

The deepest and hottest reservoir fluid has a Cl concentration of 8000 ± 500 mg/kg and a temperature of 325 °C (Ruaya et al. 1995). It is probably produced through mixing between Cl-poor meteoric waters and Cl-rich (15,000–18,000 mg/kg Cl) arc-type (andesitic) magmatic waters, with contributions of 50–60% and 40–50%, respectively. Steam loss, steam gain, and mixing with both steam condensates and shallow groundwaters cause large changes in Cl concentration, which spans the 1500–8700 mg/kg range. Sulfate concentration varies from 5 to 35 mg/kg in most neutral chloride liquids but attains 107 mg/kg in one sample of well Pal-2D. Sulfate concentration is higher in the acid fluid discharges of wells Pal-2D, CN-2D, and CN3RD, which are disregarded in this work, being not representative of the equilibrium condition with the typical hydrothermal minerals of the neutral alteration suite (sensu Reyes 1990).

3.5.2 Tongonan-Mahanagdong

The Greater Tongonan geothermal field is positioned on Leyte Island, along a Tertiary north-west/south-east trending volcanic arc related to the Philippine fault zone. The Greater Tongonan geothermal field comprises the Tongonan geothermal field in the north and the Mahanagdong geothermal field in the south (Fig. 3.37). The two geothermal fields are probably separated by a cold impermeable block

Fig. 3.37 Google Earth map showing the location of the Tongonan-Mahanagdong and Alto Peak geothermal fields

(Angcoy 2010). Many wells have excess enthalpy due to contribution of steam from a two-phase zone situated above the deep single-phase liquid zone.

In the Tongonan geothermal field, wells discharge neutral Na–Cl waters with reservoir chloride concentrations usually ranging from 6200 to 11,000 mg/kg, whereas the temperatures measured in the main production zones before discharge vary from 280 to 314 °C (Baltasar 1980).

The reservoir liquids of the Mahanagdong geothermal field are originated from a parent fluid with quartz temperature of ~300 °C, chloride concentration of ~4000 mg/kg, and $\delta^{18}O$ of −1.0‰, representing the isotopically richest value (Angcoy 2010). Close to the main outflow zone in the southeast, reservoir liquids have quartz temperature of 260–280 °C, chloride concentration of 2000–3000 mg/kg and $\delta^{18}O$ values of −2.0 to −3.0‰. The northern part of the reservoir hosts acid Cl–SO_4 waters with chloride concentrations and $\delta^{18}O$ values similar to the wells in the upflow zone, but with high concentrations of sulfate (>100 mg/kg), iron (>10 mg/kg) and magnesium (>5 mg/kg).

The geothermal fluids of both Tongonan and Mahanagdong are produced through mixing of local meteoric waters and arc-type magmatic water (Alvis-Isidro et al. 1993).

3.5.3 Alto Peak

The Alto Peak geothermal field is situated on Leyte Island to the south-east of Tongonan-Mahanagdong (Fig. 3.37). On the basis of the evidence provided by hydrothermal mineral petrology and the chemical characteristics of both fluid inclusions and fluids discharged from five deep wells, Reyes et al. (1993) postulated that the Alto Peak geothermal system comprises vapor-dominated and liquid-dominated sectors.

A gas-rich vapor phase, with CO_2 concentrations of 1.1–5.6 mol/kg, occupies the central core or chimney with a diameter of ~1 km and a height of ~3 km, connecting more extensive, very high temperature vapor-dominated zones at depth to a shallow zone occupied by steam-heated ground-waters. The central core is surrounded by a geothermal aquifer hosting neutral Na–Cl waters, with chloride concentration close to 7000 mg/kg and temperatures between 250 and 350 °C. Two-phase zones, increasingly wider with increasing depth and hosting fluid mixtures of highly variable compositions, are interposed between the vapor-dominated central chimney and the surrounding liquid-dominated zone.

Based on this distribution of fluids within the Alto Peak geothermal system, the changes with time in the composition of the well discharges is ascribable to the entrainment of variable amounts of fluids hosted in the liquid- and vapor-dominated zones crossed by the wells.

Most neutral Na–Cl waters of relatively low temperature were probably generated during an earlier phase in the evolution of the Alto Peak geothermal system, whereas the fluids at temperatures >300 °C and the hydrothermal, magmatic-hydrothermal, and contact-metamorphism alteration minerals encountered in wells AP-1D and AP-2D may be explained in terms of re-heating caused by recent emplacement of magma batches at shallow depths. The deuterium and oxygen-18 of well discharges suggest that they are mixtures made up of 40 to 50% of arc-type magmatic water and 60–50% of local groundwaters.

3.5.4 Palinpinon

The Palinpinon liquid-dominated, high-temperature geothermal system is located on Negros Island (Rae 2002; Rae et al. 2011 and references therein). The geothermal field is producing from two distinct sectors: one is called Puhagan, is situated in the central part of the field, and corresponds to the upflow zone; the other sector is known as Nasuji-Sogongon and is positioned in the south-west, where one of the two outflow zones is found (Fig. 3.38). The other outflow zone occurs to the north-east. The Palinpinon production wells cross multiple zones of permeability and discharge two-phase fluids. Measured down-hole temperatures vary from 220 to over 300 °C, with the highest temperature, 329 °C, measured at 1925 m below sea level in well PN20D. Most Palinpinon wells discharge typical neutral to slightly

Fig. 3.38 Google Earth map showing the location of the Palinpinon geothermal field. The place cards P, S, and N identify the Puhagan, Sogongon, and Nasuji sectors, respectively

alkaline chloride liquids with Cl < 7200 mg/kg and substantial concentrations of silica, sodium, potassium, and boron. These chloride liquids are produced from a parent reservoir liquid with Cl close to 4000 mg/kg and temperature of 328 °C through variable combinations of mixing, boiling, and/or conductive cooling. Mixed acid sulfate-chloride waters are discharged by some wells drilled to the south in the Nasuji-Sogongon production area, but are not considered in this work.

3.5.5 Chemistry of the Reservoir Liquids from the Geothermal Systems in the Philippines

Sodium is the prevailing cation in all the reservoir liquids from the geothermal systems in the Philippines, being all located in the [Na] sector of the triangular plot of major cations (Fig. 3.39).

In the triangular diagram of main anions (Fig. 3.40) all the reservoir liquids of interest except one are situated in the [Cl] sector, indicating that chloride is the dominant anion in all the samples apart from that collected in 2009 from well MG32D of Mahanagdong and identified by code MG32D_09. This sample is unique, being located in the [SO_4,Cl] sector.

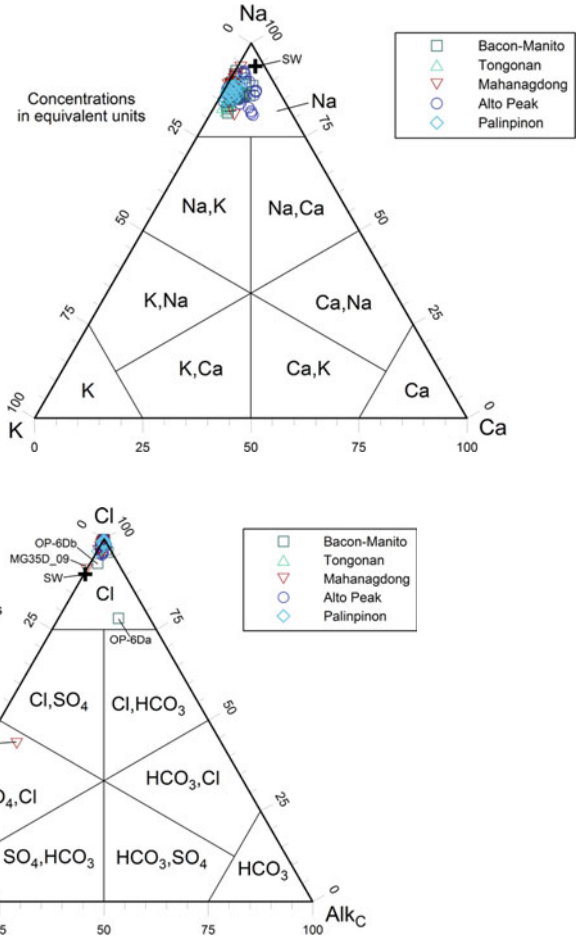

Fig. 3.39 Triangular plot of major cations for the reservoir liquids from the geothermal systems in the Philippines. Average seawater is also shown for comparison

Fig. 3.40 Triangular plot of major anions for the reservoir liquids from the geothermal systems in the Philippines. Average seawater is also shown for comparison

Moreover, all the Cl-rich reservoir liquids are positioned close to the chloride vertex, with the sole exception of the sample collected on 14/02/1991 from well OP-6D of Bacon-Manito (code OP-6 Da), which has unusually high relative contents of HCO_3, 14.4 eq%, and SO_4, 7.5 eq%, as well as an abnormally low relative content of Cl, 78.1 eq%, compared to the other Cl-rich reservoir liquids.

On the basis of the evidence provided by both triangular diagrams, all the reservoir liquids of interest belong to the Na–Cl chemical facies, apart from sample MG32D_09 which has Na–SO_4,Cl composition.

The reservoir liquids from the geothermal systems in the Philippines span a relatively wide interval of Σ_{eq}, from the 25 meq/kg of sample OP-6 Da of Bacon-Manito to the 600–620 meq/kg of the two samples collected from well 407 of Tongonan

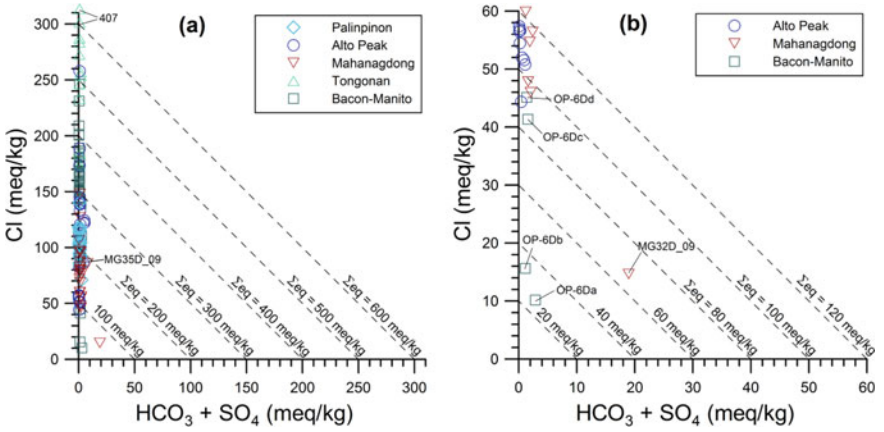

Fig. 3.41 Correlation diagrams of Cl versus SO_4 + Alk_C for the reservoir liquids from the geothermal systems in the Philippines. Different Σ_{eq} intervals are considered in the two diagrams **(a)** and **(b)** in order to accommodate all the liquids of interest

(Fig. 3.41). In addition to sample OP-6 Da, also the other three samples from well OP-6D have low Σ_{eq} values, namely 33, 84, and 95 meq/kg. Considering the total discharge enthalpy of well OP6D, ~2450 kJ/kg, the low salinities of these four samples may be due to improper liquid/vapor separation during sampling, with entrainment of vapor in the liquid phase. Similar considerations apply to sample MG32D_09 which has Σ_{eq} of 69 meq/kg and discharge enthalpy of ~2400 kJ/kg. Even if these samples are potentially not representative of reservoir liquids, they are kept in the following discussion to ascertain whether the geochemical techniques of interest are applicable or not.

Apart from these five unusual aqueous solutions, the Σ_{eq} values in the range 100–600 meq/kg of most reservoir fluids from the geothermal systems in the Philippines can be explained by mixing, in variable proportions, of Cl-poor meteoric waters and Cl-rich magmatic waters, as indicated by deuterium and oxygen-18 data (see above). Moreover, a further contribution of solutes is provided by rock dissolution sustained by titration of acid gases.

3.6 The Reservoir Liquids from the Geothermal Systems in New Zealand

All the high-temperature geothermal systems in New Zealand are located in the Taupo Volcanic Zone, TVZ (Fig. 3.42), apart from Ngawha which is situated in the Northland Peninsula (Fig. 3.43).

The geothermal systems of the TVZ were divided into arc- and rift-types by Giggenbach (1995), based on both the chemical and isotopic characteristics of gases

Fig. 3.42 Google Earth map showing the location of the geothermal fields of Wairakei, Rotokawa, Mokai, Ngatamariki, Broadlands-Ohaaki, Orakeikorako, Waiotapu, Rotorua, and Kawerau situated to the north-east of Lake Taupo

Fig. 3.43 Google Earth map showing the location of the Ngawha geothermal field

and waters discharged from hot springs and geothermal wells, namely the relative Cl, B, Li and Cs contents, the $CO_2/^3He$ and N_2/Ar ratios, and the δ^2H and $\delta^{18}O$ values of H_2O. The reservoir fluids of the systems along the Eastern side of the TVZ, such as Kawerau, Broadlands-Ohaaki and Rotokawa, are affected by addition of volatiles from subducted sediments and are richer in magmatic components than the fluids from the systems along the Western side of the TVZ, such as Wairakei and Mokai, which are similar to mantle-derived fluids. To corroborate his analysis, Giggenbach (1995) provided a number of data on the vapor and liquid phases discharged from the geothermal wells of Broadlands-Ohaaki, Kawerau, Mokai, Ngatamariki, Rotokawa, and Wairakei. These Giggenbach's data are considered in this work together with those produced by Mahon and Finlayson (1972), Hedenquist (1990) and Christenson et al. (2002) for Broadlands-Ohaaki, Chambefort et al. (2016) for Ngatamariki, Sheppard and Giggenbach (1980) and Sheppard (1984) for Ngawha, Sheppard and Lyon (1984) for Orakeikorako, Krupp and Seward (1987) and Reyes et al. (2003) for Rotokawa, Hedenquist and Browne (1989) for Waiotapu, and Truesdell and Singers (1974), Bruton (1995), Stefansson and Arnórsson (2000), and Clearwater et al. (2015) for Wairakei. The accepted chemical analyses are 41 from Broadlands-Ohaaki, 4 from Kawerau, 4 from Mokai, 7 from Ngatamariki, 12 from Ngawha, 1 from Orakeikorako, 9 from Rotokawa, 6 from Waiotapu, and 9 from Wairakei, for a total of 93 entries.

3.6.1 Broadlands-Ohaaki

This brief synthesis on the Broadlands-Ohaaki geothermal system (location in Fig. 3.42) is based on Hedenquist (1990) and Christenson et al. (2002). The geological framework of the Broadlands-Ohaaki field comprises a thick sequence of volcanic rocks resting unconformably onto the greywackes and argillites of the Mesozoic basement. Faulting affects the basement rocks causing local discontinuities and large changes in the elevation of the basement top but does not extend significantly into the overlying volcanic rocks which show, in general, good lateral continuity. Fluid circulation appears to be controlled by fractures and faults in the basement, whereas it occurs through inherently permeable rocks and formation contacts in the volcanic sequence. The geothermal system is characterized by the presence of two distinct upflow zones of reservoir fluids, both controlled by fault structures cutting the greywackes of the Mesozoic basement.

Both upflow zones have comparable salinity, but the fluids of the eastern upflow zone are enriched in B and F compared to those of the western upflow zone. The deep reservoir fluids originate from a parent (preboiled) fluid with a temperature of ~300 °C and a CO_2 content of ~2.6% by weight. Boiling is common in both upflow zones as indicated by the chemical characteristics of reservoir fluids and measured temperatures. CO_2-rich steam-heated waters are present above the boiling zones and on the margins of the system, where they dilute the deep chloride fluids. The main thermal manifestation is the Ohaaki pool, discharging neutral chloride water at 95 °C

and contributing about 10 MWt to the total natural heat flow from the system, which is estimated at ~100 MWt. Surface manifestations comprise a few warm springs on the banks of the Waikato River and some steaming grounds, with subsurface seepages also contributing to the natural heat flow. Exploration wells at depths varying from 366 to 2587 m were drilled in 1965 -1984. Temperatures of 260 ± 20 °C were measured in the feed zones of production wells.

3.6.2 Kawerau

The geological framework of the Kawerau field (location in Fig. 3.42) comprises a >1 km thick sequence of volcanic products resting unconformably onto the Mesozoic greywacke complex (Christenson 1997 and references therein). Permeability is fault- and fracture-controlled within both the greywackes and the overlying volcanics. Lacustrine and marine sediments act as discontinuous aquicludes in the volcanic sequence. Reservoir fluids flow up through steeply dipping normal faults from the greywackes into the overlying volcanic rocks, where they spread laterally entering distinct productive aquifer levels.

The chemical characteristics of the reservoir fluids circulating in both the greywackes and the volcanic rocks are affected by both boiling and dilution. Pressure draw-down and inflow of cold fluids from the marginal recharge have been induced by production from volcanic rocks whereas production from fractured greywackes has been generally stable with time. Boiling prompted by production has caused calcite scaling in boreholes and locally in reservoir rocks. The surface manifestations include steaming grounds and neutral to acid pools, springs and seeps. Reservoir fluids are close to boiling and attains temperatures >315 °C. Shallow reservoir fluids are affected by steam heating as indicated by the high concentrations of HCO_3 and/or SO_4 and slightly to strongly acidic pH, whereas the deep reservoir fluids are of the near-neutral chloride-type and gas-rich. The base fluid has estimated Cl concentration of 925 mg/kg and gas content of 2.8% by weight.

3.6.3 Mokai

This brief account on Mokai geothermal field (location in Fig. 3.42) is based on Henley and Middendorf (1985), Henley and Plum (1985), and Hedenquist et al. (1990). Six exploration wells were drilled in the Mokai field at depths of 600–2800 m. Different volcanic units (from top to bottom: shallow ignimbrites, rhyolitic domes, deep ignimbrites and tuffs) were crossed by the wells but the Mesozoic greywacke basement was not attained. Measured maximum temperatures are in the interval 194–323 °C. The first well, MK1, was drilled to a depth of 606 m and found a maximum temperature of 194 °C above a temperature inversion. Temperatures in the range 250–278 °C were measured in the main circulation loss zone of well MK2 (total

depth 1654 m) before and during discharge. High temperatures were also found in wells MK3 (total depth 1678 m) and MK5 (total depth 2592 m) up to 305 and 298 °C, respectively. Down-hole measurements indicate considerable cooling of the system close to well MK4 probably due to inflow of cooler waters. The natural heat discharge through the steam-heated thermal manifestations located within the drilled area in the Mokai field (one large fumarole, steaming grounds, acid-sulfate mud pools, and a few neutral-pH steam-heated pools) is very small, with 6 MWt only. However, a natural thermal flux of at least 80 MWt is related to the dilute chloride springs, with temperatures up to 67 °C, which are distributed in a fault-controlled gorge, 6–10 km NNE of the drilled area in the Mokai field. Hence, the upflow zone of the Mokai geothermal system is located to the south, but the major component of the surface discharge of thermal fluids is displaced to the north, largely because of the northerly hydraulic gradient of >300 m over a distance of 12 km. During this northwards travel, the deep-upflow chloride fluids are progressively diluted by addition of cold groundwater. The deep undiluted parent fluid has estimated temperature of 335 °C, chloride concentration of 2050 mg/kg, and low gas content, similar to that of Wairakei fluids.

3.6.4 Ngatamariki

The current knowledge and understanding of the Ngatamariki geothermal field (location in Fig. 3.42) has been presented by Chambefort et al. (2016). At Ngatamariki the greywackes of the Mesozoic basement have been reached only by well NM6 at a depth of ~3.4 km. They are covered by a thick sequence of volcanic and sedimentary rocks which have been attributed to different stratigraphic units. An intrusive complex, comprising a microdiorite, a quartz-diorite and a tonalite, has been encountered in wells NM4, NM8, and NM9 at depths >2.4 km approximately. The Ngatamariki geothermal system comprises a deep geothermal reservoir at temperatures of 260–285 °C covered by a clay-cap which is overlain by two separate shallow aquifers.

The fluid circulating in the Ngatamariki reservoir has Na–Cl composition, Cl concentration of 900–1000 mg/kg, near neutral pH, ~6, and low gas content, ~0.3% by weight. The reservoir fluid is chiefly made up of meteoric water with a limited contribution of magmatic water. Most natural manifestations discharge mixed chloride-bicarbonate waters with low SO_4 and slightly alkaline pH. However, 10–15 L/s of chloride waters are discharged by the most important hot spring, the South One pool, which has a surface area of ~1000 m^2. This spring is hosted into the vent of the hydrothermal eruption which occurred in 2005. Sinter is deposited by the hot spring waters in several sites. The natural background thermal flux is estimated at 40 MWt.

3.6.5 Ngawha

The Ngawha geothermal field is situated in the Northland Peninsula (Fig. 3.43). The geothermal reservoir is hosted in quartz-feldspathic greywackes and argillites, which have low inherent permeability and porosity close to zero (Cox and Browne 1998). Locally, faults and joints enhance rock permeability creating the conditions needed for the circulation of reservoir fluids which move within a myriad of joint channels interconnected in three dimensions (Browne 1980). The cap-rock overlying the geothermal reservoir is represented by a 500–600 m thick sequence of low-permeability marine sediments.

The Ngawha reservoir fluids are of neutral Na–Cl type but have unusually high concentrations of HCO_3, B, and NH_4 as well as high gas contents, of which 95% is CO_2. Boron isotope data suggest that high B concentrations are the result of rock leaching under low water/rock ratios in the capped hydrothermal system (Aggarwal et al. 2003).

The large oxygen isotope shift of Ngawha geothermal fluids, 11‰ units, was attributed to isotope exchange with the local rocks assuming either a low water/rock ratio or a very young age for the system, but without any involvement of magmatic waters (Aggarwal et al. 2003 and references therein).

3.6.6 Orakeikorako

The Orakeikorako geothermal system (location in Fig. 3.42) is situated at the south-western termination of the Paeroa Fault and might be associated to the adjacent Te Kopia geothermal system. In the mid 1960s, the four exploration wells OK-1, OK-2, OK-4 and OK6 were drilled at Orakeikorako outside the area of hot spring activity (Simpson and Bignall 2016 and references therein). These wells reached depths of 1155–1404 m, found a maximum temperature of 265 °C, but poor permeability conditions. About ¾ of the Orakeikorako natural manifestations, including many spectacular geysers, were submerged by the damming of the Waikato River in 1961 for hydroelectric power production. Today, the Orakeikorako natural manifestations consist of hot springs, geysers, minor steaming grounds, and few mud pools and cover an area of ~1.8 km^2 mainly on the eastern bank of the Waikato River. The discharged fluids have generated the Umukuri sinter, which is the most extensive deposit of this type in the TVZ, with an area close to 1 km^2, and is locally up to 18 m thick. The natural heat flow is estimated at 340 MWt.

3.6.7 Rotokawa

Similar to the other geothermal systems of the TVZ, the Rotokawa system (location in Fig. 3.42) is hosted into a sequence of Pleistocene and Recent volcanic rocks and the underlying Mesozoic greywacke basement. At least thirteen different hydrothermal explosion breccia have been recognized in surface outcrops. The largest crater is 1.5 km in diameter, was formed by a hydrothermal eruption which occurred ~6060 a ago, and is currently occupied by Lake Rotokawa, whose waters have pH close to 2. Between 1965 and 2010, a total of 31 geothermal wells have been drilled at Rotokawa reaching depths between 2500 and 3000 m. Thirteen of these wells have been drilled in 2007–2010 (Price et al. 2011). As proposed by Winick et al. (2009), the Rotokawa geothermal system comprises three main aquifers, namely the shallow aquifer, the intermediate aquifer and the deep reservoir.

Neutral-chloride waters, with Cl concentrations of 450–850 mg/kg and temperatures of 300–340 °C, circulate in the deep reservoir, which is hosted both in the volcanic units and in the underlying greywacke basement and is partially capped by a smectite-rich clay zone. In the south, reservoir fluids have higher concentrations of Cl (up to 1900 mg/kg in wells RK2 and RK3) and B (up to 62 ppm in wells RK2 and RK3) due to boiling in the natural-state conditions. Very large geochemical gradients in Cl concentration, Cl/B ratio and non-condensable gas contents occur from south to north, suggesting that the deep reservoir fluids are progressively diluted northward by cooler, marginal fluids. Based on the available dataset, it is possible to relate the deep reservoir fluids to a single parent fluid, through a combination of dilution and boiling processes, as proposed by Hedenquist et al. (1988). Nevertheless, it is not possible to exclude alternative multiple-parent models, for instance the presence of two distinct fluid sources, one in the north and the other in the south, as suggested by Giggenbach (1995). Conspicuous surface hydrothermal activity, comprising steaming grounds, fumaroles, and acid-sulfate springs, occurs in the southern part of the geothermal field. Mixed chloride-sulfate springs are found along the northern shores of Lake Rotokawa and partially contribute to the acid lake water. Springs discharging neutral chloride-bicarbonate waters are distributed along the Waikato River that dissects the geothermal field. Geysers and extensive silica terraces are absent.

3.6.8 Waiotapu

The Waiotapu geothermal field (location in Fig. 3.42) has the highest natural heat loss, up to 540 MWt, and its surface manifestations occupy the largest area in the TVZ, 17 km^2 (Simpson and Bignall 2016 and references therein). Between 1956 and 1959, seven exploratory wells (WT-1 to WT-7) were drilled at Waiotapu, to depths varying between 435 and 1100 m. Although temperatures of 200–295 °C were encountered, geothermal exploration was stopped because of the low flow rates of discharged fluids, the occurrence of calcite scaling and the choice to concentrate geothermal

development at Wairakei. The Waiotapu thermal manifestations have different characteristics depending on their location, with waters affected by acid condensates in the north and mixed chloride-sulfate springs in the south. The most famous surface manifestation, Champagne Pool, occupies a hydrothermal eruption vent and discharges undiluted, boiled reservoir fluids cooled at 75 °C. The fluids discharged from Champagne Pool generated the Primrose silica sinter terrace extending over an area of ~220 m × 90 m.

3.6.9 Wairakei

This brief synthesis on Wairakei is based on Bixley et al. (2009) and references therein. The Wairakei geothermal field is mostly positioned on the west bank of the Waikato River, just north of Lake Taupo (Fig. 3.42) and is part of the larger Wairakei–Tauhara geothermal system. The hydrological link between these two fields has been demonstrated by the close relation between the pressure changes at Wairakei and those at the Tauhara geothermal field, about 10 km to the southeast. In contrast, the Rotokawa geothermal field, 10 km to the northeast, has not responded to the pressure changes at Wairakei. Wairakei was a liquid-dominated system with a base temperature close to 260 °C, before the onset of geothermal exploitation, as pointed out by both physical measurements and geothermometric techniques. Based on the data acquired through the early wells, it was recognized from that the maximum measured temperatures approximated the boiling point for depth down to 400 m depth, roughly corresponding to sea level (Banwell 1957).

Neutral chloride waters from the geothermal reservoir were mainly discharged at the surface through the hot springs and geysers in the Geyser Valley. The chemistry of these thermal manifestations indicated that deep chloride water had experienced both dilution and boiling before discharging at the surface (Glover and Mroczek 2009). The other major area of surface activity was in the Waiora Valley where acidic chloride–sulfate or acid sulfate waters were discharged due to the higher elevation of this site. Steam discharges occurred in the Karapiti Thermal Area, in the southern part of the geothermal field. The natural heat discharge from Wairakei has been evaluated by several authors with average values close to 400 MWt. From 1950 to 2009, drilling activity resulted in more than 200 wells, completed to depths ranging from 300 to 2750 m and spread over the geothermal field, with some wells outside its boundaries. Thanks to this large number of wells, it was possible to monitor and understand the variations in the reservoir that have been caused by fluid extraction and, more recently, by injection.

3.6.10 *Chemistry of the Reservoir Liquids from the New Zealand Geothermal Systems*

All the New Zealand reservoir liquids are situated in the [Na] sector of the triangular diagram of major cations. Therefore, sodium is by far the prevalent cation with relative concentrations varying from 82 to 96 eq% (Fig. 3.44). It is followed by potassium, with relative concentrations ranging from 3 to 18 eq%. The relative K concentration increases with temperature and, in fact, is somewhat higher at Rotokawa, Mokai, and Ngatamariki compared to the other fields. The relative concentrations of Ca are low, varying from 0.1 to 2.5 eq% only.

In the triangular diagram of main anions (Fig. 3.45) most reservoir liquids are

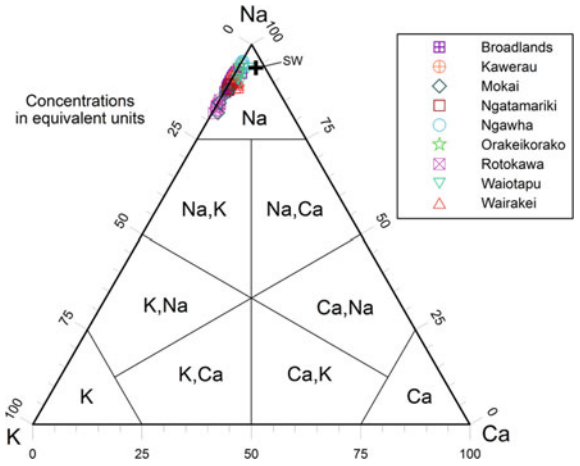

Fig. 3.44 Triangular plot of major cations for the reservoir liquids from the high-temperature geothermal fields in New Zealand

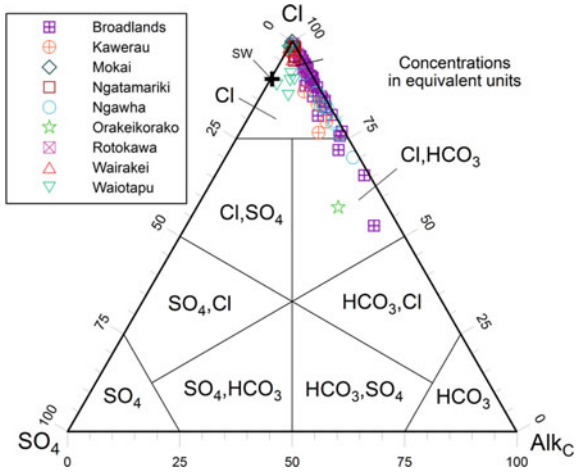

Fig. 3.45 Triangular plot of major anions for the reservoir liquids from the high-temperature geothermal fields in New Zealand

located in the [Cl] sector, and several of them, from Mokai, Ngatamariki, Rotokawa, and Wairakei, are very close to the chloride vertex. Only a few reservoir liquids from Broadlands, Orakeikorako, and Ngawha are situated in the [Cl,HCO_3] sector. Based on both triangular diagrams, it is possible to recognize the following two chemical facies:

1. The Na–Cl chemical type, which is by far the most common, comprising 88 of the 93 reservoir liquids of interest, that is 95% of the entries. Moreover, the Na–Cl reservoir liquids are found in all the considered New Zealand geothermal systems, except Orakeikorako for which one sample only is available.
2. The Na–Cl,HCO_3 chemical facies, which groups 5 reservoir liquids (5% of the cases), 3 coming from Broadlands, and 1 each from Orakeikorako and Ngawha.

The reservoir liquids from the geothermal systems in New Zealand distribute over a relatively limited interval of Σ_{eq}, from the minimum values of the Rotokawa wells, 20–48 meq/kg, to the maximum values of the Mokai wells, 88 to 133 meq/kg (Fig. 3.46).

These low to relatively low Σ_{eq} values are not surprising because the geothermal aquifers of the TVZ are mainly recharged by meteoric waters with subordinate contributions of magmatic (arc-type) waters, as indicated by isotopic data. According to Giggenbach (1995), the magmatic component contribution is $14 \pm 5\%$ for the eastern systems of the TVZ and $6 \pm 2\%$ for the western systems of the TVZ. The contribution of magmatic waters is nil at Ngawha, which is recharged by meteoric waters only as already recalled in Sect. 3.6.5.

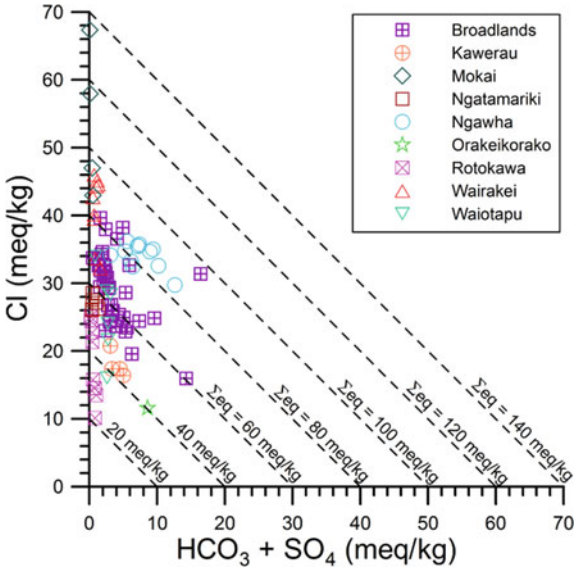

Fig. 3.46 Correlation diagram of Cl versus SO_4+ Alk_C for the reservoir liquids from the high-temperature geothermal fields in New Zealand

3.7 The Reservoir Liquids from Miscellaneous Geothermal Systems

The miscellaneous geothermal fields taken into account in this work are: Yangbajing in China (data from Ping et al. 1998a, b; Guo et al. 2014), Kizildere in Turkey (data from Guidi et al. 1988, 1990; Haizlip and Haklidir 2011; Haklidir et al. 2015; Tarcan et al. 2016), the three Italian fields of Bagnore (data from Ruggieri et al. 2004), Latera (data from Gianelli and Scandiffio 1989), and Mofete (data from Balducci and Chelini 1992), Ribeira Grande, São Miguel, Azores (data from Carvalho et al. 2006), as well as the following geothermal systems in the East African Rift System (EARS), from N to S: Asal, Djbouti (data from D'Amore et al. 1998; Sanjuan et al. 1990; Sanjuan 2010), Tendaho, Ethiopia (data from D'Amore et al. 1997; Ali 2005), Aluto-Langano, Ethiopia (data from Gizaw 1993, 1996; Teklemariam et al. 1996 and references therein), and Olkaria, Kenya (data from Muna 1982; Karingithi et al. 2010). Data on reservoir liquids from Menengai, Kenya were also compiled (from Kipng'ok 2011; Sekento 2012; Malimo 2013; Auko 2014) but were disregarded because these aqueous solutions are probably not representative of the equilibrium condition with relevant hydrothermal minerals.

The accepted chemical analyses are 32 for Yangbajing, 28 for Kizildere, 2 for Bagnore, 5 for Latera, 3 for Mofete, 15 for Ribeira Grande, 4 for Asal, 36 for Tendaho, 3 for Aluto-Langano, and 42 for Olkaria, for a total of 170 entries.

3.7.1 Yangbajing

The Yangbajing geothermal field is located on the Tibetan plateau at an altitude of 4300–4500 m asl. From the structural point-of-view, Yangbajing is positioned at an inflection point of the Nyainquentanglha slip-fault zone where its strike changes from N 60° E to N 30° E (Fig. 3.47). This strike change caused pervasive rock fracturing creating the permeability conditions needed for thermal water circulation (Ji and Ping 2000).

The Yangbajing geothermal system comprises a shallow reservoir hosted in altered granite and Quaternary sediments at depths of 180–280 m, and a deep reservoir hosted in fractured granite at depths of 950–1850 m. Temperature ranges from 150 to 165 °C in the shallow reservoir, whereas the deep reservoir is subdivided into two parts: the upper part with temperatures of 250–275 °C between 950 and 1350 m depth, and the lower part with temperatures >300 °C below 1500 m depth, (Xiaoping 2002).

Before the Yangbajain geothermal power plants began operating, the field was affected by hydrothermal explosions (e.g., in November 1975 and December 1977) and several manifestations were present. However, all primary thermal springs and pools disappeared in response to the intensive exploitation of the geothermal resource (Guo et al. 2014).

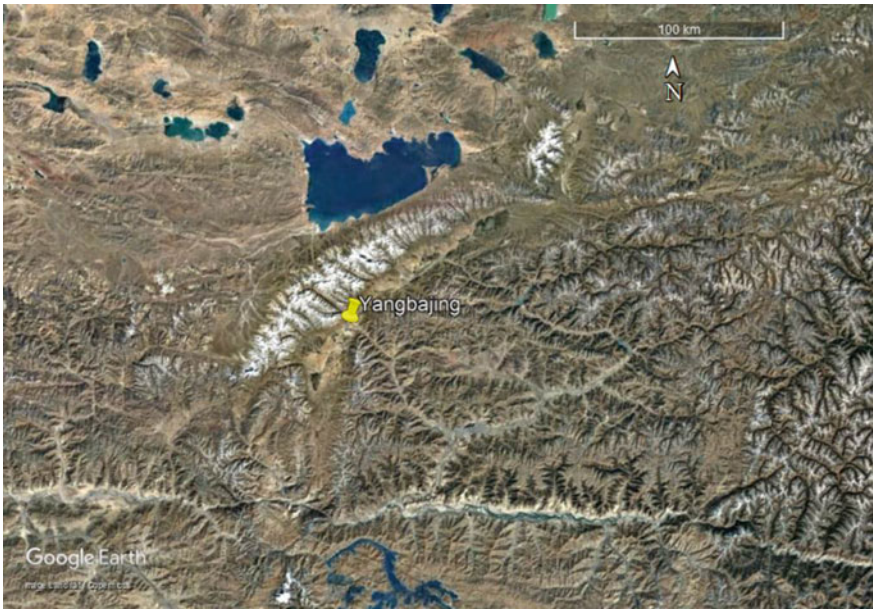

Fig. 3.47 Google Earth map showing the location of the Yangbajing geothermal field

Based on isotopic evidence, the Yangbajing geothermal fluids originate from meteoric waters. Both the shallow and the deep reservoirs host neutral chloride fluids, with chloride concentration of 1.5 and 2.8 g/kg, respectively. The fluid of the deep reservoir ascends and enters the shallow reservoir where it mixes with cooler meteoric water (Xiaoping 2002).

3.7.2 Kizildere

The Kizildere geothermal field is located in the northern sector of the Buyuk Menderes graben (Fig. 3.48), a continental rift zone whose activity begun in Early-Middle Miocene.

Quaternary alluvia crop out in the central part of the graben, where they reach a maximum thickness of some hundred meters, whereas both a Neogene series and the underlying Paleozoic basement crop out in the horsts (Guidi et al. 1988 and references therein). The basement is made up of gneisses and micaschists with lenses of marbles. The Neogene series includes prevailing clastic sediments and a sequence of limestones and marly limestones, with the local occurrence of gypsum and anhydrite. The limestones and the metamorphic basement exhibit good permeability, particularly where fractured, whereas the other Neogene deposits are impervious.

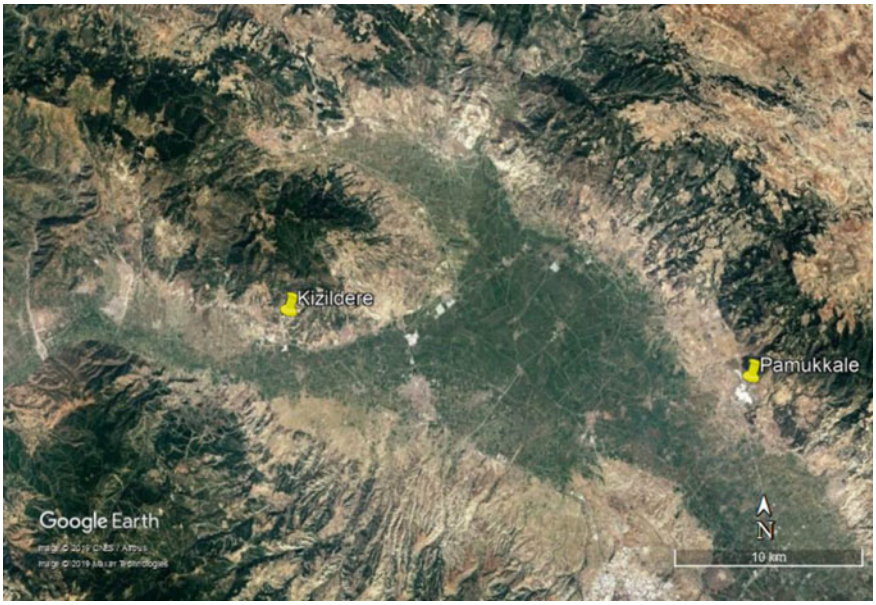

Fig. 3.48 Google Earth map showing the location of the Kizildere geothermal field and the famous Pamukkale thermal springs characterized by intense travertine deposition

Deuterium and oxygen-18 data (e.g., Özgür 1998; Tarcan et al. 2016 and references therein) indicate that the Kizildere reservoir liquids have meteoric origin, whereas the considerable oxygen isotope shift, up to ~5‰ units, is due to isotope exchange with carbonate rocks.

Temperatures are 148–198 °C in the first (shallow) reservoir, 200–212 °C in the second (middle) reservoir, and close to 240 °C in the third (deepest) reservoir, at depth of ca. 2.2 km (Tarcan et al. 2016). The Kizildere reservoir liquids have Na–HCO_3 to Na–HCO_3,SO_4 composition and high f_{CO_2}, usually in the range 35–50 bar (Guidi et al. 1988, 1990).

Today, the only thermal manifestations present in the area of the geothermal field are the fumaroles located at the northern boundary of the drilled zone, where hot springs were once found (Dominco and Samilgil 1970). This change indicates a substantial deepening of the piezometric surface caused by exploitation. Hot springs, with temperature up to the boiling point, and an old drilled well are present at Tekke Hamam, in front of Kizildere, on the opposite side of the Buyuk Menderes graben. Several hot springs are found in nearby areas. At Pamukkale there are thermal springs and extensive deposits of white travertines, visible in the Google Earth map of Fig. 3.48. These white travertines are responsible for the name of this place. In fact, pamuk is Turkish for cotton.

3.7.3 Bagnore

This brief synthesis on Bagnore is based on Calamai et al. (1970), Gianelli et al. (1988), and Bertini et al. (1995). There are two high-temperature geothermal fields in the southern sector of the Quaternary Mt. Amiata volcano (Principe et al. 2017 and references therein), one is at Bagnore while the other one is at Piancastagnaio (Fig. 3.49).

Two distinct reservoirs are present in the Bagnore geothermal field. The shallow reservoir is situated at depths of 400–1000 m, is hosted in carbonate-evaporite (anhydrite-bearing) rocks, and was exploited before the 1970s. The deep reservoir is positioned at depths of 1300–3000 m, is hosted in fractured metamorphic rocks, and has been exploited more recently.

The maximum temperature recorded in the shallow reservoir is 160 °C. The deep reservoir is water-dominated, has a hydrostatic pressure of ~200 bar at 3000 m depth, and temperatures close to 300–330 °C. The produced fluid is a two-phase mixture. The steam phase separated at wellhead at 20 bar has a high content of non-condensable gases, up to 15% by weight. The whole system is recharged by meteoric waters circulating through fractured rocks. Heat is probably contributed by a granitic intrusion which is located at an estimated depth of about 7000 m and has an expected temperature of 750–800 °C.

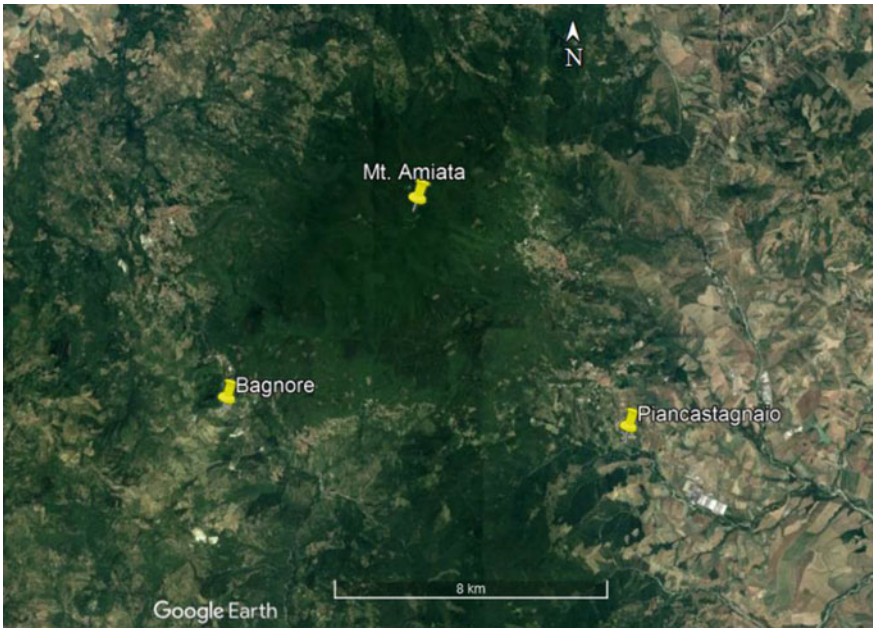

Fig. 3.49 Google Earth map showing the location of the Bagnore and Piancastagnaio geothermal fields in the southern sector of Mt. Amiata volcano

3.7.4 Latera

The Latera geothermal field is located within the homonymous caldera of 7 km × 9 km and roughly elliptical shape (Fig. 3.50). The eastern rim of the Latera caldera intersects a wider volcano-tectonic depression, which is partly filled by Lake Bolsena.

The Latera geothermal reservoir occurs at 1000–1500 m depth in a structural high made up of carbonate rocks (Cavarretta et al. 1985; Gianelli and Scandiffio 1989). The productive zones of the Latera geothermal system have hydrostatic pressures and temperatures of 200–240 °C, whereas higher temperatures were measured in some unproductive wells, such as well L10, in which the bottom-hole temperature is >400 °C at ~3300 m depth, and well L1, in which a temperature of 340 °C was measured at ~2800 m depth.

Available deuterium and oxygen-18 data (Battaglia et al. 1992) suggest that the Latera reservoir liquids have meteoric origin. Their extensive oxygen isotope shift, up to ~8‰ units, is ascribable to isotope exchange with carbonate rocks.

The conceptual model proposed by Gianelli and Scandiffio (1989) comprises a regional warm aquifer of $Ca–SO_4,HCO_3$ composition and an upflow of hot Na–Cl waters, with Cl concentration of 1500–3300 mg/kg and total CO_2 concentration of 2000–32,000 mg/kg. This model is supported by well L14, which encountered two

Fig. 3.50 Google Earth map showing the location of the Latera geothermal field within the homonymous caldera. The Latera caldera is situated to the west of the Bolsena volcano-tectonic depression, which is occupied by the homonymous lake

distinct productive zones, the first one delivering hot Na–Cl waters at 430 m depth, the second one supplying warm Ca–SO_4,HCO_3 waters at 800 m depth.

All the wells produce two-phase fluids, with discharge enthalpy ranging from 791 to 1026 kJ/kg and temperature varying from 186 to 238 °C. The water analyses of wells L2, L3D and L4 are more reliable than those of other wells because of the longer production time, in the order of several months.

The chemistry of the Latera reservoir liquids was obtained from Gianelli and Scandiffio (1989) without running WATCH because data for the separated liquid and vapor phases are not available.

3.7.5 Mofete

The Mofete geothermal field is situated within the Campi Flegrei caldera, extending west of Naples (Fig. 3.51). The caldera has a diameter of ~12 km and formed ~35,000 years ago after the Campanian Ignimbrite eruption (Rosi et al. 1983). The southern half of this volcano-tectonic depression is submerged, whereas its northern half occurs on land and includes several intra-caldera small volcanic apparatuses.

The geothermal reservoir is hosted into a volcanic sequence made up of alternating tuffs and lavas as well as quartz-feldspathic siltites below ~700 m depth. The Mofete

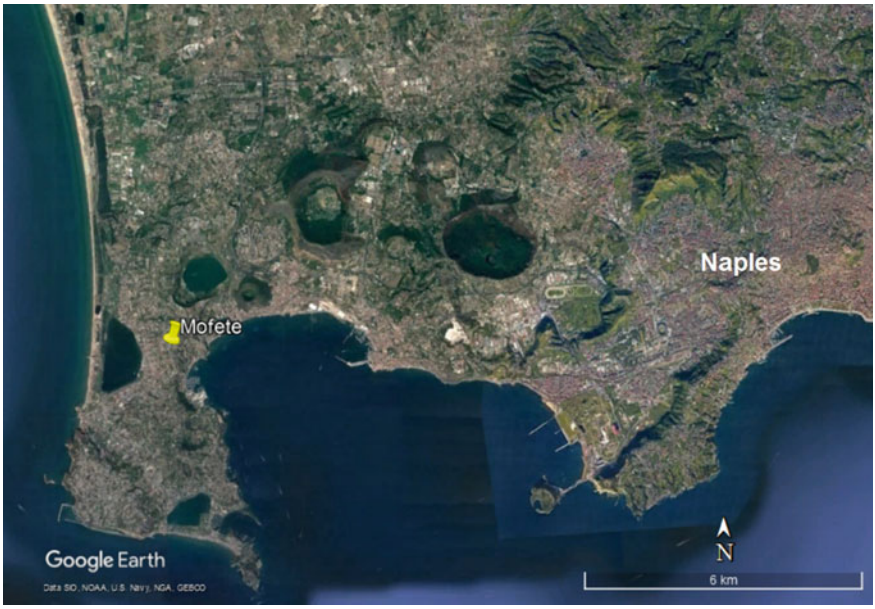

Fig. 3.51 Google Earth map showing the location of the Mofete geothermal field within the Campi Flegrei caldera, close to Naples

geothermal system includes a shallow reservoir at temperatures of 230–300 °C, which was encountered by five of the seven wells drilled in the late 1970s to early 1980s, and an intermediate-deep reservoir at temperatures of 340–350 °C which was found by two wells only (Carella and Guglielminetti 1983).

Neutral Na–Cl reservoir liquids circulate in fractured zones not cemented by hydrothermal minerals. The brines separated at atmospheric pressure exhibit considerable differences in Cl concentration, which ranges from 21,000 to 44,000 mg/kg for those coming from the shallow and intermediate reservoirs, whereas those delivered from the deep reservoir have Cl concentration of ~310,000 mg/kg (Carella and Guglielminetti 1983) and are close to saturation with halite. The system is recharged by seawater, modified by steam separation and by the irreversible mass exchanges occurring during the high-temperature interaction with reservoir rocks (Balducci and Chelini 1992).

3.7.6 Ribeira Grande

The water-dominated geothermal field of Ribeira Grande is situated within the Água de Pau stratovolcano in the central part of São Miguel Island, Azores (Fig. 3.52). The stratovolcano is truncated by an outer 4 km × 7 km caldera that formed ~33,600 years ago and an inner 2.5 km × 3 km caldera that originated ~15,200 years ago (Carvalho et al. 2006 and references therein). The geothermal system is recharged by meteoric waters, infiltrating in the upper parts and flanks of the Água de Pau volcano and flowing from south to north.

Fig. 3.52 Google Earth map showing the location of the Ribeira Grande geothermal field in the central part of São Miguel Island, Azores

Wells CL1, CL2, CL3, and CL4 have total depth of 2029, 1402, 1459, and 1500 m, respectively. Production from these wells is sustained by three different aquifers, all probably hosted in pillow lavas and situated at depths of 800 to 1300 m approximately, where temperature varies from 230 to 245 °C. A small temperature reversal occurs below ~1300 m depth in these four wells. Well PV1 is somewhat different, with a total depth of 811 m only and maximum temperatures of 220–236 °C at ~500 m depth, but again a temperature reversal is present below.

The deepest aquifer contains a single liquid phase, the intermediate aquifer hosts a two-phase (vapor + liquid) mixture with a steam fraction up to 0.08, whereas the shallower aquifer produces a single steam phase. All the wells have excess enthalpy.

The Ribeira Grande reservoir liquids are neutral, have Na–Cl composition, and Cl concentration of 1100–2600 mg/kg. Calcite scaling was directly observed in wells PV1 and CL1, but probably occurs in all geothermal wells upon flashing.

3.7.7 Asal

The Asal geothermal system, positioned in the Afar region between Lake Asal and the Gulf of Ghoubbet, is situated along the still emerged portion of an oceanic rift (Fig. 3.53).

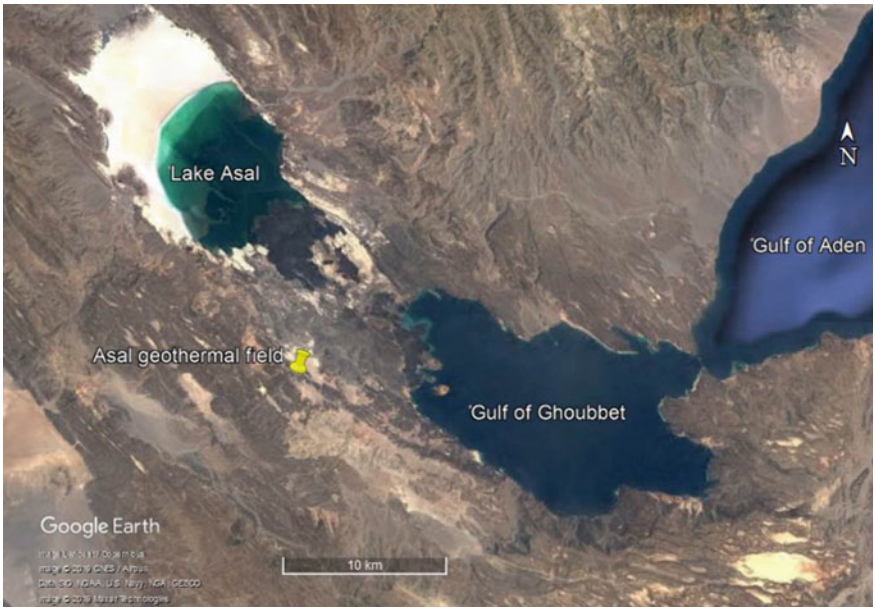

Fig. 3.53 Google Earth map showing the location of the Asal geothermal field, Djibouti, between Lake Asal and the Gulf of Ghoubbet

Six deep geothermal wells were drilled in the Asal Rift area in the 70's and 80's. Well Asal 1 produced water and steam for several months, whereas well Asal 2 produced a very small amount of fluids (Fouillac et al. 1989). The Na–Cl brine discharged from well Asal 1 has Cl concentration of 115,000–120,000 mg/kg at atmospheric conditions (Sanjuan 2010).

As reported by D'Amore et al. (1998): (1) well Asal 3 has total depth of 1316 m, a maximum temperature of 265 °C and encountered high-enthalpy fluids below 1075 m depth; (2) well Asal 4 has total depth of 2011 m, a maximum temperature of 344 °C, but it met cold water at shallow depth and it is dry below 400 m; (3) well Asal 5 has total depth of 2105 m, a maximum temperature of 359 °C, but it is dry below 400 m; (4) well Asal 6 has total depth of 1761 m, a maximum temperature of 281 °C and encountered high-enthalpy fluids at 265 °C from 1100 to 1300 m depth. Wells Asal 3 and Asal 6 produced a Na–Cl brine with Cl concentration of 103,000–106,000 mg/kg and pH 4.8–4.9 at atmospheric conditions. Sphalerite and galena scaling was detected in both wells downstream of the flash level.

As recognized by previous authors, the chemistry of the Asal reservoir liquids is controlled by high-temperature basalt-seawater interaction, associated with variable evaporation. The chemistry of the Asal reservoir liquids was obtained from D'Amore et al. (1998) and Sanjuan (2010) without running WATCH because of the unavailability of data for the separated liquid and vapor phases.

3.7.8 Tendaho

The Tendaho geothermal system is positioned in the inland portion of the Afar region (Fig. 3.54), at a distance of ~150 km from the sea coast. Most information on Tendaho was derived from Battistelli et al. (2002).

Deuterium and oxygen-18 indicate that the Tendaho geothermal reservoir is recharged by meteoric waters infiltrating at elevations of 2000–3000 m asl in the Western Ethiopian Plateau. Consistently, the shallow Tendaho geothermal reservoir hosts low-salinity brines with TDS of ~2 g/kg and low gas content, ~370 mg/kg.

Available enthalpy and temperature data for wells TD-2 and TD-4 suggest the presence in the reservoir of either a single liquid phase or bi-phase conditions with small excess enthalpy as well as the provenance of produced fluids from different feed zones. Reservoir conditions and production characteristics of wells TD-5 and TD-6 are similar to those of well TD-4.

Owing to the limited information available on enthalpy and gas chemistry, a single liquid phase was hypothesized to be present in the reservoir, at the temperature indicated by the quartz/chalcedony geothermometer, and the CO_2 and H_2S contents of all the reservoir liquids of wells TD-5 and TD-6 were assumed to be 307 mg/kg and 2.14 mg/kg, respectively, based on the gas chemistry data of wells TD-2 and TD-4 from D'Amore et al. (1997).

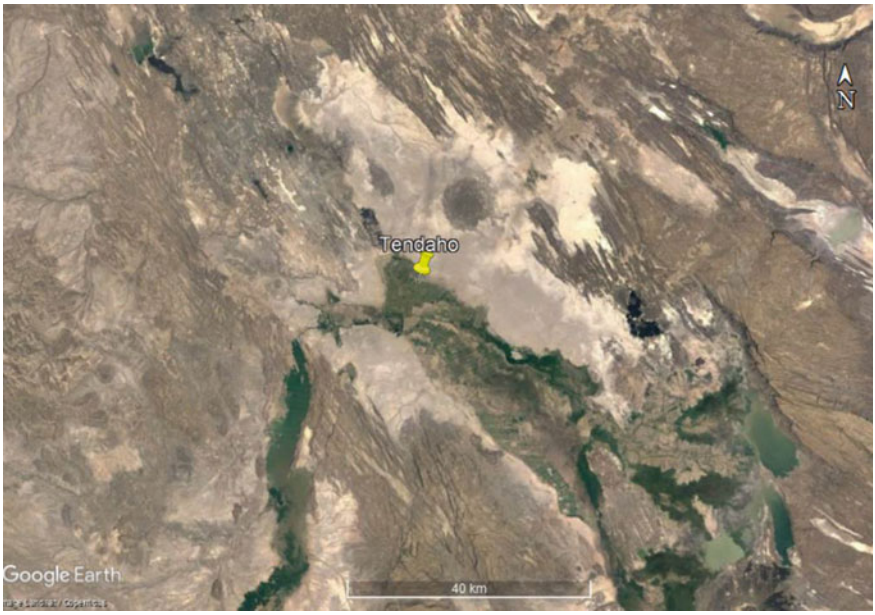

Fig. 3.54 Google Earth map showing the location of the Tendaho geothermal system in the inland portion of the Afar region, Ethiopia

3.7.9 Aluto-Langano

The Aluto-Langano geothermal field is found in the central sector of the Main Ethiopian Rift, between Lake Ziway to the north and Lake Abiyata and Lake Langano to the south (Fig. 3.55).

The Aluto-Langano geothermal system is associated with the Quaternary Aluto volcanic complex. The stable isotope values indicate that the geothermal well discharges consist essentially of meteoric water infiltrating in the volcanic complex (Rango et al. 2010 and references therein). The upflow of geothermal fluids is controlled by an active fault zone known as Wonji Fault Belt (Gianelli and Teklemariam 1993).

According to Teklemariam et al. (1996), the two hottest wells, LA-3 and LA-6, have total discharge enthalpies of 1600–1650 kJ/kg and aquifer temperatures of 320–335 °C, respectively. These data indicate the presence of bi-phase conditions with mass steam fractions of 0.11–0.15 and 0.037–0.083 in the reservoir zones encountered by wells LA-3 and LA-6, respectively. The reservoir liquids of Aluto-Langano wells LA-3 and LA-6 were disregarded because computed pH values resulted to be higher than the mineral-solution equilibrium pH values by 1.8 pH unit. A single liquid phase seems to occur in the aquifer zones connected with wells LA-4, LA-7, and LA-8, with measured temperatures of 233, 226, and 270 °C, respectively.

Fig. 3.55 Google Earth map showing the location of the Aluto-Langano geothermal system in the Main Ethiopian Rift

The chemistry of the Aluto-Langano reservoir liquids encountered by wells LA-4, LA-7, and LA-8 was directly taken from Teklemariam et al. (1996) without running WATCH because data for the separated liquid and vapor phases are unavailable.

3.7.10 Olkaria

The Olkaria geothermal field is situated to the south of Lake Naivasha in the central portion of the Kenyan Rift Valley (Fig. 3.56). The Olkaria geothermal system is related with the Quaternary Olkaria volcanic complex, where magmatic activity began during the late Pleistocene and continued until 180 ± 50 years ago when the Ololbutot comendite was erupted (Clarke et al. 1990). Incidentally, comendites are present only in the Olkaria area within the whole Kenyan Rift Valley.

The following brief synthesis on Olkaria is based on Karingithi et al. (2010). The over 100 wells drilled at Olkaria have variable discharge enthalpy. Most of the wells have excess enthalpy which is due to depressurization boiling in producing aquifers. However, contribution of steam from the steam cap present above the bi-phase reservoir of Olkaria East is responsible for the excess enthalpy of the wells drilled in this sector of the field.

Fig. 3.56 Google Earth map showing the location of the Olkaria geothermal system in the Kenyan Rift Valley

The fluids in Olkaria West and Domes sectors have high carbonate alkalinity and low chloride concentration in sharp contrast with those in the Olkaria East and Olkaria Northeast sectors which have lower alkalinity and higher chloride concentration. Moreover, the fluids encountered by the wells of Olkaria West and Domes sectors have high concentrations of CO_2, which are controlled by considerable gas fluxes from a magmatic heat source. In contrast, CO_2 concentration is relatively low in the other sectors of the Olkaria geothermal field, being buffered by the epidote-prehnite-calcite-quartz hydrothermal mineral assemblage.

Under-saturation with respect to the Ca-bearing solid phases, which are known to be present in the geothermal reservoir as hydrothermal minerals, is probably an artifact due to loss of Ca through calcite precipitation occurring in the depressurization zone around the wells.

3.7.11 Chemistry of the Reservoir Liquids from Miscellaneous Geothermal Systems

One hundred sixty six of the one hundred seventy reservoir liquids considered in this section are situated in the [Na] sector of the triangular diagram of major cations (Fig. 3.57). The four exceptions are the reservoir liquids from Asal, which are located

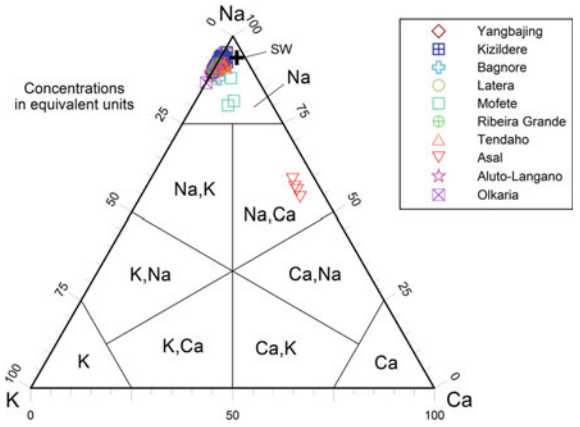

Fig. 3.57 Triangular plot of major cations for the reservoir liquids from miscellaneous geothermal systems (see legend). Average seawater is also shown for comparison

in the [Na,Ca] sector, due to gain of Ca through basalt-seawater interaction at elevated temperatures. Therefore, sodium is the prevailing cation in all the reservoir liquids of interest, with relative Na concentrations >75 eq% at Yangbajing, Kizildere, Bagnore, Latera, Mofete, Ribeira Grande, Tendaho, Aluto-Langano, and Olkaria. The Asal reservoir liquids have relative Na concentrations of 54–59 eq%, relative Ca concentrations of 35–40 eq%, relative K concentrations of 5.5–6.2 eq%, and relative Mg concentrations $\leq$0.1 eq%.

In the triangular diagram of main anions (Fig. 3.58) most reservoir liquids are located in the [Cl] sector and some of them are close to the chloride vertex. Nevertheless, several reservoir liquids are situated elsewhere, namely in the [Cl,HCO_3], [Cl,SO_4], [HCO_3,Cl], [HCO_3,SO_4], and [HCO_3] sectors, whereas no sample is found in the [SO_4,Cl], [SO_4,HCO_3], and [SO_4] sectors. Based on both triangular diagrams, it is possible to recognize eight different chemical facies. In detail:

1. The Na,Ca–Cl chemical type includes only the 4 reservoir liquids of Asal, but is the only chemical facies present in this field.

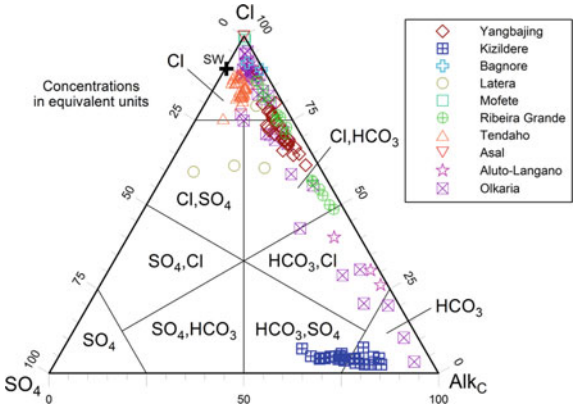

Fig. 3.58 Triangular plot of major anions for the reservoir liquids from miscellaneous geothermal systems (see legend). Average seawater is also shown for comparison

2. The Na–Cl chemical facies is by far the most common, with 88 reservoir liquids. Thirty six are from Tendaho, three are from Mofete, and two are from Bagnore, but they constitute 100% of the samples from these three geothermal fields. Twenty eighth are from Olkaria, where they represent 67% of the entries. Six are from Ribeira Grande, where they make up 40% of the items. Two are from Latera, where they account for 40% of the records. Eleven are from Yangbajing, where they represent 34% of the entries.
3. The Na–Cl,HCO_3 chemical type is rather widespread with 37 reservoir liquids. It is present at Yangbajing with 21 samples, corresponding to 66% of the entries of this site, Ribeira Grande with 8 samples, representing 53% of the items of this place, Olkaria with 7 samples, corresponding to 17% of the records of this field, and Latera with 1 sample, representing 20% of the entries of this site.
4. The Na–Cl,SO_4 chemical type groups 2 reservoir liquids only, both from Latera, where they account for 40% of the items.
5. The Na–HCO_3,Cl chemical facies comprises 8 reservoir liquids. Three are from Aluto-Langano, where they explain 100% of the items. Four are from Olkaria, where they make up 10% of the entries. One is from Ribeira Grande, where it constitutes 7% of the records.
6. The Na–HCO_3,SO_4 chemical type includes 15 reservoir liquids, all from Kizildere, where they account for 54% of the items.
7. The Na–HCO_3 chemical facies comprises 16 reservoir liquids. Thirteen are from Kizildere, where they represent 46% of the records. Three are from Olkaria, where they make up 7% of the entries.

The binary diagram of Cl versus $SO_4 + Alk_C$ (Fig. 3.59a) shows that the reservoir liquids of Asal have Σ_{eq} values varying from 3780 to 4210 meq/kg, which are 3–3.5

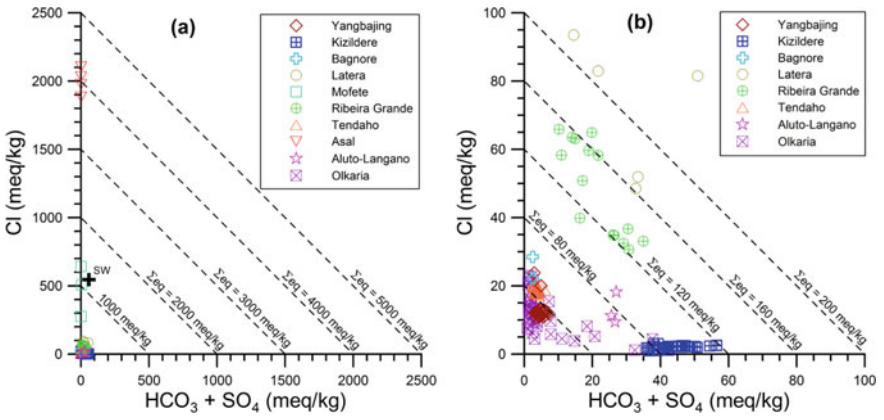

Fig. 3.59 Correlation diagrams of Cl versus $SO_4 + Alk_C$ for the reservoir liquids from miscellaneous geothermal systems (see legend). Average seawater is also shown for comparison in (**a**). Different Σ_{eq} intervals are considered in the two diagrams **(a)** and **(b)** in order to accommodate all the liquids of interest

times higher than the average seawater value, 1210 meq/kg. These very high ionic salinities are essentially controlled by the predominant role of evaporated seawater in the recharge of this geothermal circuit, in spite of the subsequent occurrence of important chemical changes caused by water-rock interaction (D'Amore et al. 1998; Sanjuan et al. 1990; Sanjuan 2010).

Two of the three reservoir liquids of Mofete have Σ_{eq} of 1020 and 1310 meq/kg, comparing with the value of seawater, which recharges this geothermal system, as already mentioned above (Fig. 3.59a). The other reservoir liquid of Mofete has lower ionic salinity, 542 meq/kg, due to dilution with meteoric waters.

The other reservoir liquids considered in this section have lower Σ_{eq} values, namely 28 – 57 meq/kg for Yangbajing, 79–110 meq/kg for Kizildere, 50–59 meq/kg for Bagnore, 170–265 meq/kg for Latera, 116–165 meq/kg for Ribeira Grande, 41–48 meq/kg for Tendaho, 76–96 meq/kg for Aluto-Langano, and 20–86 meq/kg for Olkaria (Fig. 3.59b). These low to relatively low Σ_{eq} values are expected, because deuterium and oxygen-18 data indicate that these geothermal circuits are recharged by meteoric waters (see above).

Carbon dioxide is entirely or chiefly contributed by deep sources, either mantle/magma degassing, as suggested by the $\delta^{13}C$ values of CO_2 for Yangbajing (Zhao et al. 1998), Olkaria (Darling 1998), Aluto-Langano (Darling 1998), Tendaho (D'Amore et al. 1997), and Asal (Darling 1998; D'Amore et al. 1997), or high-temperature decomposition of carbonate rocks, as indicated by the $\delta^{13}C$ values of CO_2 for Kizildere (Özgür 1998). Where the CO_2 flux from these deep sources is high, reservoir liquids have high f_{CO_2} values and Na–HCO_3 or Na–HCO_3,Cl or Na–HCO_3,SO_4 compositions, reflecting the occurrence of water-rock interaction governed by conversion of CO_2 to HCO_3^- ion.

In contrast, reservoir liquids have Na–Cl or Na–Cl,HCO_3 composition where Cl sources are more important than CO_2 sources. Dissolution of carbonate-evaporite rocks is probably responsible of the relatively high SO_4 concentrations of the Na–Cl,SO_4 reservoir liquids of Latera, as suggested by the $\delta^{34}S$ values of the hydrothermal anhydrite samples from the deep geothermal wells L1 and L2 (Cavarretta et al. 1985) and the Na–HCO_3,SO_4 reservoir liquids of Kizildere (Guidi et al. 1988, 1990).

3.8 Main Results of Speciation Calculations for the Reservoir Liquids and Implications

3.8.1 The pH Value

As already mentioned in Sect. 3.1.2, the pH value of a reservoir liquid is computed by WATCH considering the low-temperature pH value and assuming conservation of

alkalinity upon cooling from the reservoir temperature to the temperature of measurement of pH and alkalinity, apart from the increment caused by steam separation (Arnórsson et al. 1982).

Looking at the pH of reservoir liquids from a different point of view, Ellis (1970) recognized that the a_{K^+}/a_{H^+} ratio is controlled by coexistence of K-feldspar, muscovite, and a silica mineral, according to the following reaction:

$$1.5\,KAlSi_3O_8 + H^+ = 0.5\,KAl_3Si_3O_{10}(OH)_2 + 3\,SiO_2 + K^+ \tag{3.8}$$

and the a_{Na^+}/a_{H^+} ratio is buffered by coexistence albite, K-feldspar, muscovite, and a silica mineral, as described by the reaction:

$$0.5\,KAlSi_3O_8 + NaAlSi_3O_8 + H^+ = 0.5\,KAl_3Si_3O_{10}(OH)_2 + 3\,SiO_2 + Na^+. \tag{3.9}$$

Assuming that salinity is approximated by the sum of the molalities of Na^+ and K^+ ions, Ellis (1970) underscored that the pH of reservoir liquids unaffected by boiling is a function of salinity and temperature. In this way, he was able to explain the low pH values of the deep waters of high salinity and high temperature, such as those of Salton Sea in California, as well as the high pH values of the deep waters of low salinity and low temperature, such as those of Hveragerdi in Iceland.

The Ellis approach was later expanded by Chiodini et al. (1991), who used a mineral-solution equilibrium model to calculate the pH value and the concentrations of compatible solutes (Na, K, Mg, Ca, Al, SiO_2, HCO_3, SO_4, and F) for the aqueous solutions in equilibrium with the hydrothermal mineral assemblage comprising low-albite, adularia, either a Ca–Al-silicate and/or calcite (depending on CO_2 fugacity and temperature), clinochlore, muscovite, quartz, anhydrite, and fluorite, at specified temperature, CO_2 fugacity, and concentration of chloride, the only considered conservative (mobile) component (further details in Sect. 5.8). Through multiple regression analysis (MRA) of the results of the mineral-solution equilibrium model, Chiodini et al. (1991) derived the following equation:

$$pH_{mse} = 1.757 - 0.822 \cdot \log \Sigma_{eq} + 1846/T - 0.0171 \cdot \log f_{CO_2}, \tag{3.10}$$

relating the pH fixed by mineral-solution equilibrium, pH_{mse}, to total ionic salinity (Σ_{eq}, in eq/kg), temperature (in K), and CO_2 fugacity (in bar), which were treated as independent variables in MRA. MRA results also indicated that the pH fixed by mineral-solution equilibrium is controlled by total ionic salinity, temperature, and CO_2 fugacity, in order of decreasing importance. In agreement with Ellis findings, Eq. (3.10) indicates that pH_{mse} decreases with increasing Σ_{eq} and temperature and vice versa. Moreover, pH_{mse} decreases with increasing CO_2 fugacity.

As mentioned in Sect. 3.1.4, the correspondence, within ±1.3 pH unit, between the pH computed through speciation calculations usually carried out using WATCH, pH_{sc}, and mineral-solution equilibrium pH is one of the two criteria adopted to accept the analytical data of the compiled reservoir liquids. The range spanned by

pH_{sc}, 4.17–8.13, is somewhat smaller than the interval covered by pH_{mse}, 4.03–8.63. The correlation diagrams of Fig. 3.60, in which these two pH values are contrasted, provide the following indications.

1. All or most reservoir liquids of some geothermal systems have $pH_{sc} < pH_{mse}$. This is the case of the medium-temperature geothermal systems in Iceland (Fig. 3.60a), Long Valley (Fig. 3.60b), Onikobe and Oku-aizu (Fig. 3.60c), Alto Peak (Fig. 3.60d), Ngawha (Fig. 3.60e), Kizildere and Latera (Fig. 3.60f). These differences between pH_{sc} and pH_{mse} values are probably ascribable to excess of acidic species, in most cases CO_2 from deep sources. The amount of CO_2 entering these geothermal aquifers from below is so large that relevant mineral-solution reactions are not able to consume all the CO_2, whose concentration and fugacity in the reservoir liquid become higher than the values fixed by mineral-solution equilibrium. Consequently, the pH of these reservoir liquids decreases becoming lower than the value controlled by equilibrium with the minerals of the neutral alteration suite, but it does not attain the low values causing the development of the acid alteration suite (sensu Reyes 1990). The only possible exception is Onikobe, where the main acidity source is HCl, with H_2SO_4 acting as potential subordinate acidity source, as noted in Sect. 3.4.4.
2. In contrast, all or most reservoir liquids of other geothermal systems have $pH_{sc} > pH_{mse}$. Examples are Krafla, Námafjall, Hellisheidi, and Nesjavellir, (Fig. 3.60a), Salton Sea, Cerro Prieto, Los Azufres, and Berlin (Fig. 3.60b), Sumikawa, Uenotai, and Oguni (Fig. 3.60c), Tongonan (Fig. 3.60d), Wairakei (Fig. 3.60e), Ribeira Grande, Olkaria and Tendaho (Fig. 3.60f). These divergences between pH_{sc} and pH_{mse} values might be caused by CO_2 loss through aquifer boiling either in the natural (pre-exploitation) state or in response to the depressurization induced by exploitation.
3. There are also geothermal systems whose reservoir liquids have pH_{sc} values similar to pH_{mse} values, as is the case of Hveragerdi, Svartsengi, and Reykjanes (Fig. 3.60a), Dixie Valley, Heber, and Miravalles (Fig. 3.60b), Takigami (Fig. 3.60c), Palinpinon (Fig. 3.60d), Kawerau and Ngatamariki (Fig. 3.60e) and Bagnore (Fig. 3.60f). These reservoir liquids with pH_{sc} not too different from pH_{mse} are probably close to the mineral-solution equilibrium condition, which is apparently unaffected or negligibly affected by gain/loss of CO_2. Therefore, strictly speaking, only these reservoir liquids should be considered for investigating the traditional geoindicators and elaborating theoretical, activity-based geothermometers and f_{CO_2} indicators, as we plan to do in this work, whereas the reservoir liquids with pH_{sc} significantly different from pH_{mse} should be disregarded because they are not (or not completely) representative of this equilibrium condition. However, such a choice would cause a considerable loss of information due to the large number of reservoir liquids with pH_{sc} considerably different from pH_{mse}.

However, the discrepancies between pH_{sc} and pH_{mse} values could also be caused, at least in part, by uncertainties in the reconstruction of reservoir liquid chemistry and related speciation calculations, especially for the excess enthalpy wells. Accepting

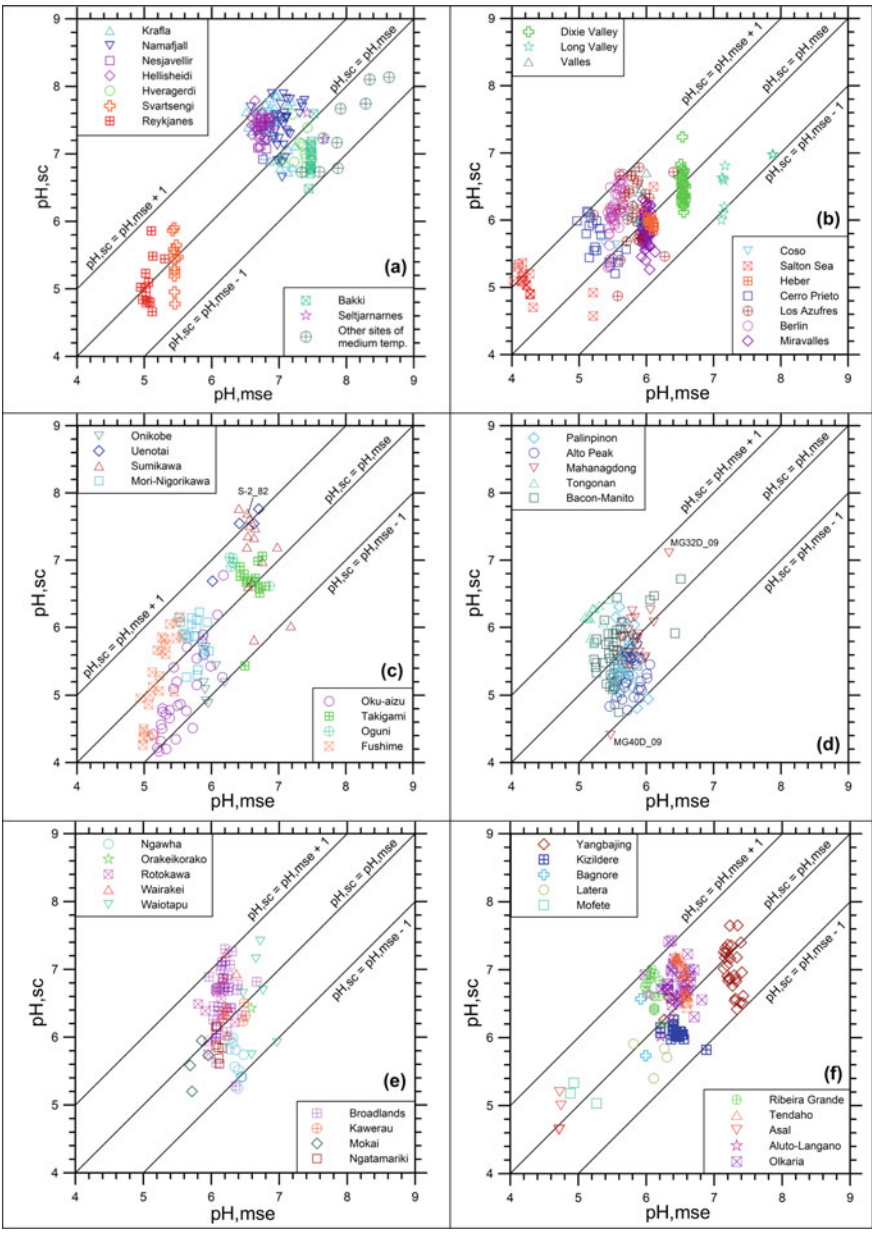

Fig. 3.60 Correlations diagrams between the pH values computed through speciation calculations usually carried out using WATCH, pH_{sc}, and the corresponding mineral-solution equilibrium pH values, pH_{mse}, for the reservoir liquids of **a** Iceland, **b** Northern and Central America, **c** Japan, **d** The Philippines, **e** New Zealand, and **f** Miscellaneous geothermal fields

this explanation, it is legitimate to take into consideration also the reservoir liquids with pH_{sc} differing from pH_{mse} by up to ±1.3 pH unit, as long as we aim at elaborating theoretical, activity-based geothermometers and f_{CO_2} indicators which do not involve pH and are based on variables which are not influenced or negligibly influenced by pH, like the concentrations and activities of non-volatile solutes. These variables, in fact, are not impacted or are marginally impacted by uncertainties in the calculation of reservoir liquid chemistry (see Sect. 3.1.2). Traditional geothermometers satisfy these criteria, but have other weaknesses, which will be discussed in Chap. 5.

3.8.2 The Fraction of Undissociated $SiO_{2(aq)}$

The fraction of undissociated $SiO_{2(aq)}$ is the ratio of the molal concentration of undissociated silicic acid, $SiO_{2(aq)}$, over the total (or analytical) molal concentration of SiO_2. The fraction of undissociated $SiO_{2(aq)}$ is strongly correlated with reservoir pH and departs significantly from unity for pH values higher than 7.5–8.0 (Fig. 3.61), as expected based on the pK of silicic acid dissociation, which varies from 8.8 to 10.1, in the 100–350 °C range (see Sect. 5.2.1 for details). Hence, for pH > 7.5–8.0, it is advisable to consider undissociated $SiO_{2(aq)}$ instead of total dissolved SiO_2 in geothermometric calculations, in spite of possible uncertainties on the pH values computed through speciation calculations. Actually, fractions of undissociated $SiO_{2(aq)}$ lower than 0.95 are rather uncommon, as they pertain to 25 reservoir liquids only, of which 7 each from Námafjall and Krafla, 2 from Yangbajing, and 1 each from Baer, Bakki, Hveragerdi, Reykholar, Reykholt, Reykjavik, Seltjarnarnes, Sumikawa, and Waiotapu.

3.8.3 The Fractions of Free Na^+, K^+, Ca^{2+}, and Mg^{2+} Ions

The fractions of free (or uncomplexed) Na^+, K^+, Ca^{2+}, and Mg^{2+} ions are the ratios of the molal concentrations of free Na^+, K^+, Ca^{2+}, and Mg^{2+} ions over the total (or analytical) molal concentrations of Na, K, Ca, and Mg, respectively.

The fractions of free Na^+, K^+, Ca^{2+}, and Mg^{2+} ions are contrasted with aquifer temperature in the correlation diagrams of Figs. 3.62, 3.63, 3.64 and 3.65, respectively. The fractions of free cations depend on the concentrations of relevant anionic ligands and the stability of pertinent ion complexes which, in turn, increases with increasing reservoir temperature. Owing to variable composition, salinity and temperature of the considered reservoir liquids there is a considerable scatter of sample points in the binary plots of Figs. 3.62, 3.63, 3.64 and 3.65.

The fractions of free Na^+ and K^+ ions and especially those of free Ca^{2+} and Mg^{2+} ions exhibit large variations (see below) because the aqueous speciation of most reservoir liquids was modeled using the B-dot equation (see Sect. 2.3.3) for

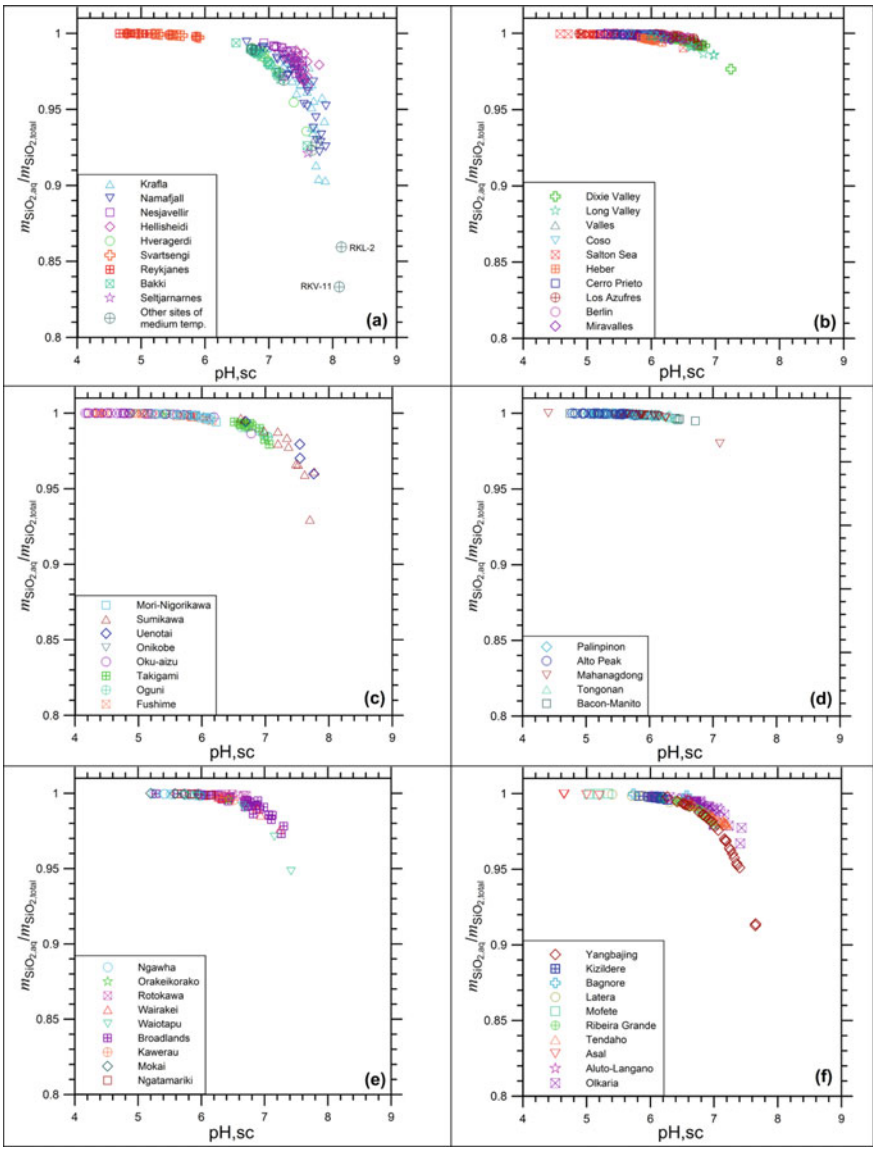

Fig. 3.61 Correlations diagrams showing the fraction of undissociated silica as a function of aquifer pH (from speciation calculations) for the reservoir liquids of **a** Iceland, **b** Northern and Central America, **c** Japan, **d** The Philippines, **e** New Zealand, and **f** Miscellaneous geothermal fields

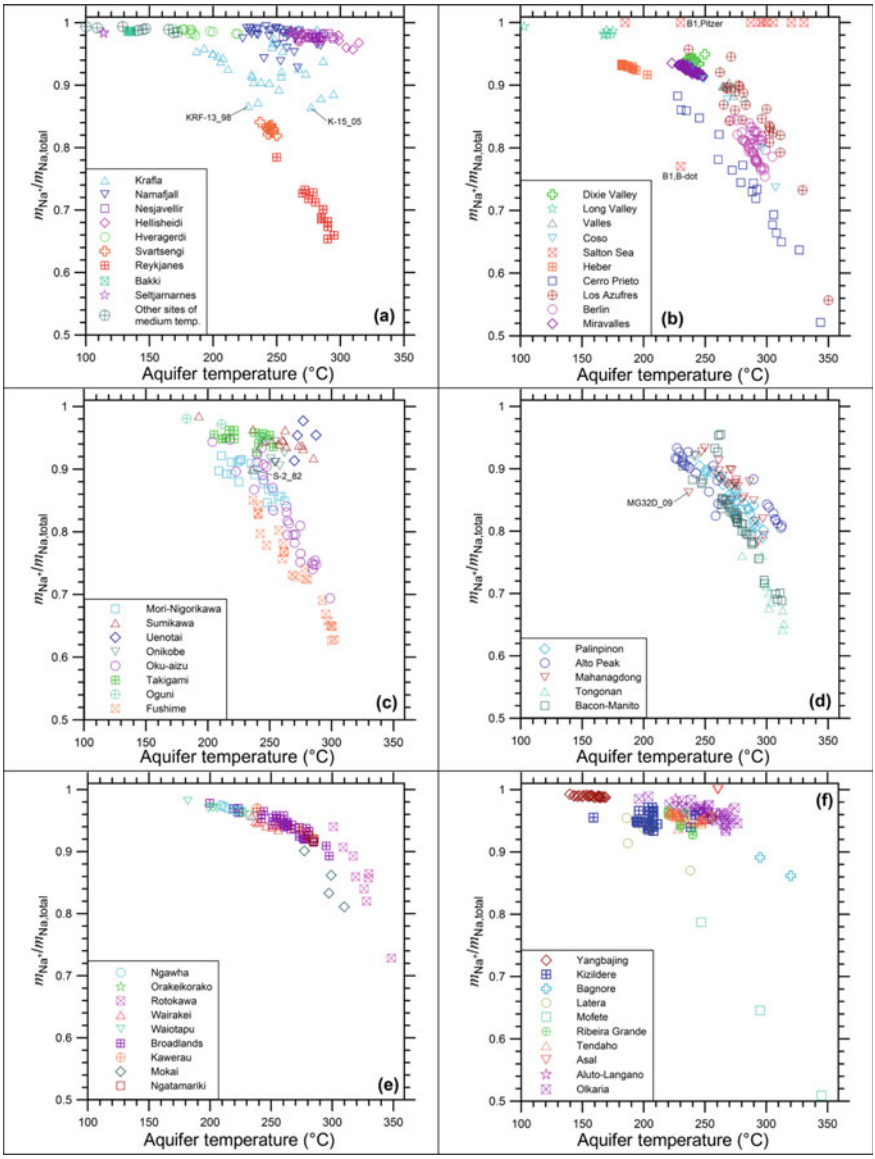

Fig. 3.62 Correlations diagrams showing the fraction of free Na^+ ion as a function of aquifer temperature for the reservoir liquids of **a** Iceland, **b** Northern and Central America, **c** Japan, **d** The Philippines, **e** New Zealand, and **f** Miscellaneous geothermal fields

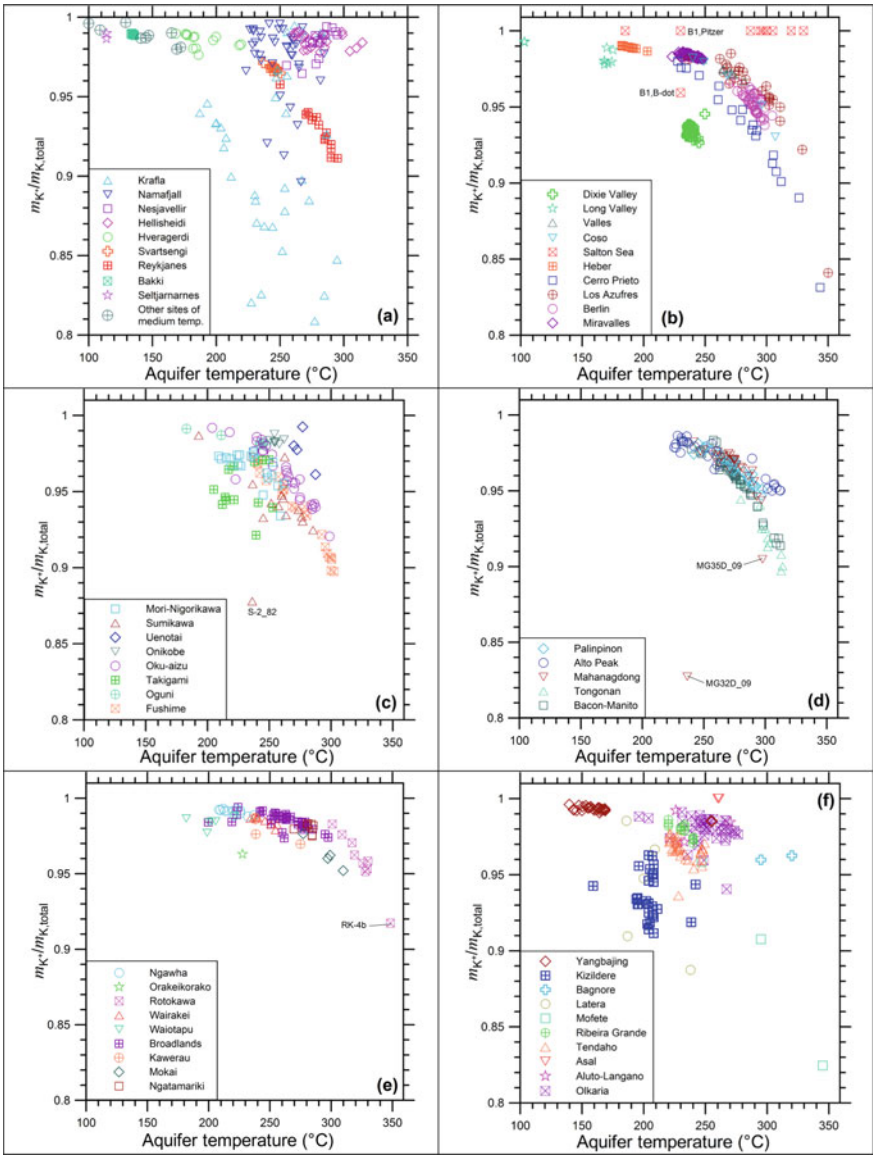

Fig. 3.63 Correlations diagrams showing the fraction of free K^+ ion as a function of aquifer temperature for the reservoir liquids of **a** Iceland, **b** Northern and Central America, **c** Japan, **d** The Philippines, **e** New Zealand, and **f** Miscellaneous geothermal fields

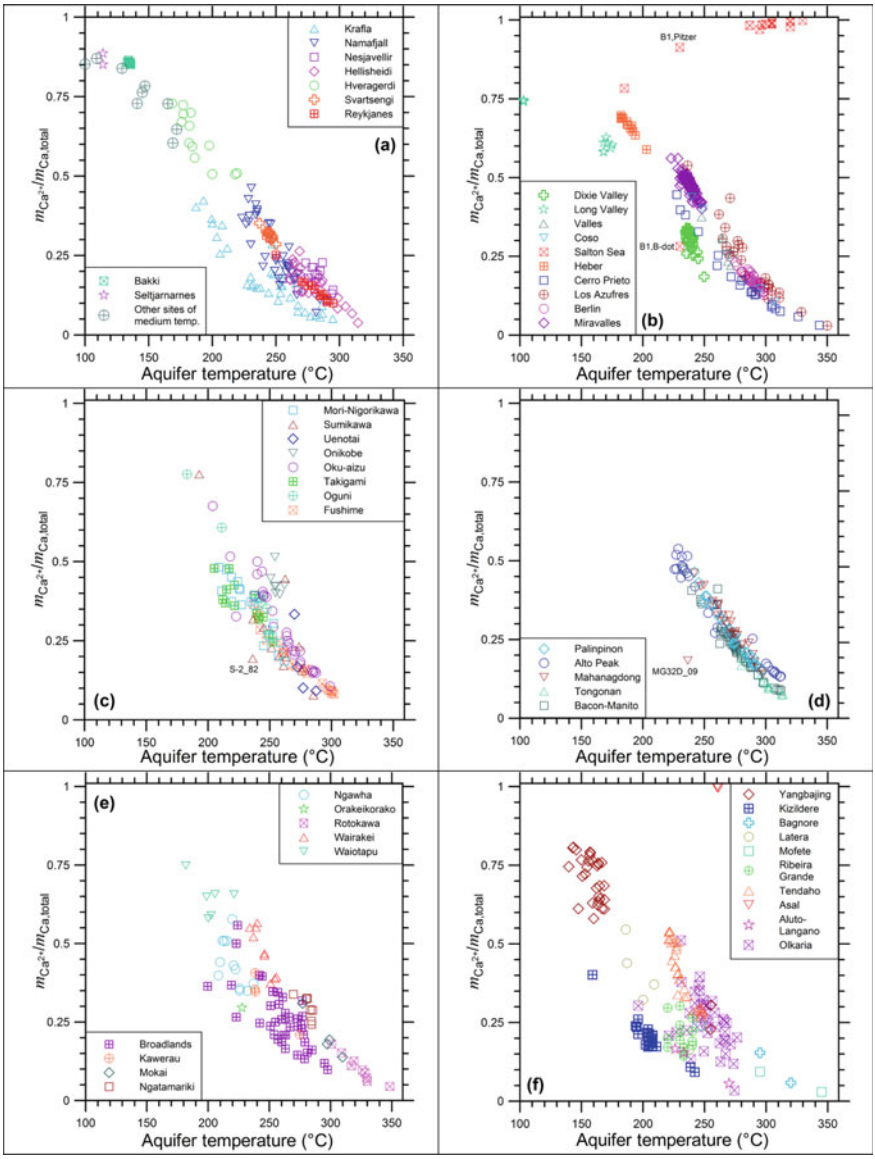

Fig. 3.64 Correlations diagrams showing the fraction of free Ca^{2+} ion as a function of aquifer temperature for the reservoir liquids of **a** Iceland, **b** Northern and Central America, **c** Japan, **d** The Philippines, **e** New Zealand, and **f** Miscellaneous geothermal fields

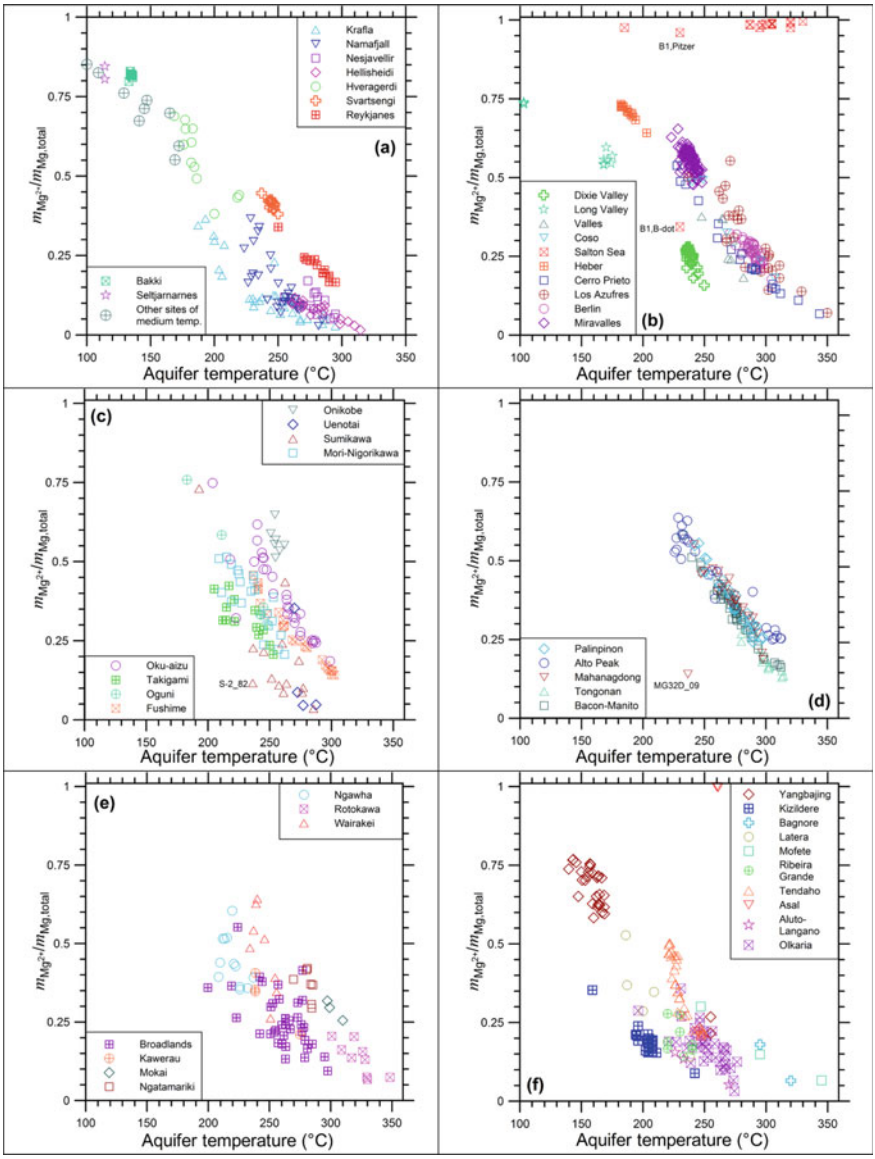

Fig. 3.65 Correlations diagrams showing the fraction of free Mg^{2+} ion as a function of aquifer temperature for the reservoir liquids of **a** Iceland, **b** Northern and Central America, **c** Japan, **d** The Philippines, **e** New Zealand, and **f** Miscellaneous geothermal fields

computing the activity coefficients of ionic species and several ion pairs were taken into account, as typically done in this approach.

In contrast, the speciation of the Salton Sea and Asal reservoir liquids were modeled using the Pitzer equations (see Sect. 2.3.4). In the Pitzer's approach, solute-solvent and solute-solute interactions are mainly explained by activity coefficients and few complex species are considered, namely NaF° for sodium, $CaCO_3^{\circ}$, $CaHCO_3^{+}$, $CaOH^{+}$, and $CaSO_4^{\circ}$ for calcium, and $MgCO_3^{\circ}$, $MgHCO_3^{+}$, and $MgOH^{+}$, for magnesium. Consequently, in the Salton Sea and Asal reservoir liquids: (1) the fraction of free K^{+} is equal to 1 because no aqueous complex of K^{+} ion is taken into account; (2) the fraction of free Na^{+} and Mg^{2+} ions are close to 1 due to the very small importance of the considered ion pairs in these aqueous solutions; (3) the fraction of free Ca^{2+} ion departs from unity in the aqueous solution of lowest temperature, from well Commercial # 113 of Salton Sea (code Com #113 in the file Reservoir_Liquids.XLS), due to the moderate importance of the $CaSO_4^{\circ}$ aqueous complex.

To be noted that the reservoir liquid of well Commercial # B1 of Salton Sea (indicated by codes Com #B1 in the file Reservoir_Liquids.XLS and B1 in the diagrams), characterized by a Cl concentration of 31,000 mg/kg and an aquifer temperature of 230 °C (which are low values for Salton Sea), was modeled adopting both approaches to appreciate the difference in the fractions of free cations.

The Fraction of Free Na^{+} Ion The fraction of free Na^{+} ion varies from 0.65 to 0.994 in the reservoir liquids of Iceland, indicating that free Na^{+} ion is the prevailing aqueous species (Fig. 3.62a). The main aqueous complexes are: (1) the $NaSO_4^{-}$ ion pair in 112 reservoir liquids, of which 33 from Námafjall, 32 from Krafla, 18 from Bakki, 13 from Hveragerdi, 5 from Nesjavellir, 3 from Hellisheidi, 2 each from Reykholt and Reykjabol, and 1 each from Baer, Efri-Reykir, Leirà, and Seltjarnarnes; (2) the $NaCl^{\circ}$ ion pair in 67 reservoir liquids, of which 25 from Svartsengi and Reykjanes (these aqueous solutions have Na–Cl composition and high salinity), 24 from Hellisheidi, 4 from Krafla, 3 from Námafjall, 10 from Nesjavellir, and 1 from Seltjarnarnes; (3) the $NaHSiO_3^{\circ}$ ion pair in three reservoir liquids from Námafjall, Reykholar, and Reykjavik.

Neglecting the hypersaline reservoir liquids of Salton Sea that were modeled using the Pitzer's equations, all the other reservoir liquids of Northern and Central America have fraction of free Na^{+} ion ranging from 0.52 to 0.994, pointing out that free Na^{+} ion is the dominating aqueous species (Fig. 3.62b). The main aqueous complexes are: (1) the $NaSO_4^{-}$ ion pair in 45 reservoir liquids, of which 35 from Dixie Valley and 10 from Long Valley, of relatively low salinity and variable composition, Na–Cl,SO_4 or Na–Cl,HCO_3 or Na–HCO_3,Cl; (2) the $NaCl^{\circ}$ ion pair in the remaining 233 reservoir liquids, of which 105 from Miravalles, 55 from Berlin, 26 from Los Azufres, 19 from Cerro Prieto, 16 from Heber, 7 from Valles, and 5 from Coso, all of medium-high salinity and Na–Cl composition.

The reservoir liquids of Japan have fractions of free Na^{+} ion varying from 0.98 to 0.63, suggesting that free Na^{+} ion is the principal aqueous species (Fig. 3.62c). The lowest fractions of free Na^{+} ion are encountered in the high-salinity, Na–Cl reservoir

liquids of Fushime and Oku-aizu. The main aqueous complexes are: (1) the $NaCl^{\circ}$ ion pair in 98 reservoir liquids, of which 31 from Oku-aizu, 25 from Fushime, 21 from Mori-Nigorikawa, 7 from Onikobe, 6 from Oguni, 3 each from Takigami and Uenotai, and 1 each from Sumikawa and Wasabizawa; (2) the $NaSO_4^-$ ion pair in the remaining 23 reservoir liquids, of which 13 from Sumikawa and 10 from Takigami.

In the reservoir liquids of the Philippines, the fraction of free Na^+ ion ranges from 0.96 to 0.64. The lowest values pertain to the Na–Cl reservoir liquids with the highest salinities, mostly from Tongonan and some from Bacon-Manito (Fig. 3.62d). The main aqueous complex after the free Na^+ ion is the $NaCl^{\circ}$ ion pair in all the reservoir liquids apart from one, the Na–SO_4,Cl reservoir liquid MG32D_09 from Mahanagdong, whose speciation is dominated by free Na^+ ion followed by the $NaSO_4^-$ ion pair.

The reservoir liquids of New Zealand have high fractions of free Na^+ ion, varying from 0.98 to 0.73. There are only eleven reservoir liquids with values lower than 0.9, of which 1 is from Broadlands, 3 are from Mokai, and 7 are from Rotokawa (Fig. 3.62e). The $NaCl^{\circ}$ ion pair is the main aqueous species after the free Na^+ ion in all the reservoir liquids of New Zealand, apart from OK-2 from Orakeikorako in which the main aqueous complex is the $NaSO_4^-$ ion pair.

Leaving aside the reservoir brines of Asal that were modeled adopting the Pitzer's approach, most miscellaneous reservoir liquids have fractions of free Na^+ ion in the interval 0.927–0.993. Only 7 reservoir liquids have lower fractions of free Na^+ ion, with the minimum value of 0.509 pertaining to reservoir liquid MF-2 from Mofete (Fig. 3.62f). The $NaCl^{\circ}$ ion pair is the major aqueous species after the free Na^+ ion in 111 reservoir liquids, of which 30 from Olkaria, 29 from Tendaho, 27 from Yangbajing, 15 from Ribeira Grande, 3 each from Aluto-Langano and Mofete, and 2 each from Bagnore and Latera. The $NaSO_4^-$ ion pair is the prevailing aqueous species after the free Na^+ ion in 55 reservoir liquids, of which 28 from Kizildere, 12 from Olkaria, 7 from Tendaho, 5 from Yangbajing, and 3 from Latera.

The Fraction of Free K^+ Ion The fraction of free K^+ ion ranges from 0.81 to 0.997 in the reservoir liquids of Iceland, indicating that free K^+ ion is the prevailing aqueous species (Fig. 3.63a). The main aqueous complexes are: (1) the KSO_4^- ion pair in 154 reservoir liquids, of which 26 from Hellisheidi, 13 from Hveragerdi, 36 from Krafla, 37 from Námafjall, 13 from Nesjavellir, 18 from Bakki, 2 each from Reykholt, Reykjabol, and Seltjarnarnes, 1 each from Baer, Efri-Reykir, Leirà, Reykholar, and Reykjavik; (2) the KCl° ion pair in the remaining 28 cases, comprising the 25 high-salinity, Na–Cl reservoir liquids of Svartsengi and Reykjanes, 2 reservoir liquids from Nesjavellir and 1 from Hellisheidi.

Ignoring the reservoir brines of Salton Sea that were modeled adopting the Pitzer's approach, all the other reservoir liquids of Northern and Central America have fraction of free K^+ ion fluctuating from 0.83 to 0.993, pointing out that aqueous speciation is dominated by free K^+ ion (Fig. 3.63b). The main aqueous complexes are: (1) the KCl° ion pair in 232 reservoir liquids, of which 55 from Berlin, 19 from Cerro Prieto, 5 from Coso, 16 from Heber, 25 from Los Azufres, 105 from Miravalles, and 7 from Valles, all characterized by medium-high salinity and Na–Cl composition; (2) the

KSO_4^- ion pair in the other 46 reservoir liquids, including 35 of Dixie Valley and 10 of Long Valley, all of comparatively low salinity and varying composition, Na–Cl,SO_4 or Na–Cl,HCO_3 or Na-HCO_3,Cl, as well as the Na–Cl reservoir liquid AZ-14 of Los Azufres that has a relatively low temperature, 236 °C, compared to the other fluids of this field.

Most reservoir liquids of Japan have fractions of free K^+ ion varying from 0.99 to 0.92. Somewhat lower values, in the interval 0.91–0.90, occur in a few high-salinity, Na–Cl reservoir liquids from Fushime (Fig. 3.63c). A Na–Cl,SO_4 reservoir liquid of relatively low salinity from Sumikawa, code S-2_82, with 406 mg Cl/kg and 401 mg SO_4/kg has an even lower fraction of free K^+ ion, 0.88. Therefore, free K^+ ion prevails in all the reservoir liquids of Japan and is accompanied by the following main aqueous complexes: (1) the KCl° ion pair in 78 reservoir liquids, of which 30 from Oku-aizu, 25 from Fushime, 14 from Mori-Nigorikawa, 7 from Onikobe, 1 each from Uenotai and Wasabizawa; (2) the KSO_4^- ion pair in the other 43 reservoir liquids, of which 14 from Sumikawa, 13 from Takigami, 7 from Mori-Nigorikawa, 6 from Oguni, 2 from Uenotai, and 1 from Oku-aizu.

In the reservoir liquids of the Philippines, the fraction of free K^+ ion varies from 0.99 to 0.83. Values lower than 0.93 are found in eight Na–Cl reservoir liquids from Tongonan, six Na–Cl reservoir liquids from Bacon-Manito, and two reservoir liquids from Mahanagdong (Fig. 3.63d). Of these two Mahanagdong reservoir liquids, MG32D_09 has Na–SO_4,Cl composition and low salinity, while MG35D_09 belongs to the Na–Cl facies, but has an unusually high SO_4 concentration. Therefore, free K^+ ion dominates the speciation of all the reservoir liquids of the Philippines and is complemented by: (1) the KCl° ion pair in 138 cases, of which 49 from Bacon-Manito, 28 from Palinpinon, 26 from Alto Peak, 24 from Mahanagdong, and 11 from Tongonan; (2) the KSO_4^- ion pair in the remaining 8 cases, of which 4 from Mahanagdong (including samples MG32D_09 and MG35D_09), 2 from Bacon-Manito, and 1 each from Alto Peak and Palinpinon.

The reservoir liquids of New Zealand are characterized by high fractions of free K^+ ion, ranging from 0.99 to 0.92. One reservoir liquid only, RK-4b from Rotokawa, has fraction of free K^+ ion lower than 0.95 (Fig. 3.63e). The KCl° aqueous complex is the main species after the free K^+ ion in 66 of these 93 reservoir liquids, of which 34 from Broadlands, 9 from Rotokawa, 7 each from Ngatamariki and Wairakei, 5 from Ngawha and 4 from Mokai. The KSO_4^- ion pair is the main species after the free K^+ ion in 27 reservoir liquids, of which 7 each from Broadlands and Ngawha, 6 from Waiotapu, 4 from Kawerau, 2 from Wairakei, and 1 from Orakeikorako.

Disregarding the high-salinity reservoir liquids of Asal that were modeled using the Pitzer's equations, all miscellaneous reservoir liquids except two have fractions of free K^+ ion higher than 0.90 up to a maximum of 0.996. The two exceptions have fractions of free K^+ ion of 0.887 and 0.825 and are from Latera and Mofete, respectively (Fig. 3.63f). The KSO_4^- ion pair is the dominant aqueous species after the free K^+ ion in 159 reservoir liquids, of which 41 from Olkaria, 36 from Tendaho, 31 from Yangbajing, 28 from Kizildere, 15 from Ribeira Grande, 5 from Latera, and 3 from Aluto-Langano. The KCl° ion pair is the principal aqueous species after the

free K^+ ion in the remaining 7 reservoir liquids, of which 3 from Mofete, 2 from Bagnore, and 1 each from Olkaria and Yangbajing.

The Fraction of Free Ca^{2+} Ion The medium-temperature reservoir liquids of Iceland and those of Hveragerdi have fractions of free Ca^{2+} ion in the interval 0.89–0.51, whereas all the other high-temperature reservoir liquids of Iceland have lower fractions of free Ca^{2+} ion, in the range 0.46–0.04 (Fig. 3.64a). The Ca speciation varies from site to site, as a function of the chemical characteristics and temperature. The main aqueous species are: (1) the $CaOH^+$ aqueous complex in 66 reservoir liquids, of which 24 from Hellisheidi, 21 from Námafjall, 14 from Nesjavellir, and 7 from Krafla; (2) the free ion Ca^{2+} in 53 reservoir liquids, of which 18 from Bakki, 13 from Hveragerdi, 10 from Námafjall, 2 each from Reykholt, Reykjabol, and Seltjarnarnes, and 1 each from Baer, Efri-Reykir, Krafla, Leirà, Reykholar, and Reykjavik; (3) the $CaSO_4^\circ$ ion pair in 30 reservoir liquids, of which 24 from Krafla and 6 from Námafjall; (4) the $CaCl^+$ ion pair in the 25 high-salinity, Na–Cl reservoir liquids from Reykjanes and Svartsengi; (5) the $CaHCO_3^+$ aqueous complex in 8 reservoir liquids, of which 4 from Krafla, 3 from Hellisheidi, and 1 from Nesjavellir.

Apart from the reservoir liquids of Salton Sea that were modeled using the Pitzer's approach, all the other reservoir liquids of Northern and Central America have fractions of free Ca^{2+} ion varying from 0.75 to 0.03 (Fig. 3.64b). The free ion Ca^{2+} is the prevailing aqueous species in 113 reservoir liquids, of which 85 from Miravalles, 16 from Heber, 10 from Long Valley, and 1 each from Coso and Los Azufres. The ion pair $CaCl^+$ is the major aqueous species in 130 reservoir liquids, of which 55 from Berlin, 25 from Los Azufres, 20 from Miravalles, 19 from Cerro Prieto, 7 from Valles, and 4 from Coso. The aqueous complex $CaSO_4^\circ$ is the main aqueous species in the 34 reservoir liquids of low-salinity and Na–Cl,SO_4 composition from Dixie Valley, while the $CaHCO_3^+$ ion pair prevails in the other reservoir liquid of low-salinity and Na–Cl,HCO_3 composition from this field.

Most reservoir liquids of Japan have fractions of free Ca^{2+} ion lower than 0.5 (Fig. 3.64c), with the lowest values, from 0.12 to 0.08 in 12 samples, of which 8 from Fushime, 2 from Uenotai, and 1 each from Ozu-aizu and Sumikawa. The free Ca^{2+} ion is the main aqueous species in 32 reservoir liquids, of which 9 from Mori-Nigorikawa, 9 from Takigami, 6 from Oguni, 5 from Oku-aizu, 2 from Sumikawa, and 1 from Onikobe. The ion pair $CaCl^+$ is the major aqueous species in 69 reservoir liquids, of which 26 from Oku-aizu, 25 from Fushime, 11 from Mori-Nigorikawa, 6 from Onikobe, and 1 from Wasabizawa. The aqueous complex $CaSO_4^\circ$ is the prevailing aqueous species in 11 reservoir liquids, of which 8 from Sumikawa and 3 from Takigami. The ion pair $CaOH^+$ is the prevalent aqueous species in 6 reservoir liquids, of which 3 from Sumikawa and 3 from Uenotai. The $CaHCO_3^+$ ion pair prevails in 2 reservoir liquids only, 1 from Mori-Nigorikawa and 1 from Takigami.

All the Na–Cl reservoir liquids of the Philippines distribute in a tight trend in the diagram of aquifer temperature versus the fraction of free Ca^{2+} ion (Fig. 3.64d), but the Na–SO_4,Cl reservoir liquid MG32D_09 from Mahanagdong deviates from this trend. The fraction of free Ca^{2+} ion ranges from 0.54 to 0.07 in these reservoir liquids. The main ion complex is the $CaCl^+$ ion pair in all these aqueous solutions

apart from the reservoir liquids OP-6 Da from Bacon-Manito and MG32D_09 from Mahanagdong, in which the prevailing aqueous complexes are the $CaHCO_3^+$ and $CaSO_4^\circ$ ion pairs, respectively.

The 93 reservoir liquids of New Zealand have fractions of free Ca^{2+} ion varying from 0.75 to 0.05, 77 have fractions of free Ca^{2+} ion lower than 0.5, while the remaining 16 entries (6 from Waiotapu, 4 from Ngawha, 4 from Wairakei, and 2 from Broadlands) have fractions of free Ca^{2+} ion higher than 0.5 (Fig. 3.64e). The main aqueous species are: (1) the $CaHCO_3^+$ ion pair in 38 reservoir liquids, of which 27 from Broadlands, 5 from Ngawha, 3 from Kawerau, 2 from Rotokawa, and 1 from Orakeikorako; (2) free Ca^{2+} ion in 29 reservoir liquids, of which 9 from Wairakei, 7 from Ngawha, 6 each from Broadlands and Waiotapu, and 1 from Kawerau; (3) the $CaCl^+$ ion pair in 26 reservoir liquids, of which 8 from Broadlands, 7 each from Ngatamariki and Rotokawa, and 4 from Mokai.

Leaving aside the reservoir brines of Asal that were modeled using the Pitzer's approach, the considered miscellaneous reservoir liquids have fractions of free Ca^{2+} ion ranging from 0.81 to 0.03, with 43 entries higher than 0.50 and 124 cases lower than this threshold (Fig. 3.64f). The main aqueous species are: (1) free Ca^{2+} ion in 86 reservoir liquids, of which 35 from Tendaho, 30 from Yangbajing, 18 from Olkaria, 2 from Latera, and 1 from Kizildere; (2) the $CaHCO_3^+$ ion pair in 66 reservoir liquids, of which 27 from Kizildere, 15 each from Olkaria and Ribeira Grande, 3 each from Aluto-Langano and Latera, 2 from Yangbajing, and 1 from Bagnore; (3) the CaF^+ ion pair in 7 reservoir liquids from Olkaria; (4) the $CaCl^+$ ion pair in 4 reservoir liquids, of which 3 from Mofete and 1 from Bagnore; (5) the $CaSO_4^\circ$ ion pair in 2 reservoir liquids, one from Olkaria and one from Tendaho; (6) the $CaOH^+$ ion pair in 1 reservoir liquid from Olkaria.

The Fraction of Free Mg^{2+} Ion The fraction of free Mg^{2+} ion is higher than 0.50 in all the reservoir liquids of medium-temperature of Iceland and in most of Hveragerdi, up to a maximum of 0.85. In contrast, all the other high-temperature reservoir liquids of Iceland have fraction of free Mg^{2+} ion in the interval 0.45–0.02 (Fig. 3.65a). The Mg speciation of the 165 reservoir liquids with Mg concentration higher than detection limit is different from one field to another, depending on chemistry and temperature. The main aqueous species are: (1) the $MgOH^+$ ion pair in 82 reservoir liquids, of which 29 from Námafjall, 20 from Hellisheidi, 19 from Krafla, 13 from Nesjavellir, and 1 from Hveragerdi; (2) the free Mg^{2+} ion in 43 reservoir liquids, of which 18 from Bakki, 11 from Hveragerdi, 3 from Námafjall, 2 each from Reykholt, Reykjabol, and Seltjarnarnes,1 each from Baer, Efri-Reykir, Leirà, Reykholar, and Reykjavik; (3) the $MgCl^+$ ion pair in the 25 high-salinity, Na–Cl reservoir liquids from Reykjanes and Svartsengi; (4) the $MgSO_4^\circ$ ion pair in 15 reservoir liquids, of which 14 from Krafla and 1 from Námafjall.

Excluding the reservoir liquids of Salton Sea that were modeled adopting the Pitzer's equations, all the reservoir liquids of Northern and Central America have fractions of free Mg^{2+} ion ranging from 0.74 to 0.07 (Fig. 3.65b). The free ion Mg^{2+} is the predominant aqueous species in 145 reservoir liquids, of which 105 from Miravalles, 16 from Heber, 10 from Long Valley, 7 from Los Azufres, 3 from Valles,

and 2 each from Cerro Prieto and Coso. The $MgCl^+$ ion pair is the principal aqueous species in 94 reservoir liquids, of which 55 from Berlin, 18 from Los Azufres, 17 from Cerro Prieto, 3 from Coso, and 1 from Valles. The $MgSO_4^\circ$ ion pair is the dominant aqueous species in 34 reservoir liquids from Dixie Valley, characterized by low-salinity and Na–Cl,SO_4 composition, whereas the $MgHCO_3^+$ ion pair is the predominant species in the other reservoir liquid of low-salinity and Na–Cl,HCO_3 composition from this site as well as in 2 reservoir liquids from Valles. The aqueous speciation of the remaining reservoir liquid from Valles is dominated by the $MgOH^+$ ion pair.

Most reservoir liquids of Japan have fractions of free Mg^{2+} ion lower than 0.5, with the lowest values, from 0.13 to 0.04 in 11 reservoir liquids, of which 8 from Sumikawa and 3 from Uenotai (Fig. 3.65c). The free ion Mg^{2+} is the principal aqueous species in 43 reservoir liquids, of which 13 from Mori-Nigorikawa, 10 from Oku-aizu, 7 from Onikobe, 5 from Oguni, 4 from Takigami, 2 from Sumikawa, and 1 from Wasabizawa. The $MgCl^+$ ion pair is the prevailing aqueous species in 49 reservoir liquids, of which 25 from Fushime, 20 from Oku-aizu, and 4 from Mori-Nigorikawa. The $MgOH^+$ ion pair is the main aqueous species in 13 reservoir liquids, of which 9 from Sumikawa, 3 from Uenotai, and 1 from Oguni. The $MgSO_4^\circ$ ion pair is the predominant aqueous species in 11 reservoir liquids, of which 8 from Takigami and 3 from Sumikawa. The $MgHCO_3^+$ ion pair is the predominant species in the remaining 6 reservoir liquids, of which 4 from Mori-Nigorikawa and 1 each from Oku-aizu and Takigami.

A tight trend comprises all the Na–Cl reservoir liquids of the Philippines in the binary plot of aquifer temperature versus the fraction of free Mg^{2+} ion (Fig. 3.65d), but the Na-SO_4,Cl reservoir liquid MG32D_09 from Mahanagdong does not belong to this trend. The fraction of free Mg^{2+} ion varies from 0.64 to 0.13 in these 145 aqueous solutions with concentration of Mg higher than detection limit. The $MgCl^+$ ion pair is the main aqueous species in 104 reservoir liquids, of which 42 from Bacon-Manito, 21 from Palinpinon, 17 from Mahanagdong, 13 from Alto Peak, and 11 from Tongonan. The free ion Mg^{2+} is the major aqueous species in 40 reservoir liquids, of which 14 from Alto Peak, 10 from Mahanagdong, and 8 each from Bacon-Manito and Palinpinon. The $MgSO_4^\circ$ ion pair prevails only in the reservoir liquid MG32D_09 from Mahanagdong.

The 81 reservoir liquids of New Zealand with Mg concentrations higher than the detection limit have fractions of free Mg^{2+} ion varying from 0.64 to 0.07, but apart from 9 entries (4 from Ngawha, 4 from Wairakei, and 1 from Broadlands), the other 72 have fractions of free Mg^{2+} ion lower than 0.5 (Fig. 3.65e). The main aqueous species are: (1) the $MgHCO_3^+$ ion pair in 36 reservoir liquids, of which 23 from Broadlands, 7 from Ngawha, and 3 each from Kawerau and Rotokawa; (2) the free Mg^{2+} ion in 26 reservoir liquids, of which 7 each from Ngatamariki and Wairakei, 6 from Broadlands, 5 from Ngawha, and 1 from Kawerau; (3) the $MgOH^+$ ion pair in 12 reservoir liquids, of which 9 from Broadlands, 2 from Rotokawa, and 1 from Wairakei; (4) the $MgCl^+$ ion pair in 7 reservoir liquids, of which 4 from Rotokawa and 3 from Mokai.

Disregarding the high-salinity reservoir liquids of Asal that were modeled adopting the Pitzer's equations and the 9 reservoir liquids with Mg concentration lower than detection limit, the other 157 miscellaneous reservoir liquids have fractions of free Mg^{2+} ion ranging from 0.77 to 0.03, with 34 cases higher than 0.50 and 123 entries lower than 0.50 (Fig. 3.65f). The main aqueous species are: (1) free Mg^{2+} ion in 56 reservoir liquids, of which 30 from Yangbajing, 24 from Tendaho, and 1 each from Latera and Kizildere; (2) the $MgHCO_3^+$ ion pair in 51 reservoir liquids, of which 26 from Kizildere, 8 from Ribeira Grande, 7 from Olkaria, 3 each from Aluto-Langano and Latera, and 2 each from Yangbajing and Bagnore; (3) the MgF^+ ion pair in 30 reservoir liquids from Olkaria; (4) the $MgOH^+$ ion pair in 15 reservoir liquids, of which 11 from Tendaho and 4 from Olkaria; (5) the $MgCl^+$ ion pair in 3 reservoir liquids from Mofete; (6) the $MgSO_4^\circ$ ion pair in 2 reservoir liquids, one from Latera and one from Tendaho.

A Final Remark The effects of ion association becomes more and more important with increasing ionic strength and temperature and, consequently, the free ion fractions deviate more and more from unity. Nevertheless, free Na^+ and K^+ ions generally represent by far the largest fraction of total dissolved Na and K, whereas free Mg^{2+} and Ca^{2+} ions often account for a minor fraction of total dissolved Mg and Ca.

3.8.4 The Activity Coefficient of Undissociated $SiO_{2(aq)}$

Consistent with the Garrels and Christ (1965) recommendation, the activity coefficients of $SiO_{2(aq)}$ is set to unity for the relatively dilute solutions, that is when the activity coefficients of individual ions are calculated by means of the B-dot equation (see Sect. 2.3.3). This approach was adopted for all reservoir liquids except the brines of Asal and Salton Sea.

In contrast, the Pitzer equations (see Sect. 2.3.4) were used to model the speciation of these brines, representing the focus of the present discussion. The activity coefficients of $SiO_{2(aq)}$ and the ionic strengths of the Asal and Salton Sea brines are contrasted in the two binary plots of Fig. 3.66a, b, in which the other reservoir liquids of Northern and Central America and the other miscellaneous reservoir liquids, respectively, are also displayed as usual. These two graphs show that the Asal brines have activity coefficient of $SiO_{2(aq)}$ oscillating from 0.915 to 1.09 and ionic strengths of 0.22–2.5 mol/kg, whereas the Salton Sea brines have activity coefficient of $SiO_{2(aq)}$ varying from 0.859 to 0.670 and ionic strengths of 4.2–5.5 mol/kg. These significant deviations from unity of the activity coefficient of $SiO_{2(aq)}$ are caused by the increasing solute-solvent and solute-solute interactions with increasing ionic strength.

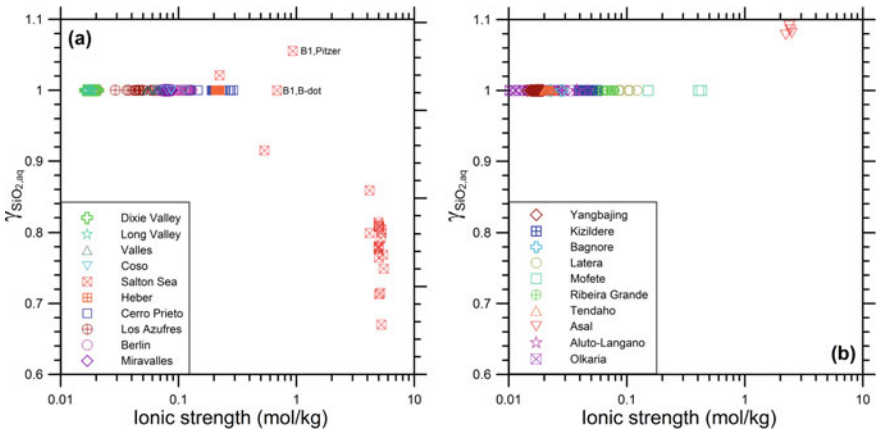

Fig. 3.66 Correlations diagrams showing the activity coefficient of undissociated $SiO_{2(aq)}$ as a function of ionic strength for the reservoir liquids of **a** Northern and Central America and **b** Miscellaneous geothermal fields

3.8.5 The Activity Coefficients of Free Na^+, K^+, Ca^{2+}, and Mg^{2+} Ions

The activity coefficients of free Na^+, K^+, Ca^{2+}, and Mg^{2+} ions are plotted versus aquifer temperature in the binary graphs of Figs. 3.67, 3.68, 3.69 and 3.70, respectively. In each diagram there are also two lines displaying the dependence of individual-ion activity coefficients on temperature at two fixed ionic strengths. These two lines were generated using the B-dot equation (see Sect. 2.3.3) and choosing two suitable ionic strengths to bracket most reservoir liquids shown in each plot. In detail:

1. For the geothermal fields in Iceland, the two selected ionic strengths are 0.0069 mol/kg, which is the average of the reservoir liquids from Krafla, Námafjall, Hellisheidi, Nesjavellir, Hveragerdi, and the medium temperature sites other than Bakki and Seltjarnarnes, and 0.34 mol/kg, which is the mean of the reservoir liquids from Reykjanes and Svartsengi.
2. For the geothermal fields in Northern and Central America, the two chosen ionic strengths are 0.018 mol/kg, which is the average of the reservoir liquids from Dixie Valley and Long Valley, and 0.22 mol/kg, which is the mean of the reservoir liquids from Cerro Prieto and Heber.
3. For the geothermal fields in Japan, the two adopted ionic strengths are 0.015 mol/kg, which is the average of the reservoir liquids from Sumikawa and Uenotai, and 0.34 mol/kg, which is the mean of the reservoir liquids from Fushime.
4. For the geothermal fields of the Philippines, the two selected ionic strengths are 0.046 mol/kg, which is the mean of the reservoir liquids encountered by well

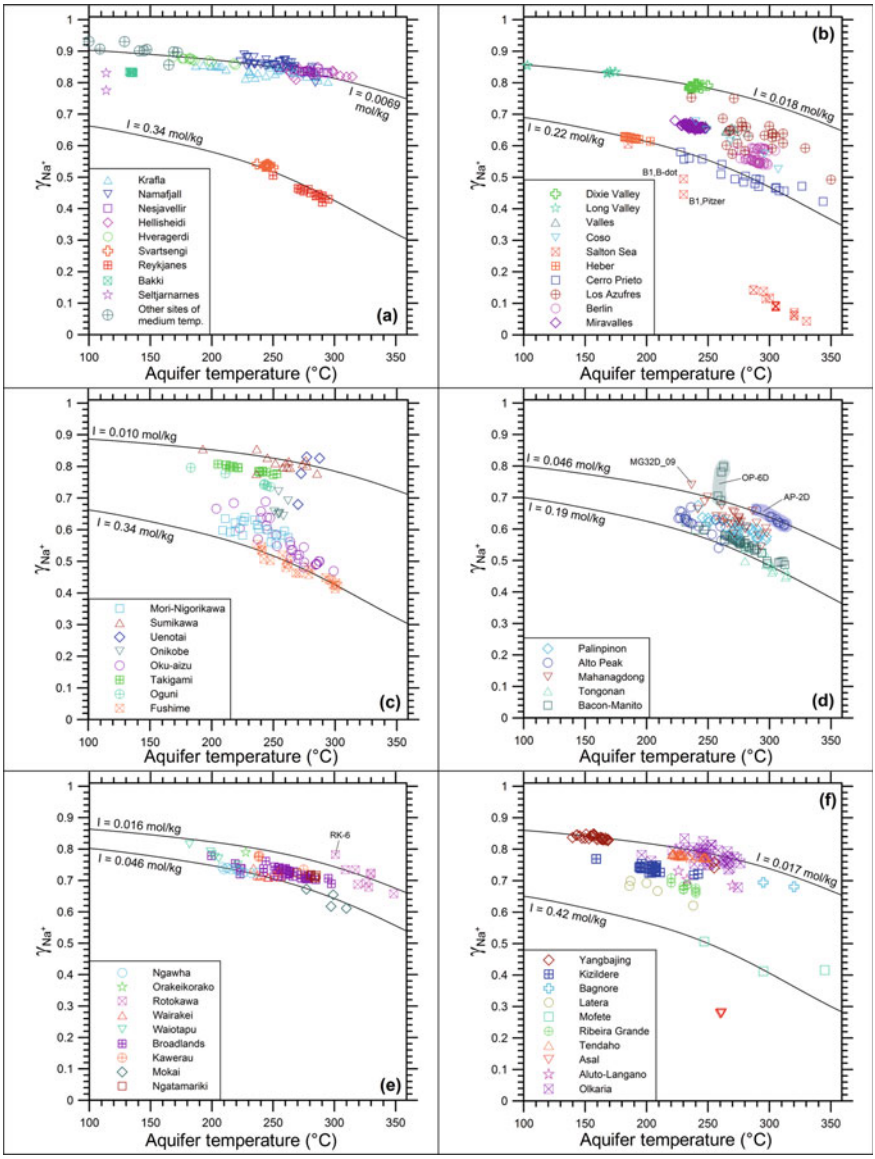

Fig. 3.67 Correlations diagrams showing the activity coefficient of free Na^+ ion as a function of aquifer temperature for the reservoir liquids of **a** Iceland, **b** Northern and Central America, **c** Japan, **d** The Philippines, **e** New Zealand, and **f** Miscellaneous geothermal fields

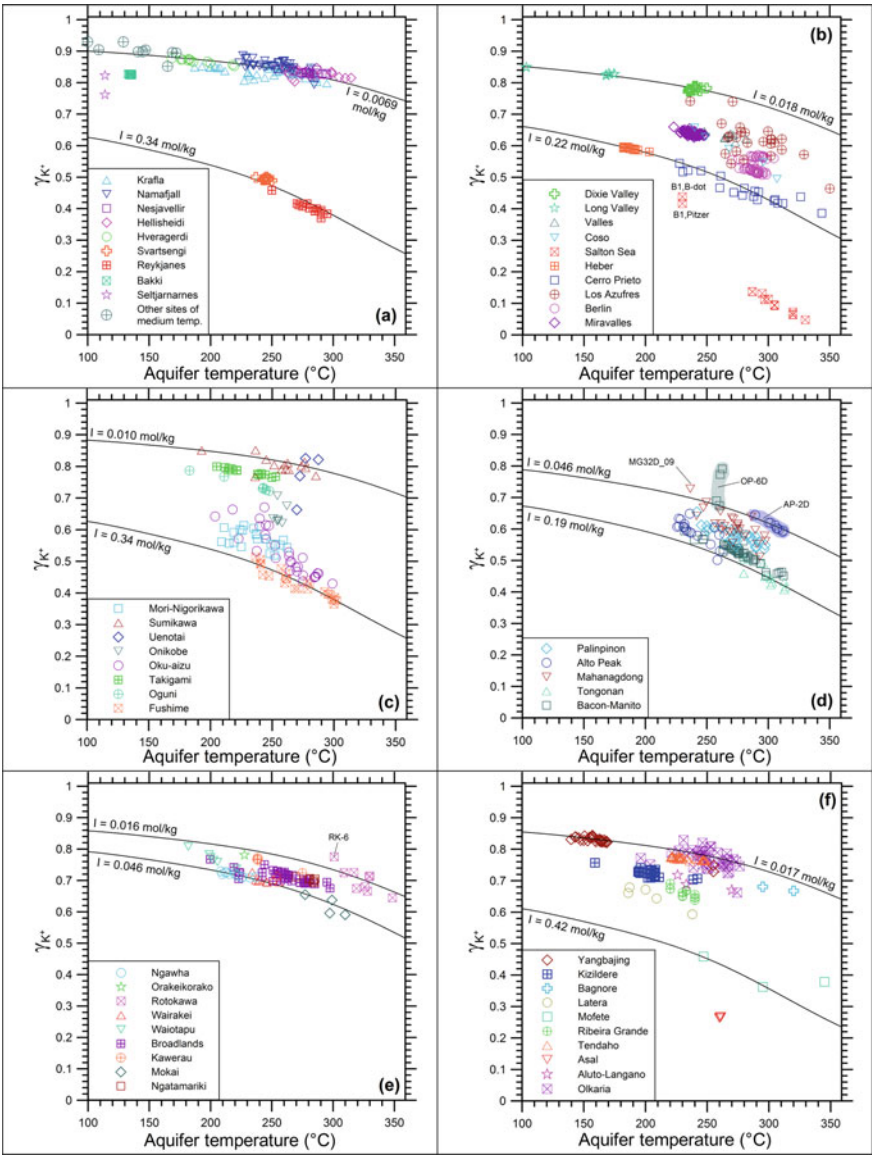

Fig. 3.68 Correlations diagrams showing the activity coefficient of free K^+ ion as a function of aquifer temperature for the reservoir liquids of **a** Iceland, **b** Northern and Central America, **c** Japan, **d** The Philippines, **e** New Zealand, and **f** Miscellaneous geothermal fields

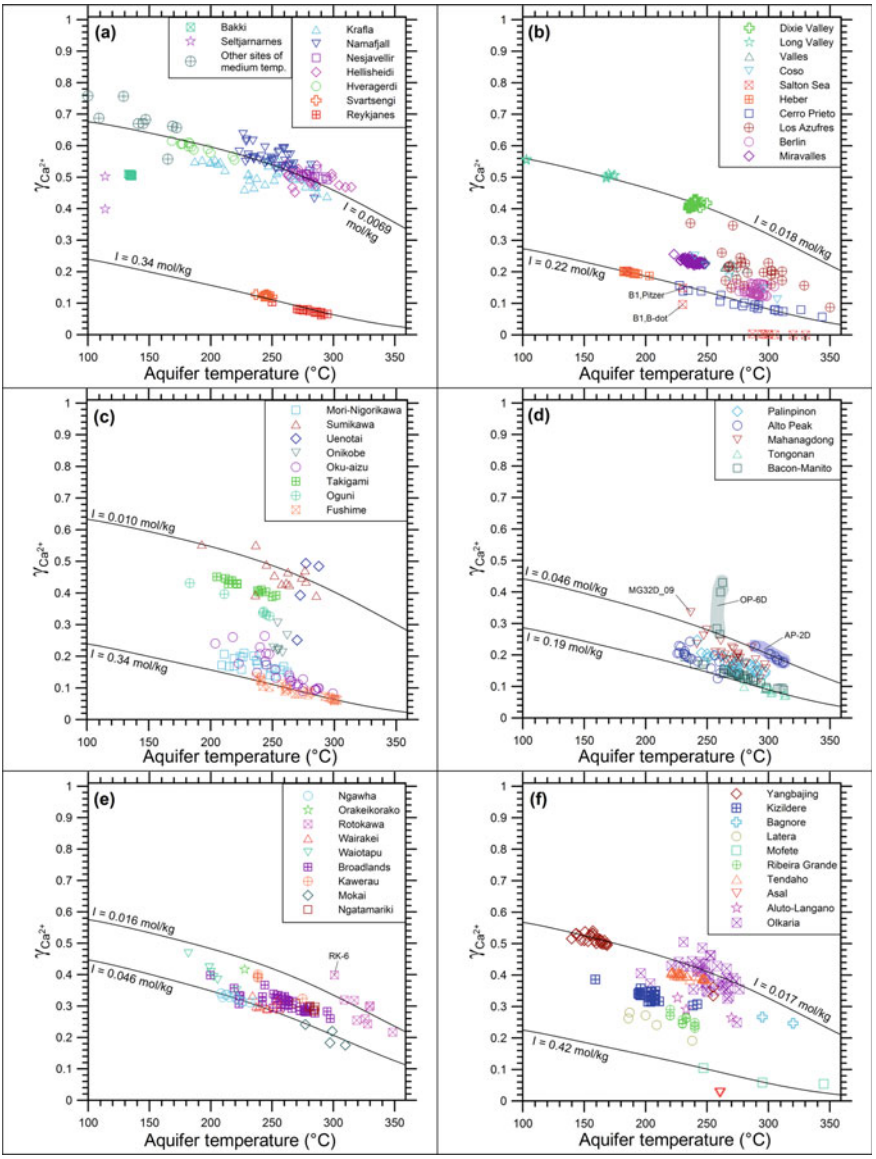

Fig. 3.69 Correlations diagrams showing the activity coefficient of free Ca^{2+} ion as a function of aquifer temperature for the reservoir liquids of **a** Iceland, **b** Northern and Central America, **c** Japan, **d** The Philippines, **e** New Zealand, and **f** Miscellaneous geothermal fields

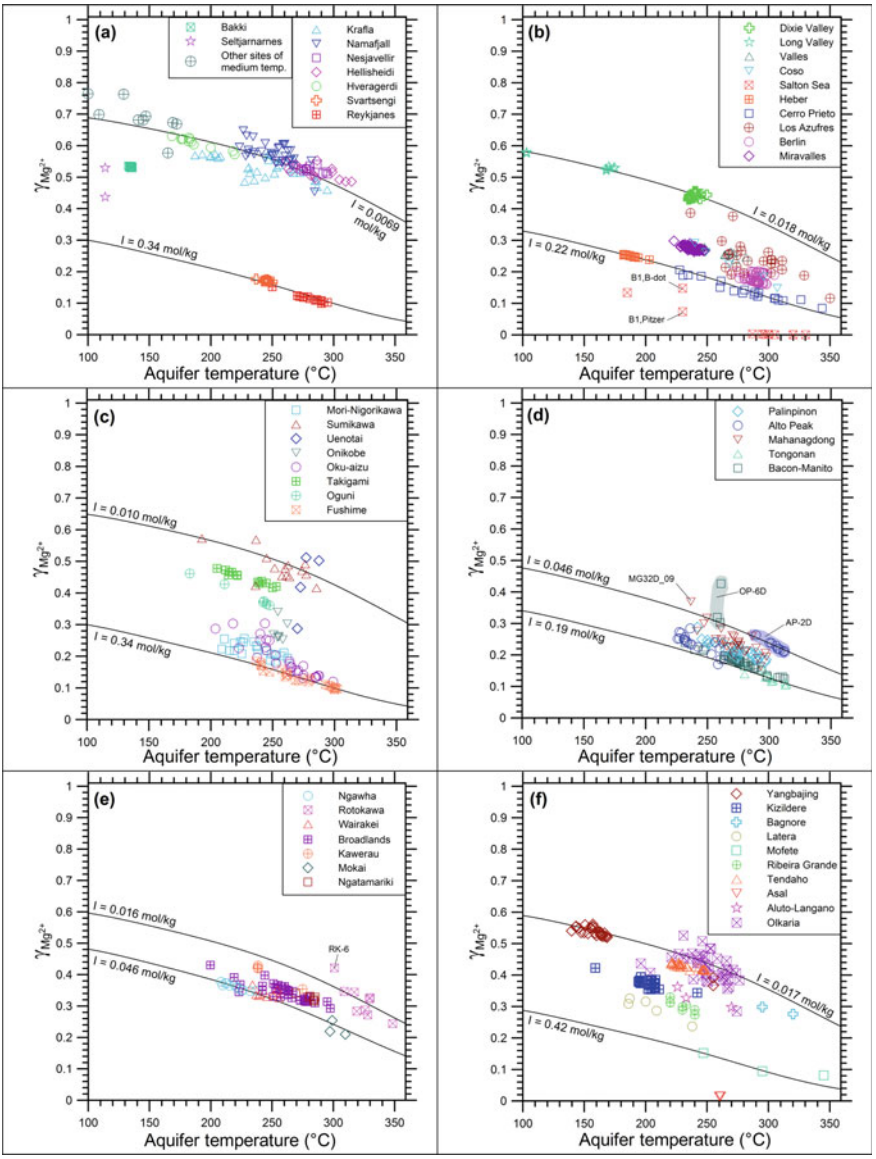

Fig. 3.70 Correlations diagrams showing the activity coefficient of free Mg^{2+} ion as a function of aquifer temperature for the reservoir liquids of **a** Iceland, **b** Northern and Central America, **c** Japan, **d** The Philippines, **e** New Zealand, and **f** Miscellaneous geothermal fields

AP2D of Alto Peak, and 0.19 mol/kg, which is the average of the reservoir liquids from Tongonan.

5. For the New Zealand geothermal fields, the two chosen ionic strengths are 0.016 mol/kg, which is the mean of the reservoir liquids from Rotokawa, and 0.046 mol/kg, which is the average of the reservoir liquids from Mokai and Ngawha.
6. For the miscellaneous geothermal fields, the two adopted ionic strengths are 0.017 mol/kg, which is the mean of the reservoir liquids from Olkaria and Yangbajing, and 0.42 mol/kg, which is the average of the reservoir liquids met by well MF-1 of Mofete.

The Activity Coefficient of Free Na^+ Ion The activity coefficient of free Na^+ ion varies from 0.420 to 0.931 for the reservoir liquids of Iceland, from 0.423 to 0.856 for the reservoir liquids of Northern and Central America apart from Salton Sea, from 0.413 to 0.855 for the reservoir liquids from the geothermal fields in Japan, from 0.447 to 0.798 for the reservoir liquids from the geothermal fields in the Philippines, from 0.611 to 0.815 for the reservoir liquids from the New Zealand geothermal fields, and from 0.412 to 0.849 for the reservoir liquids from the miscellaneous geothermal fields disregarding Asal (Fig. 3.67).

The Activity Coefficient of Free K^+ Ion The activity coefficient of free K^+ ion ranges from 0.370 to 0.930 for the reservoir liquids of Iceland, from 0.386 to 0.850 for the reservoir liquids of Northern and Central America except Salton Sea, from 0.365 to 0.852 for the reservoir liquids from the geothermal fields in Japan, from 0.407 to 0.791 for the reservoir liquids from the geothermal fields in the Philippines, from 0.591 to 0.807 for the reservoir liquids from the New Zealand geothermal fields, and from 0.363 to 0.844 for the reservoir liquids from the miscellaneous geothermal fields ignoring Asal (Fig. 3.68).

The Activity Coefficient of Free Ca^{2+} Ion The activity coefficient of free Ca^{2+} ion varies from 0.0619 to 0.758 for the reservoir liquids of Iceland, from 0.0571 to 0.558 for the reservoir liquids of Northern and Central America disregarding Salton Sea, from 0.0589 to 0.554 for the reservoir liquids from the geothermal fields in Japan, from 0.0704 to 0.430 for the reservoir liquids from the geothermal fields in the Philippines, from 0.176 to 0.467 for the reservoir liquids from the New Zealand geothermal fields, and from 0.0543 to 0.540 for the reservoir liquids from the miscellaneous geothermal fields apart from Asal (Fig. 3.69).

The Activity coefficient of free Mg^{2+} Ion The activity coefficient of free Mg^{2+} ion ranges from 0.0989 to 0.765 for the reservoir liquids of Iceland, from 0.0849 to 0.580 for the reservoir liquids of Northern and Central America neglecting Salton Sea, from 0.0941 to 0.572 for the reservoir liquids from the geothermal fields in Japan, from 0.104 to 0.426 for the reservoir liquids from the geothermal fields in the Philippines, from 0.210 to 0.431 for the reservoir liquids from the New Zealand geothermal fields, and from 0.0816 to 0.562 for the reservoir liquids from the miscellaneous geothermal fields ignoring Asal (Fig. 3.70).

Individual-Ion Activity Coefficients for the Asal and Salton Sea Reservoir Brines The individual-ion activity coefficients for the reservoir brines from Asal, of ionic strength of 2.2–2.5 mol/kg, and Salton Sea, of ionic strength of 4.2–5.5 mol/kg, whose speciation was modeled using the Pitzer's approach (see Sect. 2.3.4), are lower or even much lower than those calculated by the B-dot equation for the other reservoir liquids. This is not surprising because solute-solvent and solute-solute interactions are chiefly described by activity coefficients and considering few ion pairs, in the Pitzer's approach, as already recalled in previous section. In detail:

1. The activity coefficient of free Na^+ ion varies from 0.276 to 0.281 for the Asal reservoir brines and from 0.0436 to 0.143 for the Salton Sea reservoir brines.
2. The activity coefficient of free K^+ ion ranges from 0.262 to 0.268 for the Asal reservoir brines and from 0.0478 to 0.137 for the Salton Sea reservoir brines.
3. The activity coefficient of free Ca^{2+} ion varies from 0.0252 to 0.0276 for the Asal reservoir brines and from 5.66×10^{-5} to 3.04×10^{-3} for the Salton Sea reservoir brines.
4. The activity coefficient of free Mg^{2+} ion varies from 0.0140 to 0.0152 for the Asal reservoir brines and from 1.09×10^{-4} to 2.87×10^{-3} for the Salton Sea reservoir brines.

A Final Remark All in all, the activity coefficients of free Na^+ and K^+ ions and especially those of free Mg^{2+} and Ca^{2+} ions exhibit large deviations from unity, which become more and more important with increasing ionic strength and temperature.

3.9 Final Considerations on the Reservoir Liquids

All the 1013 reservoir liquids of high and medium temperature coming from different geothermal systems worldwide are probably mature waters, irrespective of the sources and processes contributing the main solutes and controlling the different chemical compositions, salinities, and pH values of these reservoir liquids. In other terms, all these reservoir liquids have probably attained or closely approached the condition of chemical equilibrium with the hydrothermal (secondary) minerals occurring in the geothermal reservoirs of provenance, possibly excluding a few cases, such as some reservoir liquids of Onikobe, whose chemistry is impacted by magmatic-derived HCl and H_2SO_4.

If so, it is necessary to reconsider the axiom that neutral sodium-chloride reservoir liquids are the only mature waters in equilibrium with hydrothermal minerals. This axiom applies to the geothermal systems situated along convergent plate boundaries, such as those of Central America (e.g., Miravalles and Berlin in Sect. 3.3), Japan (Sect. 3.4), the Philippines (Sect. 3.5), and New Zealand (Sect. 3.6), as well as to other geothermal systems, as shown by Ellis and Mahon (1977) and Giggenbach (1988) among the others. However, this axiom does not apply to some geothermal

systems positioned along the oceanic rift zone in Iceland, such as Krafla, Námafjall, Hveragerdi and, to some extent, Hellisheidi and Nesjavellir (Sect. 3.2), some geothermal systems located along the continental rift zone in East Africa, such as Aluto-Langano and, to some extent, Olkaria (Sect. 3.7), some geothermal systems of the Basin and Range Province in Northern America, such as Dixie Valley and Long Valley (Sect. 3.3), the fault-controlled geothermal systems of Turkey, such as Kizildere (Sect. 3.7) and, at least in part, the Ribeira Grande geothermal system in the Azores islands, occupying the triple junction between the North American, African and Eurasian Plates (Sect. 3.7).

Therefore, we suggest to adopt a comprehensive approach to water classification, including not only the triangular diagram of major anions but also the triangular diagram of main cations and suitable salinity plots, as shown in previous sections. These graphs should be prepared from the concentrations in equivalent units and a chemical terminology should be adopted. Chloride-solute diagrams and enthalpy-chloride plots (not shown here) are also essential for identifying mixing and boiling processes, as well as to reconstruct the behavior of the solutes of interest. Based on a sufficiently complete analysis of the existing geochemical data, it should be possible to distinguish mature waters suitable for geothermometry from immature waters unsuitable for geothermometry, also in surface exploration projects, in which fluids delivered from deep wells are not available.

Total concentrations of cations and SiO_2 are normally inserted into traditional geothermometers and f_{CO_2} indicators, but mineral-solution equilibrium fixes the activities of free ions and undissociated $SiO_{2(aq)}$. The activities of Na^+, K^+, Mg^{2+}, and Ca^{2+} ions and undissociated $SiO_{2(aq)}$ deviate from the total concentrations of Na, K, Mg, Ca, and SiO_2, respectively, due to the formation of ion pairs and dissociation of silicic acid, as indicated by the fractions of free Na^+, K^+, Mg^{2+}, and Ca^{2+} ions and $SiO_{2(aq)}$ (Sects. 3.8.2 and 3.8.3), and because of solute-solvent and solute-solute interactions, as described by activity coefficients (Sects. 3.8.4 and 3.8.5). Above, it was shown that the effects of these processes can cause significant differences between activities and total concentrations, a fact that must be taken in due account, as we intend to do in this work, through the elaboration of theoretical, activity-based geothermometers and f_{CO_2} indicators.

Above, it was also shown that pH is strongly impacted by uncertainties in the computation of reservoir liquids chemistry (see Sect. 3.1.2). Therefore, the new theoretical geothermometers and f_{CO_2} indicators should involve variables which are not influenced or negligibly influenced by pH, like the concentrations and activities of non-volatile solutes.

References

Abe M, Yamada M, Kawano Y, Todaka N, Tezuka S (1995) Development of the Oguni geothermal field, Japan. In: Proceedings world geothermal congress, Florence, Italy, pp 1319–1322

Adams MC, Lemieux M, Moore JN, Johnson SD (1989) Fluid chemistry and hydrology of the Heber geothermal system, California. In: Proceedings, fourteenth workshop on geothermal reservoir engineering. Stanford University, Stanford, California, 24–26 Jan 1989. SGP-TR-122, pp 81–86

Aggarwal JK, Sheppard D, Mezger K, Pernicka E (2003) Precise and accurate determination of boron isotope ratios by multiple collector ICP-MS: origin of boron in the Ngawha geothermal system, New Zealand. Chem Geol 199:331–342

Akaku K (1990) Geochemical study on mineral precipitation from geothermal waters at the Fushime field, Kyushu, Japan. Geothermics 19:455–467

Akaku K, Reed MH, Yagi M, Kai K, Yasuda Y (1991) Chemical and physical processes occurring in the Fushime geothermal system, Kyushu, Japan. Geochem J 25:315–333

Ali S (2005) Geochemical studies of the Tendaho geothermal field. In: Proceedings world geothermal congress. Antalya, Turkey

Alvis-Isidro RR, Solana RR, D'Amore F, Nuti S, Gonfiantini R (1993) Hydrology of the Greater Tongonan geothermal system, Philippines, as deduced from geochemical and isotopic data. Geothermics 22:435–449

Angcoy EC (2010) Geochemical modelling of the high-temperature Mahanagdong geothermal field, Leyte, Philippines. UNU-GTP report 2010-1, 71p

Arellano VM, Torres MA, Barragán RM (2005) Thermodynamic evolution of the Los Azufres, Mexico, geothermal reservoir from 1982 to 2002. Geothermics 34:592–616

Ariki K, Kato H, Ueda A, Bamba M (2000) Characteristics and management of the Sumikawa geothermal reservoir, northeastern Japan. Geothermics 29:171–189

Ármannsson H, Gíslason G, Hauksson T (1982) Magmatic gases in well fluids aid the mapping of the flow pattern in a geothermal system. Geochim Cosmochim Ac 46:167-177

Ármansson H (2016) The fluid geochemistry of Icelandic high temperature geothermal areas. Appl Geochem 66:14–64

Arnórsson S (1978a) Major element chemistry of the geothermal sea-water at Reykjanes and Svartsengi, Iceland. Mineral Mag 42:209–220

Arnórsson S (1978b) Precipitation of calcite from flashed geothermal waters in Iceland. Contrib Mineral Petr 66:21–28

Arnórsson S (1995a) Geothermal systems in Iceland: structure and conceptual models—I. High-temperature areas. Geothermics 24:561–602

Arnórsson S (1995b) Geothermal systems in Iceland: Structure and conceptual models—II. Low-temperature areas. Geothermics 24:603–629

Arnórsson S, Stefánsson A (2005b). Wet-steam well discharges. II. Assessment of aquifer fluid compositions. In: Proceedings world geothermal congress. Antalya, Turkey

Arnórsson S, Grönvold K, Sigurdsson S (1978) Aquifer chemistry of four high-temperature geothermal systems in Iceland. Geochim Cosmochim Acta 42:523–536

Arnórsson S, Sigurdsson S, Svavarsson H (1982) The chemistry of geothermal waters in Iceland. I. Calculation of aqueous speciation from 0 to 370 °C. Geochim Cosmochim Acta 46:1513–1532

Arnórsson S, Gunnlaugsson E, Svavarsson H (1983a) The chemistry of geothermal waters in Iceland. III. Chemical geothermometry in geothermal investigations. Geochim Cosmochim Acta 47:567–577

Arnórsson S, Gunnlaugsson E, Svavarsson H (1983b) The chemistry of geothermal waters in Iceland. II. Mineral equilibria and independent variables controlling water compositions. Geochim Cosmochim Acta 47:547–566

Arnórsson S, Björnsson S, Muna ZW, Bwire-Ojiambo S (1990) The use of gas chemistry to evaluate boiling processes and initial steam fractions in geothermal reservoirs with an example from the Olkaria field, Kenya. Geothermics 19:497–514

Arnórsson S, Stefánsson A, Bjarnason JÖ (2005) Wet-steam well discharges. I. Sampling and calculation of total discharge compositions. Proceedings World Geothermal Congress, Antalya, Turkey

Arnórsson S, Stefánsson A, Bjarnason JO (2007) Fluid-fluid interactions in geothermal systems. Rev Mineral Geochem 65:259–312

Arnórsson S, Angcoy E, Bjarnason JÖ, Giroud N, Gunnarsson I, Kaasalainen H, Karingithi C, Stefánsson A (2010) Gas chemistry of volcanic geothermal systems. In: World geothermal congress, Bali, Indonesia

Auko LO (2014) Evaluation of fluid-mineral interaction in the Menengai geothermal system, Central Rift, Kenya. UNU-GTP report 2014-8, pp 39–64

Bacon CR, Duffield WA, Nakamura K (1980) Distribution of quaternary rhyolite domes of the Coso Range, California: implications for extent of the geothermal anomaly. J Geophys Res-Sol Earth 85(B5):2425–2433

Bailey RA, Dalrymple GB, Lanphere MA (1976) Volcanism, structure, and geochronology of Long Valley caldera, Mono County, California. J Geophys Res-Solid 81(5):725–744

Balducci S, Chelini W (1992) Hydrothermal equilibria in the active Mofete geothermal system, Phlegraean Fields, Naples, Italy. Acta Vulcanol Marinelli 2:17–34

Balmes CP (1994) The geochemistry of the Mahanagdong sector, Tongonan geothermal field, Philippines. UNU-GTP report 1994-2, pp 31–52

Baltasar AJ (1980) Interpretation of the water and gas chemistry from three geothermal areas in the Philippines—Manito in Albay, Biliran Island and Tongonan in Leyte. UNU-GTP report 1980-3, 55p

Banwell CJ (1957) Borehole measurements. In: Physics of the New Zealand thermal area, bulletin 123. DSIR, Wellington, New Zealand, pp 39–72

Battaglia A, Ceccarelli A, Ridolfi A, Frohlich K, Panichi C (1992) Radium isotopes in geothermal fluids in central Italy. Proceedings of international symposium on isotope techniques in water resources development, I.A.E.A., 11–15 Mar 1991, Vienna, pp 363–383

Battistelli A, Yiheyis A, Calore C, Ferragina C, Abatneh W (2002) Reservoir engineering assessment of Dubti geothermal field, northern Tendaho rift, Ethiopia. Geothermics 31:381–406

Berehannu MM (2014) Geochemical interpretation of discharge from Reykjanes well 29 and well 32. UNU-GTP report 2014-19, pp 351–368

Bertini G, Cappetti G, Dini I, Lovari F (1995) Deep drilling results and updating of geothermal knowledge of the Monte Amiata area. In: Proceedings of the world geothermal congress, Florence, Italy, vol 2, pp 1283–1286

Bixley PF, Clotworthy AW, Mannington WI (2009) Evolution of the Wairakei geothermal reservoir during 50 years of production. Geothermics 38:145–154

Bjarnason JÖ (2010) The chemical speciation program WATCH, version 2.4. ISOR–Iceland GeoSurvey, Reykjavik, Iceland

Browne PRL (1980) Joint channels in reservoir rocks of the Ngawha geothermal field, Northland, New Zealand. In: N.Z. geothermal workshop, proceedings. University of Auckland, pp 81–84

Bruton CJ (1995) Testing EQ3/6 and GEMBOCHS using fluid-mineral equilibria in the Wairakei geothermal system. Lawrence Livermore National Laboratory report UCRL-ID-129280, 21p

Calamai A, Cataldi R, Squarci P, Taffi L (1970) Geology, geophysics and hydrogeology of the Mt. Amiata geothermal field. Geothermics 1(Special Issue):1–9

Carella R, Guglielminetti M (1983) Multiple reservoirs in the Mofete field, Naples, Italy. In: Proceedings ninth workshop geothermal reservoir engineering. Stanford University, Stanford, California, Dec 1983, SGP-TU-74, pp 53–64

Carvalho MR, Forjaz VH, Almeida C (2006) Chemical composition of deep hydrothermal fluids in the Ribeira Grande geothermal field (São Miguel, Azores). J Volcanol Geother Res 156:116–134

Cavarretta G, Gianelli G, Scandiffio G, Tecce F (1985) Evolution of the Latera geothermal system II: metamorphic, hydrothermal mineral assemblages and fluid chemistry. J Volcanol Geother Res 26:337–364

Chambefort I, Buscarlet E, Wallis IC, Sewell S, Wilmarth M (2016) Ngatamariki geothermal field, New Zealand: Geology, geophysics, chemistry and conceptual model. Geothermics 59:266–280
Charlton SR, Parkhurst DL (2002) PhreeqcI-A graphical user interface to the geochemical model PHREEQC. U.S. Geological Survey Fact Sheet FS-031-02, 2p
Chiba H (1991) Attainment of solution and gas equilibrium in Japanese geothermal systems. Geochem J 25:335–355
Chiodini G, Cioni R, Guidi M, Marini L (1991) Chemical geothermometry and geobarometry in hydrothermal aqueous solutions: A theoretical investigation based on a mineral-solution equilibrium model. Geochim Cosmochim Acta 55:2709–2727
Christenson BW (1997) Kawerau geothermal field: geochemical structure of the reservoir and its response to exploitation. Geother Res T 21:17–24
Christenson BW, Mroczek EK, Kennedy BM, van Soest MC, Stewart MK, Lyon G (2002) Ohaaki reservoir chemistry: characteristics of an arc-type hydrothermal system in the Taupo Volcanic Zone, New Zealand. J Volcanol Geother Res 115:53–82
Clarke GC, Woodhall DG, Allen D, Darling G (1990) Geological, volcanological and hydrogeological controls on the occurrence of geothermal activity in the area surrounding Lake Naivasha. Kenya, Ministry of Energy report, Kenya, 245p
Clearwater E, Seastres J Jr, Newson J, Mulusa G (2015) Modelling of scaling in a Tauhara production well. In: Proceedings world geothermal congress 2015, Melbourne, Australia, 19–25 Apr 2015, 9p
Cox ME, Browne P (1998) Hydrothermal alteration mineralogy as an indicator of hydrology at the Ngawha geothermal field, New Zealand. Geothermics 27:259–270
D'Amore F, Mejia JT (1999) Chemical and physical reservoir parameters at initial conditions in Berlin geothermal field, El Salvador: a first assessment. Geothermics 28:45–73
D'Amore F, Giusti D, Gizaw B (1997) Geochemical assessment of the Northern Tendaho Rift, Ethiopia. In: Proceedings of twenty-second workshop on geothermal reservoir engineering. Stanford University. SGP-TR-155, pp 435–445
D'Amore F, Giusti D, Abdallah A (1998) Geochemistry of the high-salinity geothermal field of Asal, Republic of Djibouti, Africa. Geothermics 27:197–210
Darling WG (1998) Hydrothermal hydrocarbon gases: 2. Application in the East African Rift System. Appl Geochem 13:825–840
Dominco E, Samilgil E (1970) The geochemistry of the Kizildere geothermal field, in the framework of the Saraykoy-Denizli geothermal area. Geothermics 2:553–560
Ellis AJ (1970) Quantitative interpretation of chemical characteristics of hydrothermal systems. Geothermics 2:516–528
Ellis AJ, Mahon WAJ (1977) Chemistry and geothermal systems. Academic Press, 392p
Farrar CD, Sorey ML, Roeloffs E, Galloway DL, Howle JF, Jacobson R (2003) Inferences on the hydrothermal system beneath the resurgent dome in Long Valley Caldera, east-central California, USA, from recent pumping tests and geochemical sampling. J Volcanol Geoth Res 127:305–328
Ferrari L, Garduño VH, Pasquarè G, Tibaldi A (1991) Geology of Los Azufres Caldera, Mexico, and its relationships with regional tectonics. J Volcanol Geoth Res 47:129–148
Fouillac AM, Fouillac C, Cesbron F, Pillard F, Legendre O (1989) Water-rock interaction between basalt and high-salinity fluids in the Asal Rift, Republic of Djibouti. Chem Geol 76:271–289
Fournier RO (1977) Chemical geothermometers and mixing models for geothermal systems. Geothermics 5:41–50
Furuya S, Aoki M, Gotoh H, Takenaka T (2000) Takigami geothermal system, northeastern Kyushu, Japan. Geothermics 29:191–211
Garrels RM, Christ CL (1965) Solutions, minerals, and equilibria. Harper & Row, New York, p 450
Gherardi F, Panichi C, Yock A, Gerardo-Abaya J (2002) Geochemistry of the surface and deep fluids of the Miravalles volcano geothermal system (Costa Rica). Geothermics 31:91–128
Gianelli G, Scandiffio G (1989) The Latera geothermal system (Italy): chemical composition of the geothermal fluid and hypotheses on its origin. Geothermics 18:447–463

Gianelli G, Teklemariam M (1993) Water-rock interaction processes in the Aluto-Langano geothermal field (Ethiopia). J Volcanol Geother Res 56:429–445
Gianelli G, Puxeddu M, Batini F, Bertini G, Dini I, Pandeli E, Nicolich R (1988) Geological model of a young volcano-plutonic system: the geothermal region of Monte Amiata (Tuscany, Italy). Geothermics 17:719–734
Giggenbach WF (1980) Geothermal gas equilibria. Geochim Cosmochim Acta 44:2021–2032
Giggenbach WF (1988) Geothermal solute equilibria. derivation of Na–K–Mg–Ca geoindicators. Geochim Cosmochim Acta 52:2749–2765
Giggenbach WF (1995) Variations in the chemical and isotopic composition of fluids discharged from the Taupo Volcanic Zone, New Zealand. J Volcanol Geoth Res 68:89–116
Giggenbach WF (1997a) The origin and evolution of fluids in magmatic-hydrothermal systems. In: Geochemistry of hydrothermal ore deposits, 3rd edn. In: Barnes HL (ed) Wiley, pp 737–796
Giggenbach WF, Corrales Soto R (1992) Isotopic and chemical composition of water and steam discharges from volcanic-magmatic-hydrothermal systems of the Guanacaste Geothermal Province, Costa Rica. Appl Geochem 7:309–332
Giroud N (2008) A chemical study of arsenic, boron and gases in high-temperature geothermal fluids in Iceland. Ph.D. thesis, Faculty of Science, University of Iceland, 110p
Gizaw B (1993) Aluto-Langano geothermal field, Ethiopian Rift Valley: physical characteristics and the effects of gas on well performance. Geothermics 22:101–116
Gizaw B (1996) The origin of high bicarbonate and fluoride concentrations in waters of the Main Ethiopian Rift Valley, East African Rift system. J Afr Earth Sci 22(4):391–402
Glover RB, Mroczek EK (2009) Chemical changes in natural features and well discharges in response to production at Wairakei. New Zealand. Geothermics 38:117–133
Glover RB, Lovelock B, Ruaya JR (1981) A novel way of using gas and enthalpy data. In: Proceedings of 3rd N.Z. geothermal workshop. University of Auckland, pp 163–169
Goff F, Shevenell L, Gardner JN, Vuataz F-D, Grigsby CO (1988) The hydrothermal outflow plume of Valles Caldera, New Mexico, and a comparison with other outflow plumes. J Geophys Res-Sol Earth 93(B6):6041–6058
Goff F, Bergfeld D, Janik CJ Counce D, Murrell M (2002) Geochemical data on waters, gases, scales, and rocks from the Dixie Valley Region, Nevada (1996–1999). Los Alamos report LA-13972-MS, 71p
González-Partida EG, Tello-Hinojosa ET, Pal-Verma M (2000) Análisis geoquímico e isotópico de aguas geotérmicas y manantiales para definir el estado de equilibrio agua-roca del reservorio de Los Azufres, Michoacán, México. Ing Hidraul Mex 15:88–99
González-Partida E, Carrillo-Chávez A, Levresse G, Tello-Hinojosa E, Venegas-Salgado S, Ramirez-Silva G, Pal-Verma M, Tritlla J, Camprubi A (2005) Hydro-geochemical and isotopic fluid evolution of the Los Azufres geothermal field, Central Mexico. Appl Geochem 20:23–39
Gudmundsson BT, Arnórsson S (2002) Geochemical monitoring of the Krafla and Námafjall geothermal areas, N-Iceland. Geothermics 31:195–243
Guidi M, Marini L, Cioppi D (1988) Geotermometria chimica su acque geotermiche provenienti da serbatoi carbonatici. CNR-PFE report, 38p
Guidi M, Marini L, Principe C (1990) Hydrogeochemistry of Kizildere geothermal system and nearby region. Geother Res T 14:901–908
Guo Q, Nordstrom DK, McCleskey RB (2014) Towards understanding the puzzling lack of acid geothermal springs in Tibet (China): insight from a comparison with Yellowstone (USA) and some active volcanic hydrothermal systems. J Volcanol Geother Res 288:94–104
Haizlip JR, Haklidir FST (2011) High noncondensible gas liquid dominated geothermal reservoir Kizildere, Turkey. Geother Res T 35:615–618
Haklidir FT, Sengun R, Haizlip JR (2015) The geochemistry of the deep reservoir wells in Kizildere (Denizli City) geothermal field (Turkey). In: Proceedings world geothermal congress 2015—Melbourne, Australia, 19–25 Apr 2015, 4p

Hardardóttir V (2011) Metal-rich scales in the Reykjanes geothermal system, SW Iceland. Sulfide minerals in a seawater-dominated hydrothermal environment. Ph.D. thesis, Faculty of Science, University of Ottawa, 288p

Hardardóttir V, Brown KL, Fridriksson T, Hedenquist JW, Hannington MD, Thorhallsson S (2009) Metals in deep liquid of the Reykjanes geothermal system, southwest Iceland: implications for the composition of seafloor black smoker fluids. Geology 37:1103–1106

Hedenquist JW (1986) Geothermal systems in the Taupo volcanic zone; their characteristics and relation to volcanism and mineralisation. In: Smith IEM (ed) Late Cenozoic volcanism in New Zealand, vol 23. Bulletin—Royal Society of New Zealand, pp 134–168

Hedenquist JW (1990) The thermal and geochemical structure of the Broadlands-Ohaaki geothermal system, New Zealand. Geothermics 19:151–185

Hedenquist JW, Browne PR (1989) The evolution of the Waiotapu geothermal system, New Zealand, based on the chemical and isotopic composition of its fluids, minerals and rocks. Geochim Cosmochim Acta 53:2235–2257

Hedenquist JW, Lowenstern JB (1994) The role of magmas in the formation of hydrothermal ore deposits. Nature 370:519–526

Hedenquist JW, Mroczek EK, Giggenbach WF (1988) Geochemistry of the Rotokawa geothermal system: summary of data, interpretation and appraisal for energy development. Chemistry Division DSIR Technical Note 88/6, 63p

Hedenquist JW, Goff F, Phillips FM, Elmore D, Stewart MK (1990) Groundwater dilution and residence times, and constraints on chloride source, in the Mokai geothermal system, New Zealand, from chemical, stable isotope, tritium, and ^{36}Cl data. J Geophys Res-Sol Earth 95(B12):19365–19375

Helgeson HC (1968) Geologic and thermodynamic characteristics of the Salton Sea geothermal system. Am J Sci 266:129–166

Helgeson HC, Delany JM, Nesbitt HW, Bird DK (1978) Summary and critique of the thermodynamic properties of rock-forming minerals. Am J Sci 278A:229p

Henley RW, Middendorf KI (1985) Geothermometry in the recent exploration of Mokai and Rotokawa geothermal fields, New Zealand. Geoth Res T 9:317–324

Henley RW, Plum H (1985) Chemistry of geothermal fluids discharged from exploration wells at Mokai/New Zealand. Z Dtsch Geol Ges 136:235–251

Henley RW, Truesdell AH, Barton JP (1984) Fluid-mineral equilibra in hydrothermal systems. Rev Econ Geol 1:268p

Heřmanská M, Stefánsson A, Scott S (2019) Supercritical fluids around magmatic intrusions: IDDP-1 at Krafla, Iceland. Geothermics 78:101–110

Iglesias ER, Arellano VM, Garfias A, Miranda C, Aragon A (1985) A one-dimensional vertical model of the Los Azufres, Mexico, geothermal reservoir in its natural state. Geother Res T 9:331–336

Izquierdo G, Aragón A, Portugal E, Arellano VM, de León J, Álvarez J (2006) Mineralogía de la zona mineralizada de sílice-epidota (ZMSE) del yacimiento geotérmico de Cerro Prieto, BC, México. Geotermia 19:2–12

James ED, Hoang VT, Epperson IJ (1987) Structure, permeability and production characteristics of the Heber, California geothermal field. Ln: Proceedings, twelfth workshop on geothermal reservoir engineering. Stanford University, Stanford, California, 20–22 Jan 1987. SGP-TR-109, pp 267–271

Ji D, Ping Z (2000) Characteristics and genesis of the Yangbajing geothermal field, Tibet. In: Proceedings of the world geothermal congress, Kyushu-Tohoku, Japan, vol 28, pp 1083–1088

Jordan OT (1982) Implications of solution-mineral equilibria on the exploitation of the S-Negros geothermal field, Philippines. UNU-GTP report 1982-7, 67p

Karingithi CW, Arnórsson S, Grönvold K (2010) Processes controlling aquifer fluid compositions in the Olkaria geothermal system, Kenya. J Volcanol Geoth Res 196:57–76

Kipng'ok J (2011) Fluid chemistry, feed zones and boiling in the first geothermal exploration well at Menengai, Kenya. UNU-GTP report 2011-15, pp 281–302

Klein CW, Iwata S, Takeuchi R, Naka T (1991) Prediction and prevention of silica scaling at low levels of oversaturation: case studies, and calculations for Uenotai geothermal field, Akita Prefecture, Japan. In: Proceedings, sixteenth workshop on geothermal reservoir engineering. Stanford University, Stanford, California, 23–25 Jan 1991. SGP-TR-134, pp 165–176

Krupp RE, Seward TM (1987) The Rotokawa geothermal system, New Zealand: an active epithermal gold-depositing environment. Econ Geol 82:1109–1129

Kuriyama T (1985) Geothermal system in the Yuzawa-Ogachi area, Northern Honshu. J Geotherm Res Soc Jpn 7:311–328 (in Japanese with English abstract)

Lemmon EW, McLinden MO, Friend DG (2017) Thermophysical properties of fluid systems. In: Linstrom PJ, Mallard WG (eds) NIST chemistry Webbook, NIST standard reference database number 69. National Institute of Standards and Technology, Gaithersburg MD. http://webbook.nist.gov/

Mahon WAJ, Finlayson JB (1972) The chemistry of the Broadlands geothermal area, New Zealand. Am J Sci 272:48–68

Malimo SJ (2012) Aquifer fluid modeling and assessment of mineral-gas-liquid equilibria in the Namafjall geothermal system. NE-Iceland. UNU-GTP report 2012-3, 57p

Malimo SJ (2013) Fluid chemistry of Menengai geothermal wells, Kenya. Geother Res T 37:425–430

Mañon A, Mazor E, Jimenez M, Sanchez A, Fausto J, Zenizo C (1977) Extensive geochemical studies in the geothermal field of Cerro Prieto, Mexico. US-DOE report LBL-7019, contract W-7405-ENG-48, 113p

Marini L, Yock Fung A, Sanchez E (2003) Use of reaction path modeling to identify the processes governing the generation of neutral Na–Cl and acidic Na–Cl–SO_4 deep geothermal liquids at Miravalles geothermal system, Costa Rica. J Volcanol Geoth Res 128:363–387

Michels DE (1986) SSSDP fluid compositions at first flow test of State 2-14. Geother Res T 10:461–465

Monastero FC, Katzenstein AM, Miller JS, Unruh JR, Adams MC, Richards-Dinger K (2005) The Coso geothermal field: a nascent metamorphic core complex. Geol Soc Am Bull 117:1534–1553

Moore JN, Adams MC, Bishop BP, Hirtz P (1989) A fluid flow model of the Coso geothermal system: data from production fluids and fluid inclusions. In: Proceedings, fourteenth workshop on geothermal reservoir engineering. Stanford University, Stanford, California, 24–26 Jan 1989, SGP-TR-122, pp 139–144

Muna ZW (1982) Chemistry of well discharges in the Olkaria geothermal field, Kenya. UNU-GTP report 1982–8, 38p

Naka T, Okada H (1992) Exploration and development of Uenotai geothermal field, Akita Prefecture, northeastern Japan. Resour Geol 42:223–240 (in Japanese with English abstract)

Nielson DL, Hulen JB (1984) Internal geology and evolution of the Redondo Dome, Valles Caldera, New Mexico. J Geophys Res Sol Earth 89(B10):8695–8711

Nitta T, Adachi M, Takahashi M, Inoue K, Abe Y (1991) Heavy metal precipitation from geothermal fluid of 87N-15T production well in the Okuaizu geothermal field, Tohoku district, Japan. Resour Geol 41:231–242 (in Japanese with English abstract)

Nitta T, Tsukagoshi S, Adachi M, Seo K (1995) Exploration and development in the Okuaizu geothermal field, Japan. Resour Geol 45:201–212 (in Japanese with English abstract)

Nordstrom DK, Plummer LN, Wigley TML, Wolery TJ, Ball JW, Jenne EA, Bassett RL, Crerar DA, Florence TM, Fritz B, Hoffman M, Holdren GR, Lafon GM, Mattigod SV, McDuff RE, Morel F, Reddy MM, Sposito G, Thrailkill J (1979) A comparison of computerized chemical models for equilibrium calculations in aqueous systems. In: Jenne EA (ed) Chemical modeling in aqueous systems, ACS symposium series, vol 93, pp 857–892

Okada H, Yasuda Y, Yagi M, Kai K (2000) Geology and fluid chemistry of the Fushime geothermal field, Kyushu, Japan. Geothermics 29:279–311

Özgür N (1998) Geochemical signature of the Kizildere geothermal field, western Anatolia, Turkey. Int Geol Rev 44:153–163

Pang Z-H (2006) pH dependant isotope variations in arc-type geothermal waters: new insights into their origins. J Geochem Explor 89:306–308
Panichi C (2004) Geochemical impact of re-injecting geothermal waste waters: example, Larderello, Italy. In: Gieré R, Stille P (eds) Energy, waste, and the environment: a geochemical perspective, vol 236. Geological Society, London, Special Publications, pp 337–354
Parkhurst DL, Appelo CAJ (2013) Description of input and examples for PHREEQC version 3: a computer program for speciation, batch-reaction, one-dimensional transport, and inverse geochemical calculations. Techniques and Methods 6-A43. U.S. Geological Survey
Ping Z (1991) Gas geothermometry and chemical equilibria of fluids from selected geothermal fields. UNU-GTP report 1991-14, 46p
Ping Z, Jian J, Haizheng Z, Ji D, Tingli L (1998a) Chemical composition of thermal water in the Yangbajing geothermal field, Tibet. Sci Geol Sin 33:61–72 (in Chinese with English abstract)
Ping Z, Tingli L, Jian J, Haizheng Z (1998b) Characteristics of gas geochemistry in Yangbajing geothermal field, Tibet. Chin Sci Bull 43:1770–1777
Price L, Powell TS, Atkinson L (2011) Geothermal fluid evolution at Rotokawa: hydrothermal alteration indicators. Geother Res T 35:977–982
Principe C, Lavorini G, Vezzoli LM (eds) (2017) Il Vulcano di Monte Amiata. Edizioni Scientifiche e Artistiche, 399p
Rae AJ (2002) Alteration systematics and mineralising potential of the Palinpinon geothermal field, Negros Island, Philippines. Ph.D. thesis, University of Tasmania, Australia, 243p
Rae AJ, Cooke DR, Brown KL (2011) The trace metal chemistry of deep geothermal water, Palinpinon geothermal field, Negros Island, Philippines: implications for precious metal deposition in epithermal gold deposits. Econ Geol 106:1425–1446
Rango T, Petrini R, Stenni B, Bianchini G, Slejko F, Beccaluva L, Ayenew T (2010) The dynamics of central Main Ethiopian Rift waters: Evidence from δD, $\delta^{18}O$ and $^{87}Sr/^{86}Sr$ ratios. Appl Geochem 25:1860–1871
Reed MJ (1976) Geology and hydrothermal metamorphism in the Cerro Prieto geothermal field, Mexico. In: Proceedings 2nd U.N. symposium on development and use of geothermal resources, vol 1, San Francisco, pp 539–547
Reed MJ (1989) Thermodynamic calculations of calcium carbonate scaling in geothermal wells, Dixie Valley geothermal field, U.S.A. Geothermics 18:269–277
Reed MH (1997) Hydrothermal alteration and its relationship to ore fluid composition. In: Barnes HL (ed) Geochemistry of hydrothermal ore deposits, 3d edn. Wiley, pp 517–611
Reed MH (1998) Calculation of simultaneous chemical equilibria in aqueous-mineral-gas systems and its application to modeling hydrothermal processes. In: Richards J, Larson P (eds) Techniques in hydrothermal ore deposits geology. Reviews in economic geology, vol 10, pp 109–124
Reed MH, Spycher NF (1984) Calculation of pH and mineral equilibria in hydrothermal waters with application to geothermometry and studies of boiling and dilution. Geochim Cosmochim Acta 48:1479–1492
Reed MH, Palandri J, Clemente V, Cabahug R (2014) Computation of reservoir geochemical conditions from excess-enthalpy wellhead samples. Geother Res T 38:461–464
Remoroza AI (2010) Calcite mineral scaling potentials of high-temperature geothermal wells. Master's thesis, Faculty of Science, University of Iceland, 99p
Renderos RE (2002) Chemical characterization of the thermal fluid discharge from well production tests in the Berlín geothermal field, El Salvador. UNU-GTP report 2002-12, pp 205–231
Reyes AG (1990) Petrology of Philippine geothermal systems and the application of alteration mineralogy to their assessment. J Volcanol Geoth Res 43:279–309
Reyes AG, Giggenbach WF, Saleras JRM, Salonga ND, Vergara MC (1993) Petrology and geochemistry of Alto Peak, a vapor-cored hydrothermal system, Leyte Province, Philippines. Geothermics 22:479–519
Reyes AG, Trompetter WJ, Britten K, Searle J (2003) Mineral deposits in the Rotokawa geothermal pipelines, New Zealand. J Volcanol Geoth Res 119:215-239

Rosi M, Sbrana A, Principe C (1983) The Phlegraean fields: structural evolution, volcanic history and eruptive mechanisms. J Volcanol Geoth Res 17:273–288
Ruaya JR, Buenviaje MM, Solis RP, Gonfiantini R (1995) Chemical and isotopic studies of fluids in the Bacon-Manito geothermal field, Philippines. In: Isotope and geochemical techniques applied to geothermal investigations. IAEA-TECDOC-788, pp 185–208
Ruggieri G, Giolito C, Gianelli G, Manzella A, Boiron MC (2004) Application of fluid inclusions to the study of Bagnore geothermal field (Tuscany, Italy). Geothermics 33: 675–692
Sakai Y, Matsunaga E, Kubota Y (1993) Geothermal energy development in the Sumikawa field, Northeast Japan. Resour Geol 43:409–425 (in Japanese with English abstract)
Sanjuan B (2010) Use of a new sodium/lithium (Na/Li) geothermometric relationship for High-Temperature (HT) geothermal fluids derived from seawater/basalt interaction processes: application to the Djibouti case. In: Third East African Rift Geothermal Conference ARGEO-C3, 21p
Sanjuan B, Michard G, Michard A (1990) Origine des substances dissoutes dans les eaux des sources thermales et des forages de la région Asal-Ghoubbet (République de Djibouti). J Volcanol Geother Res 43:333–352
Sasada M (1987) Fluid inclusions in calcite scale from DY-1 drill hole, Hohi geothermal area, Japan. J Geotherm Res Soc Jpn 9:197–205
Scott SW (2011) Gas chemistry of the Hellisheidi geothermal field. Master's thesis. REYST/Faculty of Science, University of Iceland, 81p
Scott S, Gunnarsson I, Arnórsson S, Stefánsson A (2014) Gas chemistry, boiling and phase segregation in a geothermal system, Hellisheidi, Iceland. Geochim Cosmochim Acta 124:170–189
See FS (1995) Anhydrite deposition in Cawayan wells, Bacman geothermal field Philippines: prediction and possible remedies. UNU-GTP report 13, pp 321–348
Sekento LR (2012) Geochemical and isotopic study of the Menengai geothermal field, Kenya. UNU-GTP report 2012-31, pp 769–792
Seki Y (1990) Gas concentration in aquifer fluid prior to boiling in the Oku-aizu geothermal system, Fukushima, Japan. Geochem J 24:105–121
Seki Y (1991) The physical and chemical structure of the Oku-aizu geothermal system, Japan. Geochem J 25:245–265
Seki Y, Liou JG, Guillemette R, Sakai H, Oki Y, Hirano T, Onuki H (1983) Investigation of geothermal systems in Japan I. Onikobe geothermal area. Hydroscience and Geotechnology Laboratory, Saitama University, Memoir No. 3, 206p
Sheppard DS (1984) Fluid chemistry of Ngawha reservoir. In: Proceedings 6th New Zealand geothermal workshop, pp 151–154
Sheppard DS, Giggenbach WF (1980) Chemistry of the well discharges at Ngawha. In: Proceedings of New Zealand geothermal workshop, University of Auckland, pp 91–95
Sheppard DS, Lyon GL (1984) Geothermal fluid chemistry of the Orakeikorako field, New Zealand. J Volcanol Geother Res 22:329–349
Simpson MP, Bignall G (2016) Undeveloped high-enthalpy geothermal fields of the Taupo Volcanic Zone, New Zealand. Geothermics 59:325–346
Smith RL, Bailey RA (1966) The Bandelier Tuff: a study in ash-flow eruption cycles from zoned magma chambers. Bull Volcanol 29:83–104
Stefánsson A, Arnórsson S (2000) Feldspar saturation state in natural waters. Geochim Cosmochim Acta 64:2567–2584
Suzuki M, Futagoishi M, Inoue T, Yamada K, Obara K, Fujino T (2000) Conceptual hydrogeological model of the Wasabizawa geothermal field, Akita Prefecture, Japan. In: Proceedings of the world geothermal congress 2000, Kyushu-Tohoku, Japan, pp 2241–2245
Takenaka T, Furuya S (1991) Geochemical model of the Takigami geothermal system, northeast Kyushu, Japan. Geochem J 25:267–281
Takenaka T, Gotoh H, Yamamoto Y, Furuya S (1995) Exploration and development of the Takigami geothermal system, Kyshu, Japan. J Soc Resour Geol 45:361–376 (in Japanese with English abstract)

Takeno N (2000) Thermal and geochemical structure of the Uenotai geothermal system, Japan. Geothermics 29:257–277
Tarcan G, Özen T, Gemici Ü, Çolak M, Karamanderesi İH (2016) Geochemical assessment of mineral scaling in Kızıldere geothermal field, Turkey. Environ Earth Sci 75:1317, 19p
Teklemariam M, Battaglia S, Gianelli G, Ruggieri G (1996) Hydrothermal alteration in the Aluto-Langano geothermal field, Ethiopia. Geothermics 25:679–702
Tempel RN, Sturmer DM, Schilling J (2011) Geochemical modeling of the near-surface hydrothermal system beneath the southern moat of Long Valley Caldera, California. Geothermics 40:91–101
Thompson JM, Fournier RO (1988) Chemistry and geothermometry of brine produced from the Salton Sea scientific drill hole, Imperial Valley, California. J Geophys Res-Sol Earth 93(B11):13165–13173
Tonani FB, Nagao K, Moore J, Natale G, Sperry T (1998) Water and gas geochemistry of the Cove-Fort Sulphurdale geothermal system. In: Proceedings, twenty-third workshop on geothermal reservoir engineering. Stanford University, Stanford, California, 26–28 Jan 1998
Truesdell AH (1979) Aquifer boiling may be normal in exploited high-temperature geothermal systems. In: Proceedings, fifth workshop on geothermal reservoir engineering. Stanford University, Stanford, California, 12–14 Dec 1979
Truesdell AH, Janik CJ (1986) Reservoir processes and fluid origins in the Baca geothermal system, Valles Caldera, New Mexico. J Geophys Res-Sol Earth 91(B2):1817–1833
Truesdell AH, Nakanishi S (2005) Chemistry of neutral and acid production fluids from the Onikobe geothermal field, Miyagi Prefecture, Honshu, Japan. In: Use of isotope techniques to trace the origin of acidic fluids in geothermal systems. IAEA-TECDOC-1448, pp 169–193
Truesdell AH, Singers W (1974) The calculation of aquifer chemistry in hot-water geothermal systems. J Res US Geol Surv 2:271–278
Truesdell AH, Thompson JM, Coplen TB, Nehring NL, Janik CJ (1981) The origin of the Cerro Prieto geothermal brine. Geothermics 10:225–238
Truesdell AH, Lippmann MJ, Quijano JL, D'Amore F (1995) Chemical and physical indicators of reservoir processes in exploited high-temperature, liquid-dominated geothermal fields. In: Proceedings of the world geothermal congress, Florence, Italy, vol 3, pp 1933–1938
Ueda A, Kubota Y, Katoh H, Hatakeyama K, Matsubaya O (1991) Geochemical characteristics of the Sumikawa geothermal system, northeast Japan. Geochem J 25:223–244
Waibel AF (1987) An overview of the geology and secondary mineralogy of the high temperature geothermal system in Dixie Valley, Nevada. Geot Res Council Bull 11:479–486
White AF (1986) Chemical and isotopic characteristics of fluids within the Baca geothermal reservoir, Valles Caldera, New Mexico. J Geophys Res-Sol Earth 91(B2):1855–1866
White AF, Peterson ML (1991) Chemical equilibrium and mass balance relationships associated with the Long Valley hydrothermal system, California, USA. J Volcanol Geoth Res 48:283–302
Williams AE, McKibben MA (1989) A brine interface in the Salton Sea geothermal system, California: fluid geochemical and isotopic characteristics. Geochim Cosmochim Acta 53:1905–1920
Wilson BM (2007) Igneous petrogenesis. A global tectonic approach. Springer, 466p
Winick J, Powell T, Mroczek E (2009) The natural-state geochemistry of the Rotokawa reservoir. In: New Zealand geothermal workshop 2009, Proceedings, 16–18 Nov 2009, Rotorua, New Zealand, 8p
Wohletz K, Heiken G (1992) Volcanology and geothermal energy. University of California Press, 432p
Wolery TJ (1992) EQ3NR, a computer program for geochemical aqueous speciation-solubility calculations: Theoretical manual, user's guide and related documentation (version 7.0). Report UCRL-MA-110662 PT III. Lawrence Livermore National Laboratory, Livermore
Wolery TJ, Daveler SA (1992) EQ6, A computer program for reaction path modeling of aqueous geochemical systems: Theoretical manual, user's guide, and related documentation (version 7.0). Report UCRL-MA-110662 PT IV. Lawrence Livermore National Laboratory, Livermore

Xiaoping F (2002) Conceptual model and assessment of the Yangbajing geothermal field, Tibet, China. UNU-GTP report 2002-5, pp 27–52
Yamada M, Iguchi K, Nakanishi S, Todaka N (2000) Reservoir characteristics and development plan of the Oguni geothermal field, Kyushu, Japan. Geothermics 29:151–169
Yock Fung A (1998) Chemical and isotopic studies in the Miravalles geothermal field, Costa Rica. UNU-GTP report 1998-17, pp 461–499
Yoshida Y (1991) Geochemistry of the Nigorikawa geothermal system, southwest Hokkaido, Japan. Geochem J 25:203–222
Zaporozec A (1972) Graphical interpretation of water-quality data. Ground Water 10:32–43
Zhanshi Z (2001) Water-rock interaction in the Bakki low-temperature geothermal field, SW-Iceland. UNU-GTP report 2001-17, pp 405–434
Zhanxue S (1998) Geothermometry and chemical equilibria of geothermal fluids from Hveragerdi, SW-Iceland, and selected hot springs, Jiangxi province, SE-China. UNU-GTP report 1998-14, pp 373–402
Zhao P, Dor J, Liang T, Jin J, Zhang H (1998) Characteristics of gas geochemistry in Yangbajing geothermal field, Tibet. Chin Sci Bull 43:1770–1777